Notch signalling and the cell cycle regulate Trunk Neural Crest collective migration

Alhashem, Zain

Awarding institution:
King's College London

RANDALL
centre for cell and molecular biophysics

KING'S College LONDON

Notch signalling and the cell cycle regulate Trunk Neural Crest collective migration

Doctor of Philosophy in Randall Centre for Cell and Molecular Biophysics Research

Zainalabdeen Alhashem

Supervisor: Claudia Linker

Randall Centre for Cell and Molecular Biophysics

Word count: 36358

Contents

Abstract

Neural crest cells are a multipotent population that migrate extensively during development and differentiate into a plethora of derivatives. Trunk neural crest (TNC) migrate collectively forming single cell chains, in which the leader cell directs movement and is trailed by followers. We have previously shown that leader and follower identities are established before migration initiation, but how migratory identities are acquired is not understood. In this work, we investigated the mechanisms of migratory identity acquisition and how these affect TNC differentiation capacities. First, we asked if leader and follower cells arise from a common progenitor. We found that a single progenitor divides asymmetrically giving rise to one leader and one follower cell, while all other TNC progenitors give rise to two follower cells. Next, we investigated the mechanisms by which TNC identities are defined. Interestingly, we found that communications via Notch regulate migratory identity acquisition. Our data show that leader cells are defined upon high Notch levels, while followers present low Notch activity. Alteration of Notch activity in TNC leads to the establishment of a more homogeneous population unable to migrate coherently. Concurrently, we observed that leaders are larger than follower cells, and sought to investigate the role of cell cycle dynamics in this difference. We found that leaders and followers exhibit different division patterns and cell cycle dynamics. Although the total duration of the cell cycle is similar, the durations of G_1 and S-phases are inversely proportional. Leaders spend the majority of the cell cycle in S-phase, while followers present a longer G_1-phase. Our data show that differences in cell cycle patterns are under the regulation of Notch signalling. Finally, we investigated whether leader and follower cells present differences in their long-term fate. We found that unlike followers, leaders divide asymmetrically giving rise to a new leader and a follower cell. This division asymmetry translates into a long term fate asymmetry. The sibling that retains the leader's identity gives

rise to the sympathetic chain ganglia, while its follower sibling differentiates into a Schwann cell. On the other hand, followers divide symmetrically, giving rise to the dorsal root ganglia or Schwann cells. In this work, we have shown that coordination between Notch signalling and the cell cycle pathway regulate TNC migratory identity and fate.

Introduction

Cell migration

Cell migration is a fundamental process for life, from development to maintenance and repair in simple unicellular organisms like the amoeba, to all complex multi-cellular organisms. Broadly, cell migration refers to the movement of a cell from one location to another. Different types of motilities have been described, including mesenchymal, amoeboid or collective migration.

Two models have been put forward to explain the intracellular mechanisms driving migration: the cytoskeletal model and the membrane flow model. The cytoskeletal model hinges on cell migration occurring through the rapid polymerisation of actin filaments at the anterior or the 'leading edge' of the cell, creating a cytoskeletal protrusion of filopodia and lamellipodia which pushes the cell membrane towards the frontal edge, resulting in forward movement (Blanchoin et al., 2014). These protrusions are marked by integrins, transmembrane receptors that bind to ECM and facilitate adhesion, providing mechanical traction by which a cell can use to 'anchor' and move forward (Huttenlocher and Horwitz, 2011). In tandem, the posterior end, or 'trailing edge', retracts through microtubule remodelling of the cytoskeleton, resulting in a contractile force that creates cell translocation (Ganguly et al., 2012). The differences between the anterior and posterior ends of the cell are referred to as cell polarity, which are observed in all migrating cells and define the directionality of movement.

The second model explaining migration is the membrane flow model in which the leading edge of the cell is extended by adding cell membrane from endocytic compartments, which in turn is stabilised through actin polymerisation (Bretscher, 1983). Some studies have shown the leading edge to be the site where the endocytic cycle ends, it has been suggested that there is an endocytosis of integrins from the trailing edge that is trafficked to the leading

edge where it is exocytosed and reused (Nader et al., 2016). It is likely that these two models work in conjunction to propagate cell migration.

Collective Cell Migration

Collective migration is the movement of a group of cells that coordinate their behaviours and read external cues as a whole. This type of migration can occur in large cohesive groups in which cells keep close contact to each other, or in a more singular behaviour in which cells make sparse contact, described as mesenchymal collective migration (Friedl and Gilmour, 2009). Collective cell migration has been extensively studied in various model organisms. Examples of collective cell migration include border cells migration, trachea formation in *Drosophila* (Figure 1A and B); angiogenesis, posterior lateral line (Figure 1C) and neural crest (NC) in zebrafish (Figure 1E); and head mesendoderm in *Xenopus* (Figure 1F; (Scarpa and Mayor, 2016)).

During collective migration, cells can display different spatial arrangements, from loosely connected chains of mesenchymal cells to tightly packed masses. Within the migrating group, division of labour appears to fall in to two categories of cells: Leaders and Followers. Leader cells are defined as those at the invasive front of the group and are thought to be able to set the directionality of collective migration. On the other hand, Follower cells trail the Leaders and cannot influence the directionality of migration. An example of this categorisation of behaviour is evident in the vasculature where endothelial cells migrate collectively to drive angiogenesis. The leading or tip cell, is trailed by the follower stalk cells (Ubezio et al., 2016). A further example of identity led collective migration is in the tracheal formation of Drosophila, epithelial cells in the developing fly migrate in an interconnected, bud-like manner with the leading cells guiding the following group through cell-cell adhesion (Ghabrial and Krasnow, 2006).

Recent studies have clearly revealed that NC also migrate collectively (Figure 1E), but the mechanisms that control this migration appear to be different depending on the anteroposterior origin of the NC cells (Szabó et al., 2016; Richardson et al., 2016). Importantly, in cancer metastasis an invading group of cells that maintain contact, has been frequently observed in many types of cancer, including colorectal, breast, lung, thyroid, melanoma, and salivary adenoid cystic carcinoma, among others (Nagai et al., 2020). The collective cell behaviour of cancer cells in many aspects resembles that of embryos, suggesting that the underlying mechanisms regulating collective migration during embryogenesis may be at play during cancer development.

The coordination of collective migration requires communication within the group attained through the balance of different mechanisms that keep the group moving forward while simultaneously maintaining cohesion. In angiogenesis, cadherins, VEGF and Notch signalling have been shown to be crucial for collective migration. While studies of trachea formation indicate an important role for the FGF and Notch pathways. It is worth noting that in trachea formation and during angiogenesis (Figure 1A and B), Notch signalling has been shown to be fundamental in defining the identity of leader and follower cells. On the other hand, during posterior lateral line formation the SDF-CXCR pathway has been shown fundamental for chemotaxis and migration of this population (Haas and Gilmour, 2006). The mechanisms controlling the collective migration of NC populations have not been fully established. Nevertheless, it has been shown that SDF-CXCR signalling plays an important role (Theveneau et al., 2010), while a VEGF cell generated gradient has been proposed as a mechanisms establishing directionality of movement (McLennan et al., 2015b, 2010). Other signalling pathways, such as the complement component C3 and intracellular members of Wnt signalling, have also been shown to play a role in coordinating collective migration (Szabó and Mayor, 2018; Shellard and Mayor, 2016).

Figure 1

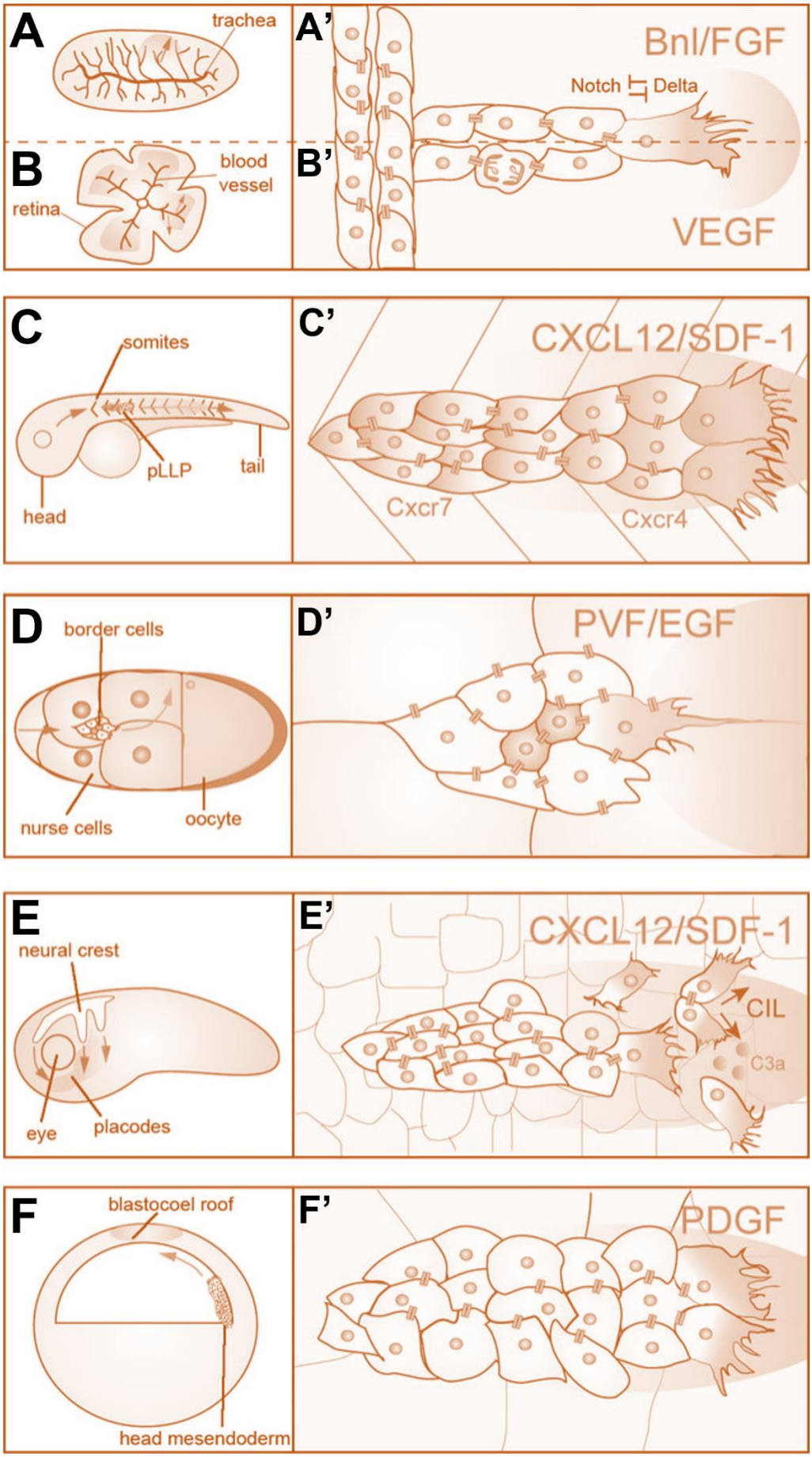
A
trachea
A'
Bnl/FGF
Notch
Delta
B
blood vessel
retina
B'
VEGF
C
somites
pLLP
tail
head
C'
CXCL12/SDF-1
Cxcr7
Cxcr4
D
border cells
nurse cells
oocyte
D'
PVF/EGF
E
neural crest
eye
placodes
E'
CXCL12/SDF-1
CIL
C3a
F
blastocoel roof
head mesendoderm
F'
PDGF

Figure 1: Models of collective cell migration in development.

(A) Branching morphogenesis of Drosophila trachea.

(A') Chemoattractant Bnl/FGF signalling induces tip cell state in drosophila trachea via Delta/Notch lateral inhibition.

(B) Blood vessel sprouting in the mouce retina.

(B') VEGF signaling induces tip cell state in endothelial cells via Delta/Notch lateral inhibition.

(C) Lateral line primoprdium migration through the myoseptum in zebrafish.

(C') Myoseptum produces the chemoattractant CXCL12/SDF-1, while leader cells at the front express CXCR4 and the rear cells express CXCR7.

(D) Border cells migration in Drosophila egg chamber, where border cells migrate between nurse cell.

(D') Chemoattractants PVF-1 and EGF guide border cell migration by polarizing the protrusions of the cell.

(E) Neural crest migration in Xenepous.

(E') Neural crest delaminate and migrate through the head by polarising the front cells via contact inhibition of locomotion, local attraction via C3a/C3aR and chemotaxis towards the chemoattractant SDF-1.

(F) Head mesendoderm migration in xenpepous.

(F') Head mesendoderm migrate towards the blastocoel roof following the chemoattractant PDGF.

Adapted from (Scarpa and Mayor, 2016).

The neural Crest

First described in chick embryos by His in 1868, the NC are a transient population of multipotent cells that arise early in vertebrate development (Bronner and LeDouarin, 2012). In 1969, the quail-chick chimeric system pioneered by Le Douarin allowed to reliably study the ontogeny of NC and their lineages (Lièvre and Douarin, 1975). In these experiments, a donor quail's neural tube (including the NC) was transplanted into a host chick embryo, creating a chimera, which displayed distinct feather pigmentation patterns. Darker feathers were derived from the quails' donor cells, while lighter feathers arise from the host chick cells. Importantly, quail cells were also distinguishable by their unique double nucleolus morphology, which allowed tracking donor cells to their final position in histological sections. This breakthrough allowed researchers to realise the extent to which NC colonise the embryo's tissues and recognize the plethora of derivatives this population give rise to (Douarin et al., 2004).

The NC are induced during gastrulation, between the prospective neural and epithelial tissues. A cascade of molecular events, including inductive signals secreted by the neuroepithelium and the underlying mesodermal tissues, establishes the NC population at the neural plate border region (Huang and Saint-Jeannet, 2004). A precise ratio of bone morphogenetic protein (BMP), Wnt, retinoic acid, fibroblast growth factors (FGF) and Notch signalling drive NC induction (Klymkowsky et al., 2010). These signalling pathways lead to the expression of the transcription factors, *Snail/Slug, FoxD3* and *SoxE*, which initiate a cascade of events leading to the establishment of the NC population, their subsequent delamination and migration (Sauka-Spengler and Bronner-Fraser, 2008; Meulemans and Bronner-Fraser, 2004). It has been shown that a similar molecular cascade leads to the delamination of cancer cells, a process known as epithelial to mesenchymal transition (EMT), of which the *Snail/Slug* family of transcription factors are master regulators (Medici et al., 2008, p.3). NC cells initiate EMT by upregulating the cell adhesion molecule N-cadherin and downregulating E-cadherin, through transcriptional repression by *Snail/Slug* (Cheung et al., 2005). The transcription factors *Snail/Slug, FoxD3* and *SoxE* further cooperate the switch of N-cadherin to *de novo* expression of the weaker adhesion molecules cadherin 7 and 11 in the trunk, whereas in the cranial region, additional transcriptional regulation from *Ets1, Sox5* and p53 become involved in the EMT process(Scarpa et al., 2015; Rinon et al., 2011; Théveneau et al., 2007; Perez-Alcala et al., 2004).

Interestingly, NC follow different patterns of delamination depending on their anteroposterior origin. In the cranial region, NC delaminate from the neuroepithelium in one

wave at different stages of development depending on the animal model observed. In *Xenopus* and mice, cranial NC (CNC) delaminate early as the neural plate remains open, in avian embryos this population delaminates later while the neural folds undergo fusion. The trunk NC (TNC) on the other hand, delaminate progressively leaving a resident population of cells in the dorsal neural tube regions, while cells at the ventral border invade adjacent tissues (Figure 2B). TNC migration initiation occurs through several days of development in all animal models (Gammill and Roffers-Agarwal, 2010)

NC can be classified in four different domains according to their anteroposterior origin and the derivatives they form (Figure 2A; (Rocha et al., 2020)): the cranial NC (CNC), the cardiac NC, the trunk NC (TNC), and the vagal and sacral NC.

(i) CNC migrate dorsolaterally underneath the dorsal epithelium and differentiate into facial connective tissue, cartilage and bone, as well as entering the pharyngeal arches to form the bones of the middle ear and jaw (Cordero et al., 2011).

(ii) Cardiac NC are found posterior to the cranial region, and despite their name these are able to give rise to similar cell types as the CNC in addition to the muscoloconnective tissue of arterial walls, contributing to the septation of the heart.

(iii) Trunk NC arise from the dorsal side of the neural tube and migrate invading adjacent tissues through two different pathways: the dorsolateral path, where TNC migrate underneath the skin epithelium and differentiate into melanocytes; and the ventromedial pathway, also known as the medial pathway, where TNC migrate deep in the embryo between the neural tube and the somites (Figure 3A). TNC migrating through the medial pathway, arrest shortly ventral to the neural tube and give rise to neurons and glia of the dorsal root ganglia; TNC that move further ventral, form Schwann cells enveloping nerve axons; TNC that undergo the ventral most migration form parasympathetic nerve cells, sympathetic ganglia and cells of the adrenal medulla (Serbedzija et al., 1994).

(iv) Vagal NC arise between the cardiac and TNC, together with sacral NC, that originate from the posterior most region of the embryo, colonize the digestive tract and form the enteric nervous system of the gut. It has been shown that failure of this migration results in the absence of peristaltic movements and a working colon (Pomeranz et al., 1991).

The mechanisms regulating NC migration have not been completely elucidated, but several modes of interaction between CNC cells have been established, including contact inhibition of locomotion (CIL) and co-attraction (Co-A).

CIL, described in 1950s (Abercrombie and Heaysman, 1954), explains how cells change direction of movement upon collision. Cells that migrate into each other generate a transient adhesion upon contact, repolarise and reinitiate movement in different directions. Such mechanism result in the dispersion of cells from an initially tightly packed group. Experiments in *Xenopus* and zebrafish have shown CIL is important for the dispersion and polarised migration of CNC (Theveneau and Mayor, 2012). At a molecular level, N-Cadherin has been shown to play a pivotal role in CNC CIL, through the activation of the non-canonical Wnt planar polarity pathway at the point of contact. Activation of Wnt components result in the downstream activation of Rho GTPases, which in turn inhibits Rac1causing retraction of membrane protrusions at the contact point and repolarisation of the cells (Theveneau et al., 2010). Nevertheless, NC migrate in cohesive groups thus while CIL accounts for the dispersion of the group, additional components must be at play to maintain the group cohesion (Szabó et al., 2016). Co-attraction play this role, maintaining the NC together and explaining the maintenance of a coherent migratory population. It has been shown that CNC secrete the chemo-attractant C3a, forming a gradient of this factor. As CNC detach from the group in response to CIL, it is the gradient of C3a that redirect their movement to follow this gradient back to the group (Carmona-Fontaine et al., 2011). The combination of CIL and Co-A in this manner allows the group to maintain polarised movement and ensures that cells remain together as a cohesive group (Shellard and Mayor, 2016).

A cell-induced gradient model has also been proposed to play a role in the directionality of CNC movement. Computational modelling of CNC migration in chick embryos, suggest that cells at the migratory front of the group, termed trailblazer cells, respond to a cell-induced chemotactic gradient of Vascular Endothelial Growth Factor (VEGF). Such gradient directs the movement of the group acting as a short-range guidance signal (McLennan et al., 2010). However, experimental evidence from zebrafish and chick embryos has shown that CNC are composed of a homogenous population of cells that undergo constant cell rearrangements and rely on cell-cell interactions to migrate directionally (Richardson et al., 2016). To date, no experimental evidence supports the proposed VEGF gradient or the existence of different cell identities (leader/follower) in the CNC population, hence it would be surprising if leader/follower dynamics play an important role in the regulation of CNC migration.

While the full complexity of signalling, cell-cell interactions, and extracellular factors governing NC migration remains to be fully elucidated, disruption of their migration results in severe pathologies collectively known as neurocristopathies. This diverse

classification includes disease derived from the lack or malfunctioning of NC, like Hirschsprung Disease, neurofibromatosis type I, melanoma and craniofrontonasal syndrome, among others (Vega-Lopez et al., 2018). The NC have also been linked to the neurological disease multiple sclerosis, where no specific cause is known, and treatment options are restricted (Behan and Chaudhuri, 2010).

NC are not only implicated in various pathologies but share commonalities with cancer cells. During cancer metastases, cancer cells undergo a process of EMT, invasion and long-distance migration like NC cells; these three processes can be studied *in vivo* during NC development, where it may be possible to extrapolate the molecular processes underlying NC migration to invasive cancer cells. Additionally, NC are particularly appropriate to model NC-derived cancers such as melanomas and neuroblastomas, where studies have shown the migration of these cancers to have underlying N-cadherin and CXCR4-mediated chemotaxis, similar to those in observed in NC (Mrozik et al., 2018; O'Boyle et al., 2013; Meier et al., 2007). Furthermore, transcriptional factors such as *Snail/Slug,* Sox10 and E/N cadherin are not only involved in EMT, migration and maintenance of NC, but are also implicated in the formation of tumours and induction of invasive behaviour. These similarities are suggestive of NC as a potential model for cancer metastasis, and as the understanding of NC migration deepens, these may shed light on the mechanisms at play during cancer metastasis.

The role that the NC play in vertebrate development and disease is of vast importance, where better understanding of the mechanisms underlying NC development would lead to better understanding of vertebrate development, evolution and neurocristopathies. Nevertheless, numerous questions regarding NC development remain unanswered, among others, how are the identities of NC sub-populations defined? What mechanisms and signalling pathways designate NC cell fate? How do NC find their migration routes and define their destination sites?. The NC are an evolutionary innovation of vertebrates and several model organisms are available for their study to answer such questions, these models include chick, Xenopus, mouse and zebrafish. Each model organism has its advantages with chick, xenopus and zebrafish providing large number of peogeny and ease of manipulation and imaging, while the mouse offers a powerful genetic model to study gene function during development within a mammalian context (Barriga et al., 2015). However out of the these models and for the purpose of our research, the zebrafish remains a very attractive model to study NC development due to their genetic tractability and optical transparency.

Figure 2

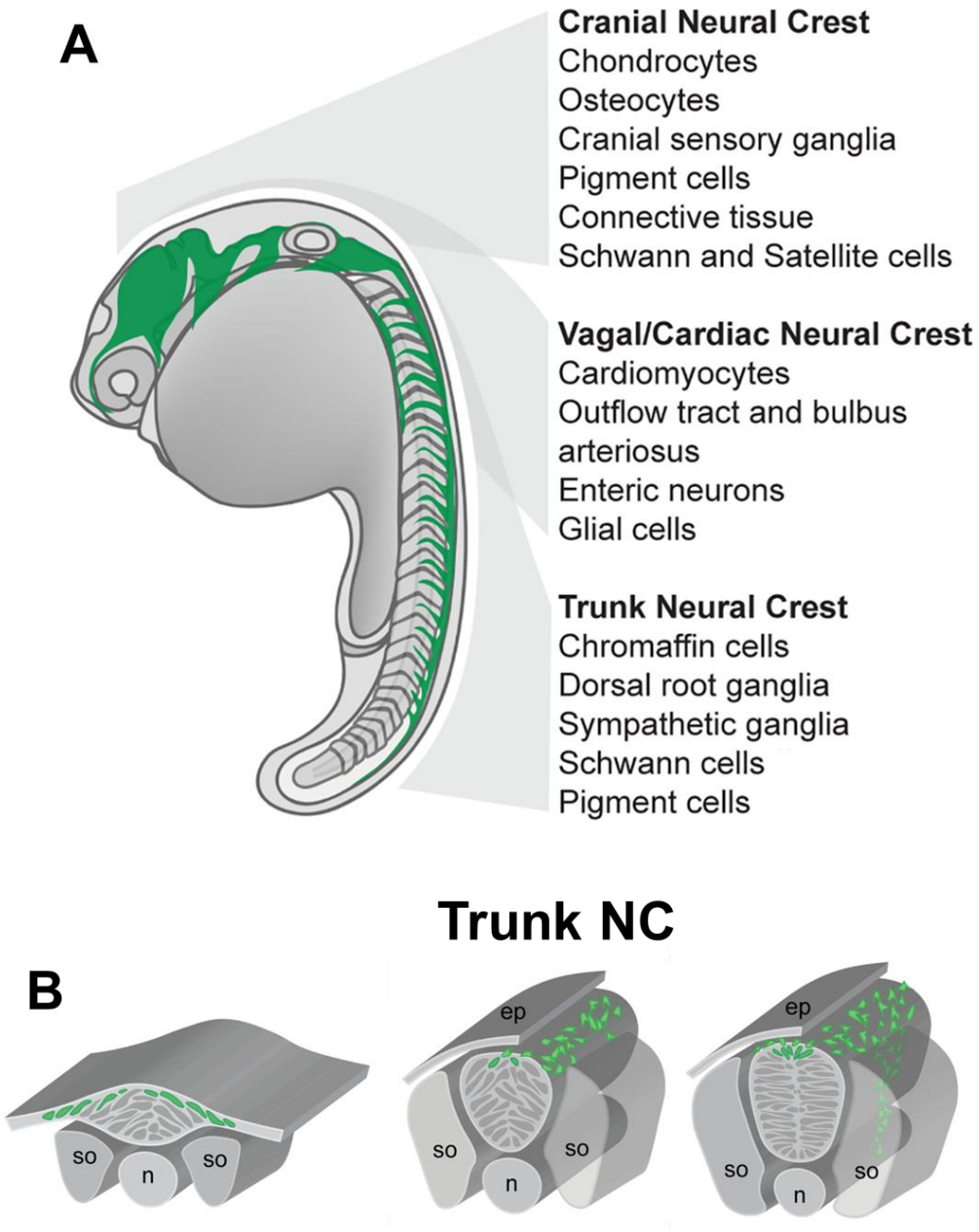

Figure 2: Neural crest regionalization an derivatives.

(A) Illustration of a 24hpf zebrafish embryo showing the domains of each NC sub-population according to their anteroposterior levels.

(B) Schematic of TNC position during neurulation and subsequent TNC delamination and migration through the ventromedial pathway between the somites and the neural tube. so: somites, n: notochord, ep: epidermis, TNC cells in green.

Adapted from (Rocha et al., 2020).

Trunk Neural Crest migration

In zebrafish, Trunk Neural Crest migrate from the dorsal side of the neural tube via two routes: first, the ventro-medial pathway in which TNC migrate between the neural tube and the dermomyotome forming glia and neurons of the sympathetic and parasympathetic ganglia and chromaffin cells; subsequently, TNC emigrate through the dorso-lateral pathway, migrating over the dermomyotome to invade the dermis and form the pigments and connective tissues of the skin (Figure 3A; (Bronner and Simões-Costa, 2016; Raible et al., 1992)). Interestingly, it has been shown that the regulative interactions between TNC are important for the formation of TNC derivatives suggesting that interaction among NC can play a role in migration (Raible and Eisen, 1996).

Trunk Neural Crest (TNC) migrate into the ventro-medial pathway, from the dorsal most region of the neural tube, termed the premigratory area, forming single cell chains. Experiments using high resolution fluorescent time-lapse imaging have demonstrated the presence of different cell identities within the TNC population (Figure 3C), namely Leaders, Followers and Pre-migratory (PM) cells. A single Leader cell initiates the migration of each chain from the premigratory area, tracked by follower cells that form the body of the chain (Figure 3B). Leader cells remain at the front of the chain throughout migration and are the only cells capable of instructing directional movement. Followers on the other hand, actively reshuffle and lack directed movement in the absence of a leader. Highly dynamic cell-cell contacts between all the cells in the chain are necessary for movement and are maintained throughout migration (Richardson et al., 2016).

In a bid to reveal more about trunk NC, a laser ablation study conducted by our lab demonstrated the differences between cranial and trunk NC, as well as the variations between sub-populations of the migrating TNC cells. In zebrafish, ablation of the CNC leading cells does not affect the migration, as the cells further behind in the group can replace the ablated

population and continue migrating without delay. These findings are mirrored by experiments in chick, showing that the CNC are formed by a homogeneous group in which all cells can adopt the leading position. In the trunk region, however, the situation is radically different. Further experiments showed that leader and follower cells represent distinct identities and fulfil specific roles during migration. First, leader and follower cells exhibit different morphologies, with the former presenting more elongated phenotypes (Figure 3E and F) and larger cell volumes (Figure 3D). It has also been observed that such differences arise before the initiation of migration, suggesting that leader and follower identities are established prior to migration initiation, and not acquired as a consequence of movement. Furthermore, ablation experiments show that leader and follower identities are permanent and are not interchangeable during migration. Upon leader laser ablation, the follower cell immediately behind protrudes into the empty space but is unable to migrate beyond this point. Likewise, follower cells further back in the chain continue to be motile and can advance to the site of ablation but are unable to move beyond this point, generating an accumulation of cells at the site of ablation. After leader ablation, migration is resumed only when a new cell arising from the PM-pool rapidly moves to the front of the group and assumes the leader's role. Interestingly, it was shown that PM cells that rescue migration upon leaders' ablations present morphological characteristics of leaders, being larger that neighbouring cells before the initiation of movement (Richardson et al., 2016).

Differences in morphology and the inability to interchange roles during migration, clearly show that leader and follower identities are set prior to migration initiation, when both populations are part of the PM pool. These results leave open the question of what are the molecular and cellular mechanisms regulating TNC migration and leaders/follower identities allocation.

Figure 3

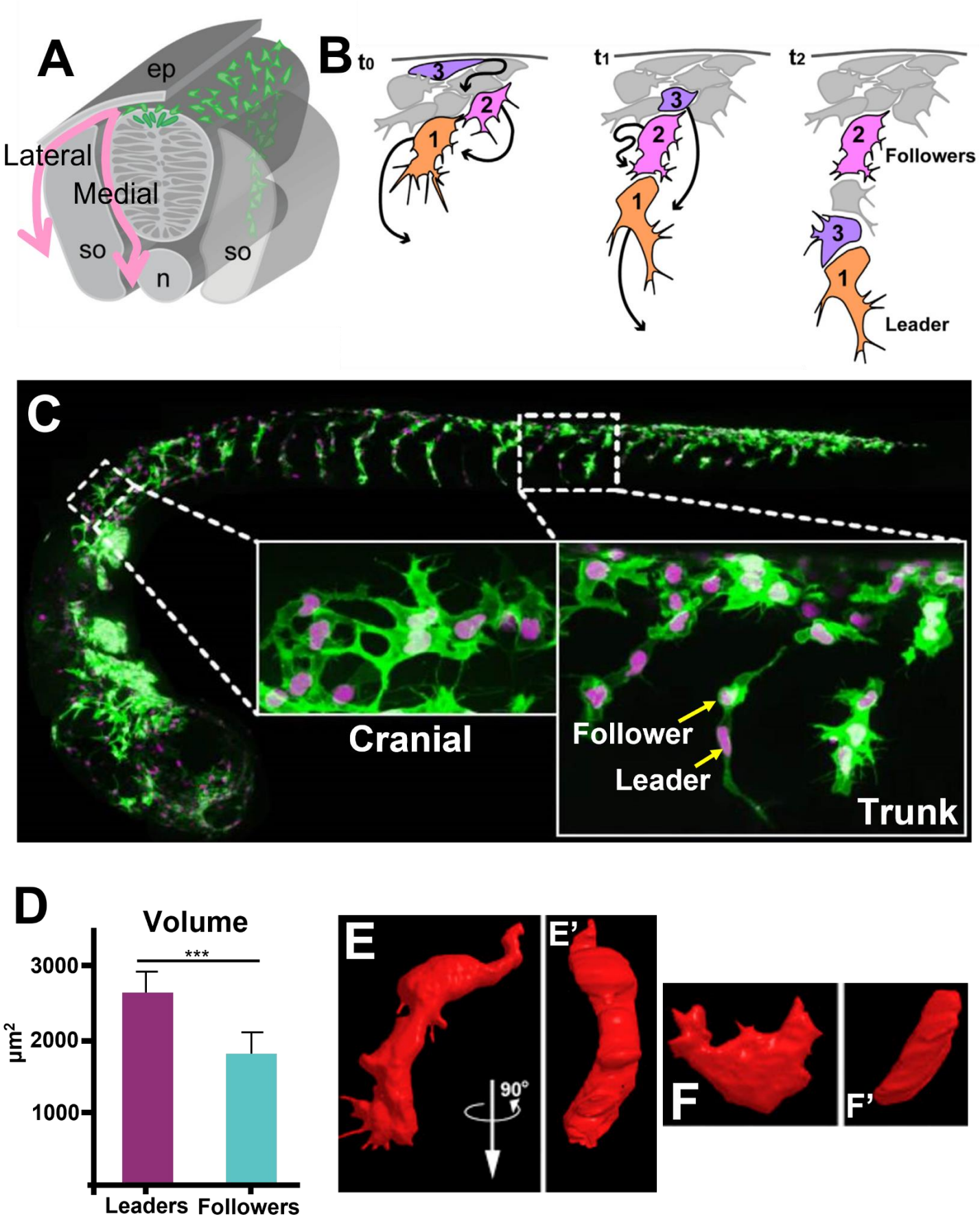
A
ep
Lateral
Medial
so
so
n
B
t0
t1
t2
3
2
1
Followers
Leader
C
Cranial
Follower
Leader
Trunk
D
Volume
***
3000
2000
1000
µm²
Leaders
Followers
E
E'
90°
F
F'

Figure 3: Trunk NC migration in zebrafish.

(A) Illustration of TNC medial pathway between the somites and the neural tube and lateral migratory pathway between the epidermis and somites; adapted from (Rocha et al., 2020). So: somites, n: notochord, ep: epidermis, TNC in green.

(B) Schematic summary of TNC migration, leaders guide the trailing followers in single cell chains between the somites and neural tube. Leaders in orange; followers in purple, pink or grey.

(C) Confocal image of a whole Sox10:mG embryo at 24hpf; insets show enlargement of the cranial and trunk NC. Nuclei in magenta and membranes in green, anterior to the left.

(D) Cell volume of leaders and followers TNC measured during migration.

(E) 3D rendering of a leader TNC showing leader's larger volume and elongated morphology. **(E')** a 90 degrees rotation of E.

(F) 3D rendering of a follower TNC. **(F')** a 90 degrees rotation of F. Adapted from (Richardson et al., 2016).

Aims

This work aims to investigate the following questions:

1. Do leaders and followers arise from a common progenitor?
2. Do leaders and followers exhibit different cell cycle dynamics?
3. What signalling pathways distinguish leaders from followers?
4. Are there interactions between these signalling pathways?
5. What is the mode of leaders and followers divisions? Symmetric or asymmetric?
6. Do leaders and followers give rise to different derivatives?

Chapter 1: Introduction

The cell cycle

Leader cells are remarkably larger than followers and this difference in size appears to be a determinant of their identity, as PM-rescuer cells show similar large volumes to leaders following leaders ablation (Richardson et al., 2016). Thus we performed a literature search of processes that regulate cell size. Interestingly, cell volume can change as cells progress through the cell cycle (Zatulovskiy and Skotheim, 2020), and thus differences in cell cycle between leaders and followers are an interesting avenue to explore.

The cell cycle is an ordered set of events, resulting in cell growth, duplication of DNA and division into two daughter cells (Fig 4). The cell cycle is divided into interphase, mitosis and cytokinesis. Interphase is the longest phase of the cell cycle consisting of G_0 (quiescent) phase, G_1 (growth) phase, S (DNA duplication) and G2 (second growth) phases. Each phase of the cell cycle has to be timely regulated, where G_1 and S-phases are reported to be the longest, while mitosis and cytokinesis take the shortest times in the cell cycle (Vermeulen et al., 2003). Cell cycle is driven by Cyclins and Cyclin dependant kinases (CDKs) which oscillate throughout the cycle, controlling its progression (Figure 4). Each cyclin has a CDK partner, which is activated upon binding. Active CDKs can phosphorylate different cellular targets and trigger progression through the cell cycle (Lim and Kaldis, 2013).

Mitogens and proliferation stimuli instruct cells to enter the cell cycle by inducing a cascade of intracellular events that result in the production of G_1 cyclins-CDKs complexes, such as Cyclins D/E and CDK4/6, which activity lead to the phosphorylation and inactivation of the retinoblastoma protein (Rb) and the release of and activation of the E2F transcription factor. Active E2F drives the expression of Cyclin E/A and CDK2, which together induce the entry into S-phase by activating the transcription of genes required for DNA replication (Lodish et al., 2000). Several checkpoints exist in the cell cycle to ensure faithful cell

division, of the most important are the restriction checkpoint in G_1 phase, which delays or halts the cell cycle in G_1 in response to DNA damage or any cell defects ; second, the DNA replication checkpoint that operates during S-phase and ensures the fidelity of DNA replication before allowing progression into G2. Cellular stress or defects lead to the activation of these checkpoints resulting in either cell cycle delay, exit or apoptosis (Barnum and O'Connell, 2014). Entry into the G2 phase, after DNA synthesis during the S-phase, is regulated by cyclin A and CDK1 and 2 complexes. During G2, cells undergo a second round of growth that abuts in division. Transition from G2 to the M phase is regulated by the expression of Cyclin B and CDK1. Any growth or DNA replication aberrations prior to this transition will activate the Wee1 kinase family, which in turn phosphorylates and inactivate CDK1 ensuring that cells do not undergo mitosis (Perry and Kornbluth, 2007).

Figure 4

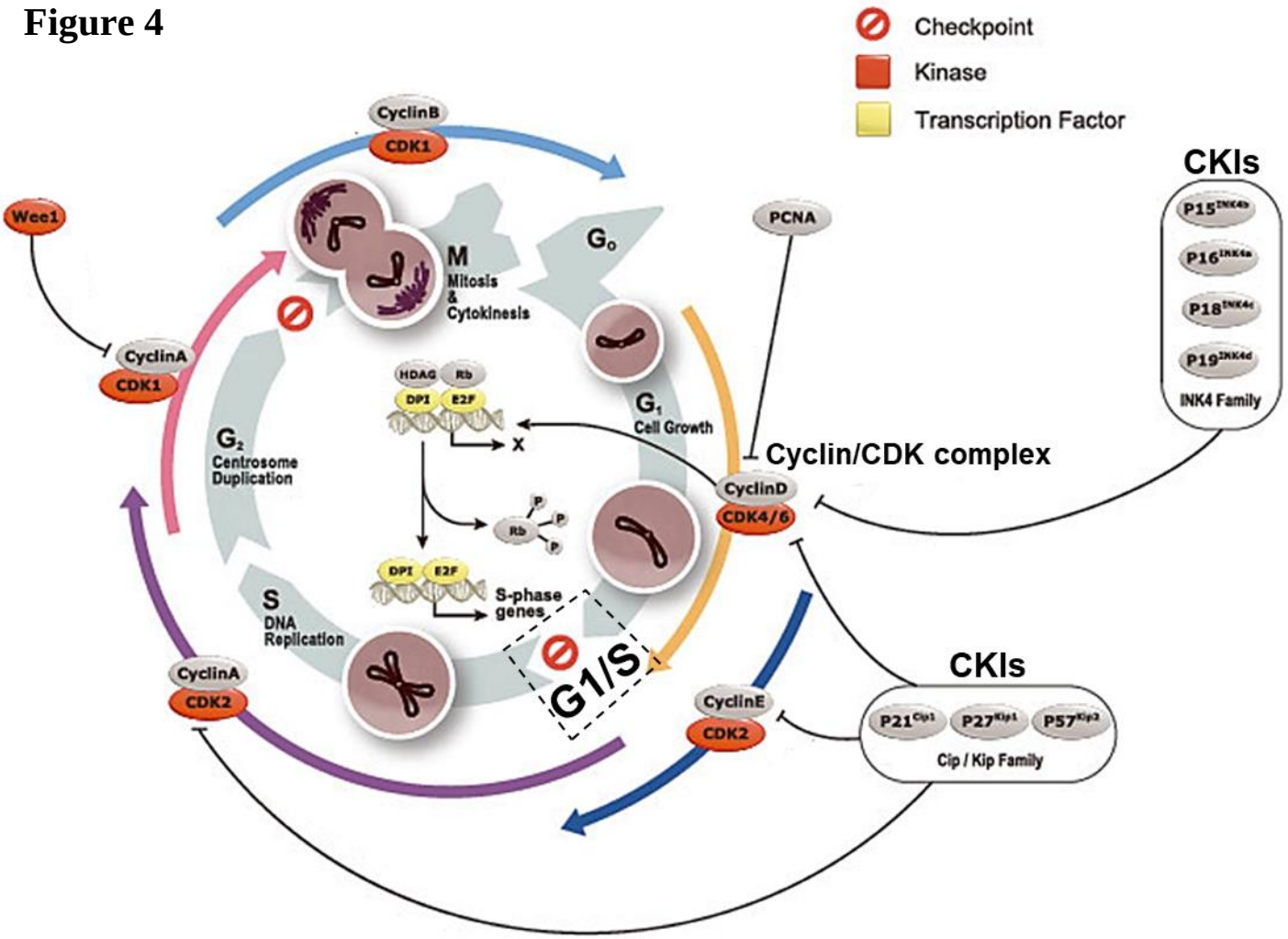

Figure 4: The cell cycle.

Schematic showing the drivers and inhibitors of each cell cycle phase. CyclinD/CDK4/6 complex drives progression through G_1-phase by phosphorylating different targets such as RB freeing the transcription factor E2F, which binds ro DP1 and drives the expression of proteins necessary for G_1/S transition. CyclinE/CDK2 and CyclinA/CDK2 complexes drive progression through S-phase, followed by CyclinA/CDK1 and CyclinB/CDK1 driving the progression through G_2- and M-phases. Several checkpoints exist to ensure correct progression through the cell cycle. Also, CKIs such as Ink4 (P15, P16, P18, P19) and Cip/Kip (P21, P27, P57) families act as inhibitors of cell cycle progression. PCNA, Ink4 and Cip/Kip CKIs inhibit G1 cyclin/CDk complex, Cip Kip CKIs inhibt G1/S transition and S phase cyclin/CDK complex, while Wee1 inhibit G2 cyclin/CDK complex.

Black dotted box indicate G_1/S transition; CDK: Cyclin dependant kinase, CKIs: Cyclin-dependant kinase inhibitors, RB: Retinoblastoma protein. Adapted from ('Cell Cycle | GeneTex', n.d.)

Cell cycle regulation of fate determination

One possible mechanism of cell cycle regulation of fate acquisition is that cell differentiation can be determined by a cell cycle clock, in which fate acquisition depends on cell cycle progression via a mechanism that counts cell divisions. Alternatively, a cell might adapt a specific fate as a function of its age and on the cell cycle phase the cell is in (Fichelson et al., 2005), somatic cells utilise telomeres length to count cell divisions and age, where telomeres shorten with each round of division until it reaches a critical length triggering cell senescence (Herbig et al., 2006).

The cell cycle has been shown to regulate cell fate determination in *Drosophila* in lineages arising from the Neuroblasts (NB) and sensory organ precursors (SOP). NB undergo asymmetric cell division giving rise to another NB cell and a ganglion mother cell (GMC), which upon division give rise to two neurons. It has been shown that NB and GMC cells are devoid of G_1 phase due to the high expression of S-phase promoting factors, such as Cyclin E, and the absence of its inhibitor Dacapo. In consequence, these cells follow a shorter cell cycle pattern comprised of S-G2-M, and fate determination takes place during either the S or the G2 phases (Cui and Doe, 1995). Similarly, in the bristle lineage, SOP cells undergo a series of divisions that give rise to precursor cells, which in turn result in five terminally differentiated cells (Hartenstein and Posakony, 1989). It has been observed that some precursor cells lack the G_1, while others have a very short G_1 phase. On the other hand, terminal cells withdraw from the cell cycle after their final mitosis, undergoing G_1 phase arrest due to the expression of the cyclin-dependant kinase inhibitor Dacapo, which prevents cells from entering S-phase. Therefore, precursor cells become determined during the G_2 phase similar to NB, GMC and SOP cells, while terminal cells such as the socket and hair cells acquire fate in G_1 phase (Nooij et al., 1996) (de Nooij et al., 1996). Moreover, fate determination can be attained through the regulation of Notch signalling by the cell cycle machinery. Notch activity can be

enhanced during G_1/S transition through the stabilization of NICD and cells can become refractory to this signalling during G2/M by active degradation of NICD (V Ambros, 1999; Nusser-Stein et al., 2012). This mechanism limits the time window of Notch activity and coordinates cell cycle progression with fate specification (Hunter et al., 2016). Taken together, cell cycle plays an important role in fate determination in many systems, and thus it provides a plausible mechanism worth investigating in the context of the regulation of migratory identity acquisition in TNC.

Cell cycle regulation of migration

Cell cycle progression and cell migration are two fundamental cellular processes that operate throughout development; hence it is important to understand the crosstalk and reciprocal regulation between these processes. Experiments in chick demonstrated that cell cycle progression through G1/S transition is essential for NC delamination. Using chemical cell cycle inhibitors, Burstyn-Cohen and co-authors found that arresting cells in G_1 resulted in in NC delamination and migration defects, while arresting cell cycle at other phases had no effect on NC migration (Burstyn-Cohen and Kalcheim, 2002). A subsequent study by the same group showed that NC emigrate in S-phase of the cell cycle (Burstyn-Cohen et al., 2004), which is in contrast to a later study that suggested NC emigrate at random points in the cell cycle (Ridenour et al., 2014). In vitro studies using cancer cells showed that arresting cell cycle can have an anti-metastatic effect, where cancer cells fail to migrate and invade other tissues (Shapiro and Harper, 1999). Moreover, the rapid progression through the cell cycle ensures efficient migration of zebrafish primordial germ cells, whereas cell cycle defects result in ineffective arrival at the migration target (Pfeiffer et al., 2018). Also, Cell migration and cell cycle progression are temporally coordinated in keratinocyte sheets, where Rac1 promotes both cell migration and cell cycle progression (Hirata et al., 2020). It has been shown that the essential G_1-cyclin D1 is sufficient to drive G1/S transition and induces cell

migration in fibroblasts (Chen et al., 2020). On the other hand, evidence exist that cancer cells invasion through the basement membrane requires cell cycle arrest to switch cells from a proliferative to an invasive state (Kohrman and Matus, 2017). Hence, the relationship between cell cycle progression and acquisition of migratory behaviours, while extremely important, remains unclear.

Chapter 1: Results
Cell cycle regulation of TNC migration

TNC leader and follower identities are established before migration initiation and one of the first characteristics that distinguishes these cells is their difference in size. As mentioned, cell cycle progression regulates cell growth and can have an impact on cell fate determination and migratory behaviours. Hence, we investigated at which point in development leader and follower differences are first established, do these cells show differences in their cell cycle patterns and whether cell cycle progression plays any role in the migratory behaviours.

1.1 Leaders arise from asymmetric divisions, while symmetric divisions give rise to followers

TNC migrate collectively as single file cell chains with a leader cell at the front that directs the movement of the group, and three to five follower cells that trail the leader. We first set to analyse at which point leader and follower cells become different. To this end, we investigated whether leader and follower cells arise from the same or from distinct progenitor pools. Three scenarios were possible, a progenitor cell gives rise to i) a leader and a non-NC cell; ii) two leader cells that migrate at contralateral sides of the embryo; or iii) one leader and one follower cell that populate the same migratory chain. To investigate these possibilities, we retrospectively tracked leader and follower cells to the division that gives rise to them. To this end, we performed live imaging of FoxD3:mCherry; H2AFVA:H2A-GFP embryos. The FoxD3:mCherry transgene labels all NC by the expression of cytoplasmic red fluorescent protein allowing to identify all NC cells from an early developmental stage (Lukoseviciute et al., 2018). On the other hand, the H2AFVA:H2A-GFP transgene (Pauls et al., 2001) drives expression of nuclear GFP in all cells of the embryo, permitting to track every cell nuclei and its divisions. This combined labelling allowed to retrospectively track leader and follower cells, defined by their migratory position in the chain, to their point of birth in the premigratory area. Our data show that a large number of TNC divide before migration initiation, between 12 and

16 hours post fertilization (hpf) at the level of somites 6-10. Interestingly, we found that a single progenitor cell per segment gives rise to a leader and a follower cell (Figure 8A), while all other progenitors give rise to two follower cells (Figure 8C). Moreover, we found that the leaders' progenitors are spatially restricted only dividing at the anterior most quarter of the premigratory region in all segments (Figure 8F), while followers' progenitors divisions do not show spatial restriction. Interestingly, measurement of cell area showed that the leader's progenitor divides asymmetrically giving rise to one big daughter (102 ± 20 μm^2 mean ± SD; Supplementary movie S1) that becomes the leader cell, and a smaller sibling fated to be a follower (72 ± 9 μm^2; Figure 8B, 8E), on the other hand, followers' progenitors divisions are symmetric, giving rise to two siblings of similar size (averaged 87 ± 27 μm^2; Figure 8D, 8E).

These data show that differences in size between leader and follower cells arise at birth by the asymmetric division of a single progenitor cell in each segment.

1.2 Sibling cells do not maintain coherence during migration

Next, we analysed whether sibling cells maintain contact and undergo coherent movement during TNC migration. After the asymmetrical division of the leader's progenitor, the bigger sibling quickly extends protrusions and emigrates from the premigratory area within 3.5 ± 1.8 hours becoming the leader cell (Figure 8A). On the other hand, the smaller sibling remains motile in the premigratory area, only joining the migratory chain later in development as a follower. Interestingly, after the symmetric division of a follower's progenitor a similar pattern is observed, siblings join the migratory chain at different times and do not maintain contact during migration.

These data show that sibling cells do not retain contact, nor maintain coherence during TNC migration.

Figure 8

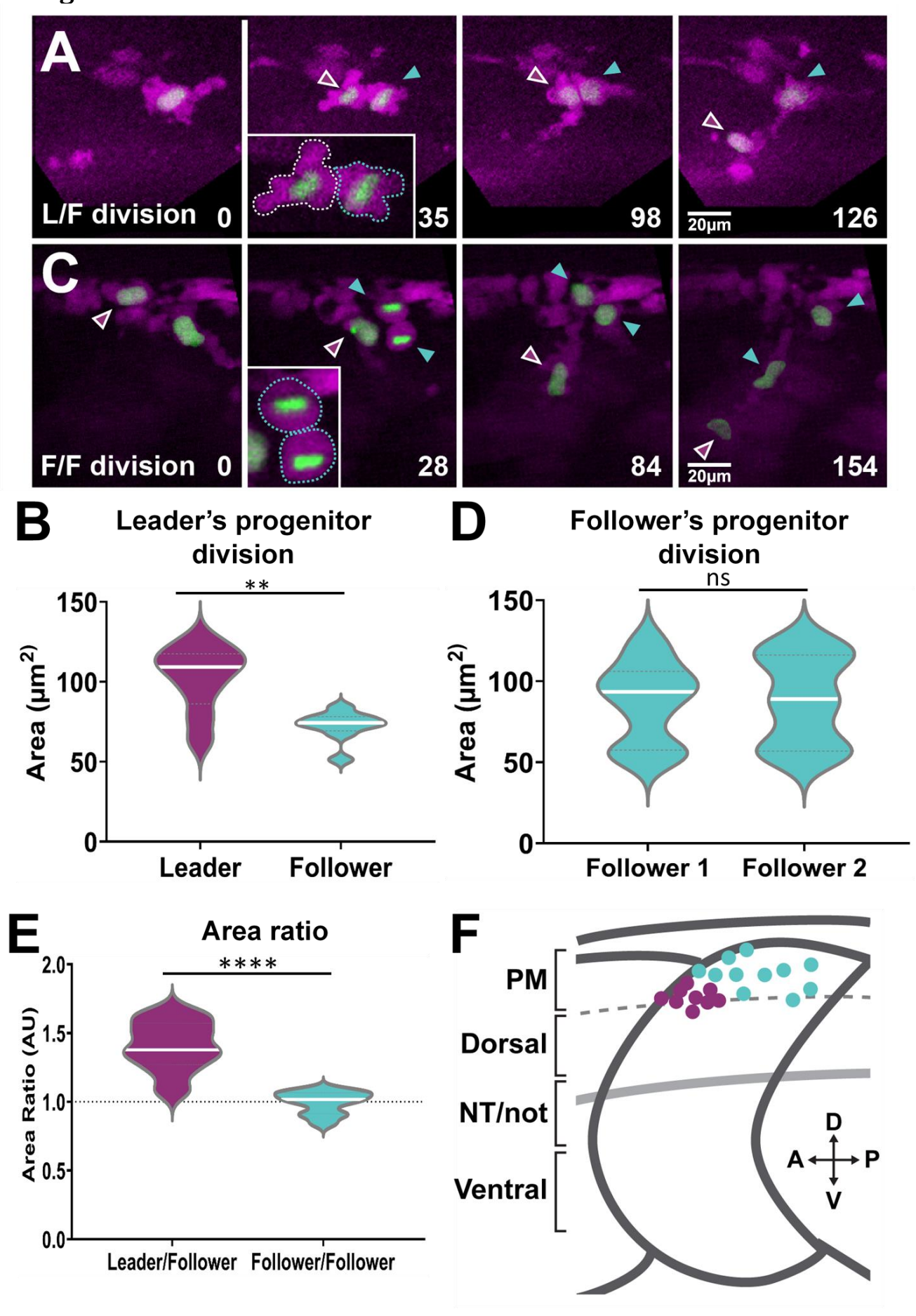
A
L/F division 0
35
98
20μm
126
C
F/F division 0
28
84
20μm
154
B
Leader's progenitor division
**
Area (μm2)
150
100
50
0
Leader
Follower
D
Follower's progenitor division
ns
Area (μm2)
150
100
50
0
Follower 1
Follower 2
E
Area ratio
****
Area Ratio (AU)
2.0
1.5
1.0
0.5
0.0
Leader/Follower
Follower/Follower
F
PM
Dorsal
NT/not
Ventral
D
A
P
V

Figure 8: Leaders' progenitor divides asymmetrically.

(A) Selected frames from in vivo time-lapse of leaders' progenitor division.

(B) Quantification of leaders' progenitor daughter cells area immediately after division (n= 9 divisions in 7 embryos; Mann-Whitney U test, p=0.0056).

(C) Selected frames of followers' progenitor division.

(D) Quantification of followers' progenitor daughter cells area immediately after division (n= 10 divisions in 4 embryos; Mann-Whitney U test, p>0.9999).

(E) Quantification of the area ratio of sibling cells after division.

Leaders' progenitor division give rise to leader and follower cells. Followers' progenitor to two followers(Mann-Whitney test, p<0.0001).

(F) Progenitors' cells position of division on a model embryo schematic (lateral view) PM: premigratory area; NT/not: neural tube/notochord boundary; A: anterior; P: posterior; D: dorsal and V: ventral region of the somite.

White line in graphs indicates the median. Time in minutes. Purple shows leader and turquoise follower cells.

1.3 Leader and follower cells present characteristic division patterns

Our data show that leader and follower cells present different sizes at birth and initiate migration at different times after birth. Moreover, previously we have shown that these size differences remain and are amplified during migration (Richardson et al., 2016). Since cell cycle plays an important role in the regulation of cell size, these results led us to hypothesise that leader and follower cells may differ in their cell cycle progression. First, we analysed whether leader and follower cells differ in the time and/or position of division before and during migration (referred to as division pattern thereafter). To this end, we performed live imaging of Sox10:mG embryos (Richardson et al., 2016), where the NC promotor Sox10 drives expression of nuclear RFP (H2B-mCherry) and membrane GFP. This double labelling allows to clearly establish when and where mitosis takes place. We found that 64% of premigratory cells have initiated migration by 24hpf. Within this population, two patterns of divisions where distinguishable: i) D>M, cells that Divide in the premigratory area and then Migrate (Figure

9A); or ii) M>D, cells that first initiate Migration and then Divide (Figure 9B; Supplementary movie S2). Interestingly, the vast majority of cells (90%) divide before migration initiation, and only 10% of cells divide along the migratory path.

Next, we asked whether the different division patterns observed correlate with the migratory identity of the cells. Interestingly, the majority of cells that divide before migration initiation exhibit a follower identity (90%), while cells that divide along their migratory path exhibit a leader identity (86%; Figure 9C). These data suggest that leader and follower cells may progress through the cycle at different rates, if this is the case, leader cells may all undergo division at specific axial positions in the migratory path, as they would present similar cell cycle progression rate to each other. To this end, we measured the ventral distance at which TNC mitotic figures are observed. On average, leader cells divide at 65.3 ± 9.6 μm from the dorsal margin of the embryo, within the neural tube/notochord boundary (NT/not); while follower cells divide at 42 ± 12.4 μm on average, with 73% of follower cells dividing in the premigratory area and 17% in the dorsal most region of the somite, and only 10% of follower cells divide at the NT/not boundary (Figure 9D and E).

Taken together these data show that leader and follower cells undergo characteristic patterns of division during migration. Leader cells initiate migration and only divide after crossing the neural tube/notochord boundary. In contrast, most followers divide in the premigratory area before migration initiation, or in the dorsal most region of the somite.

Figure 9

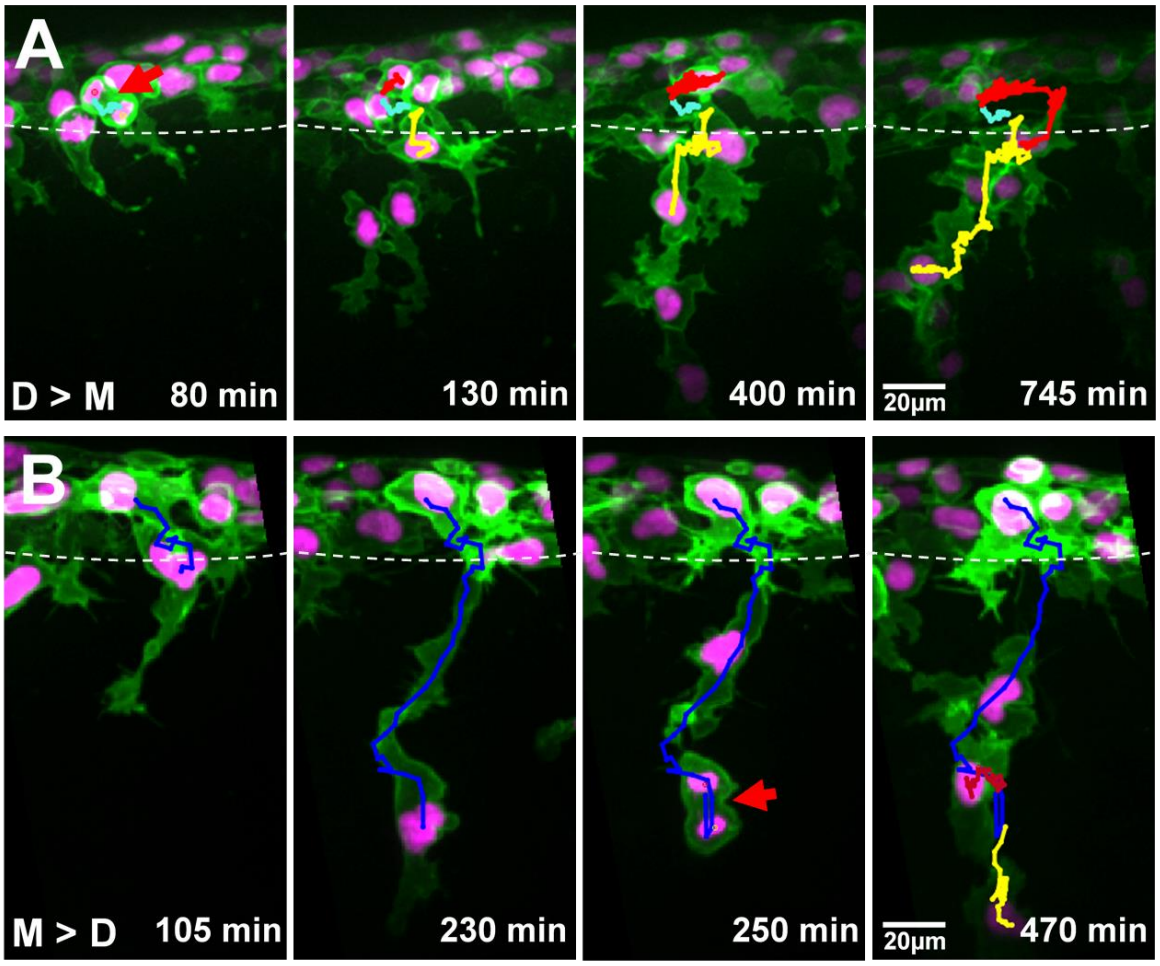
A
D > M
80 min
130 min
400 min
20μm
745 min
B
M > D
105 min
230 min
250 min
20μm
470 min

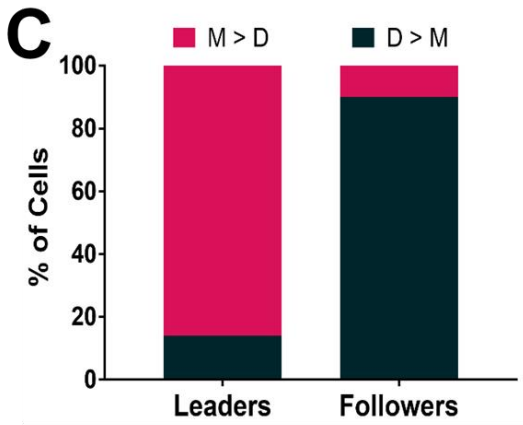
C
M > D
D > M
% of Cells
100
80
60
40
20
0
Leaders
Followers

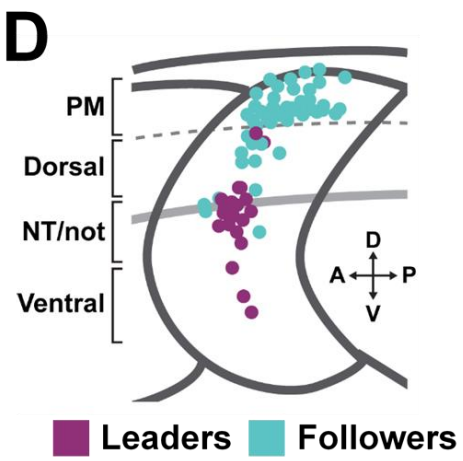
D
PM
Dorsal
NT/not
Ventral
D
A
P
V
Leaders
Followers

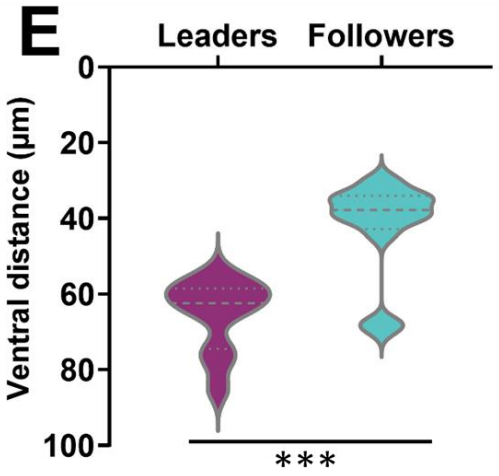
E
Leaders
Followers
Ventral distance (μm)
0
20
40
60
80
100
***

Figure 9: Division patterns of leader and follower cells.

(A) D>M pattern where a TNC divides before migration initiation. Selected frames from in vivo time-lapse of Sox10:mG embryo imaged from 16hpf to 28hpf showing the tracks of the follower cell before division in cyan and of the daughter cells in yellow and red.

B) M>D pattern where a cell migrates and divides while migrating. Selected frames from in vivo time-lapse of Sox10:mG embryo imaged from 16hpf to 28hpf showing the tracks of the leader cell before division in blue and of the daughter cells in yellow and red.

(C) Quantification of division patterns for leader (n= 21 cells from 7 embryos) and follower cells (n= 43 cells from 7 embryos). Red M>D, black D>M.

(D) Division Positions of leader and follower cells plotted on a model embryo schematic (n number as in C).

(E) Quantification of the ventral distance of the division positions. (n number as in C; Mann-Whitney U test, p=0.0002).

White dotted line indicates the edge of premigratory area, leaders in purple and followers in turquoise.

1.4 Leaders and followers TNC initiate migration at different phases of the cell cycle

Our previous data indicate that TNC division patterns correlate with their migratory identity and suggest that leader and follower cells may progress through the cell cycle at different rates. Next, we sought to fully characterise TNC cell cycle progression, defining the total duration of the cell cycle for each cell type and at which phase of the cell cycle migration is initiated. From the division patterns described we can make several predictions: i) cells with the same migratory identity present similar cell cycle durations; ii) leaders, which divide at the neural tube/notochord boundary initiate migration halfway through the cell cycle either at late G_1 or at S-phase; iii) followers on the other hand that divide in the premigratory area are likely to initiate migration during G_1.

First, we utilised immunohistochemistry of antibodies that label different phases of the cell cycle to define the phase at which leaders and followers initiate migration. Sox10:H2B-

mCherry-Kalt4 embryos were stained with Cyclin D1 to mark G1 phase, or PCNA PC10 antibodies to mark S-phase at different times of development (16, 20 and 24hpf; Figure 10). Although, we did obtain some staining of Cyclin D1 (Figure 10A-C) and PCNA (Figure 10D-F) in NC, the staining was inconsistent and whereas we expect these antibodies to label most cells in the embryo, we mostly observed staining in NC only, which led us to believe these labelling patterns were artefactual. Following few rounds of optimization, we concluded that these antibodies were not suitable for such analysis.

Subsequently, we decided to directly visualise TNC cell cycle progression in vivo using the cell cycle reporter PCNA-GFP (Leung L. et al., 2011). Embryos of the NC reporter Sox10:H2B-mCherry-Kalt4 were injected with 30 pg/ul PCNA-GFP mRNA at 1-4 cells stage (Figure 11A). The expression of the PCNA-GFP was observed throughout the embryo from 5hpf, while good expression of the TNC nuclear-RFP labelling was observed from 15hpf. Using time-lapse imaging, we observed a dynamic localization of PCNA-GFP through the cell cycle. In G_1, PCNA-GFP is expressed uniformly in the nucleus; in S-phase PCNA-GFP expression increases showing a punctuated pattern, puncta increase in number and fluorescent intensity as cells progress through S-phase; as cells enter G_2, GFP expression decreases and puncta disappear leaving uniform labelling of the nucleus, and expression decreases to minimum levels during M phase before nuclear envelop breakdown (Figure 11B-C; Supplementary movie S3).This pattern makes it possible to track TNC cell cycle progression in real-time. With this tool on hand, we found that leaders and followers initiate migration at different phases of the cell cycle. Interestingly, the majority of leader cells initiate migration in S-phase (77%; Figure 11D and F), while most follower cells emigrate during G_1 (73%; Figure 11E and G; Supplementary movie S4).

Since PCNA is an auxiliary protein that plays a role in DNA replication, it is possible that its overexpression introduced artefacts. Hence, we sought to use a different cell cycle reporter to confirm our findings and rule out this possibility. To this end, we used the FUCCI reporter (Figure 12A), which consist of RFP tagged Cdt1 that is expressed in $G_{1,}$ and GFP tagged Geminin that is highly expressed in S-phase and weakly during G_2 (Figure 12B). Using Light Sheet Microscopy, we generated time-lapse movies of the transgenic line Sox10:FUCCI, in which only NC cells are labelled ((Rajan et al., 2018); Figure 12C and D). Consistent with the PCNA data, we found that in the Sox10:FUCCI transgenic, the majority of leaders initiate migration in S phase (79%; Figure 12E and F), while most followers emigrate in G_1 (77%; Figure 12E and G; Supplementary Movie S5). These results confirm our previous data and show that PCNA overexpression is not altering the cell cycle progression of TNC. Taken together these data show that leaders initiate migration during S-phase, while followers emigrate from the premigratory area while in G_1.

Figure 10

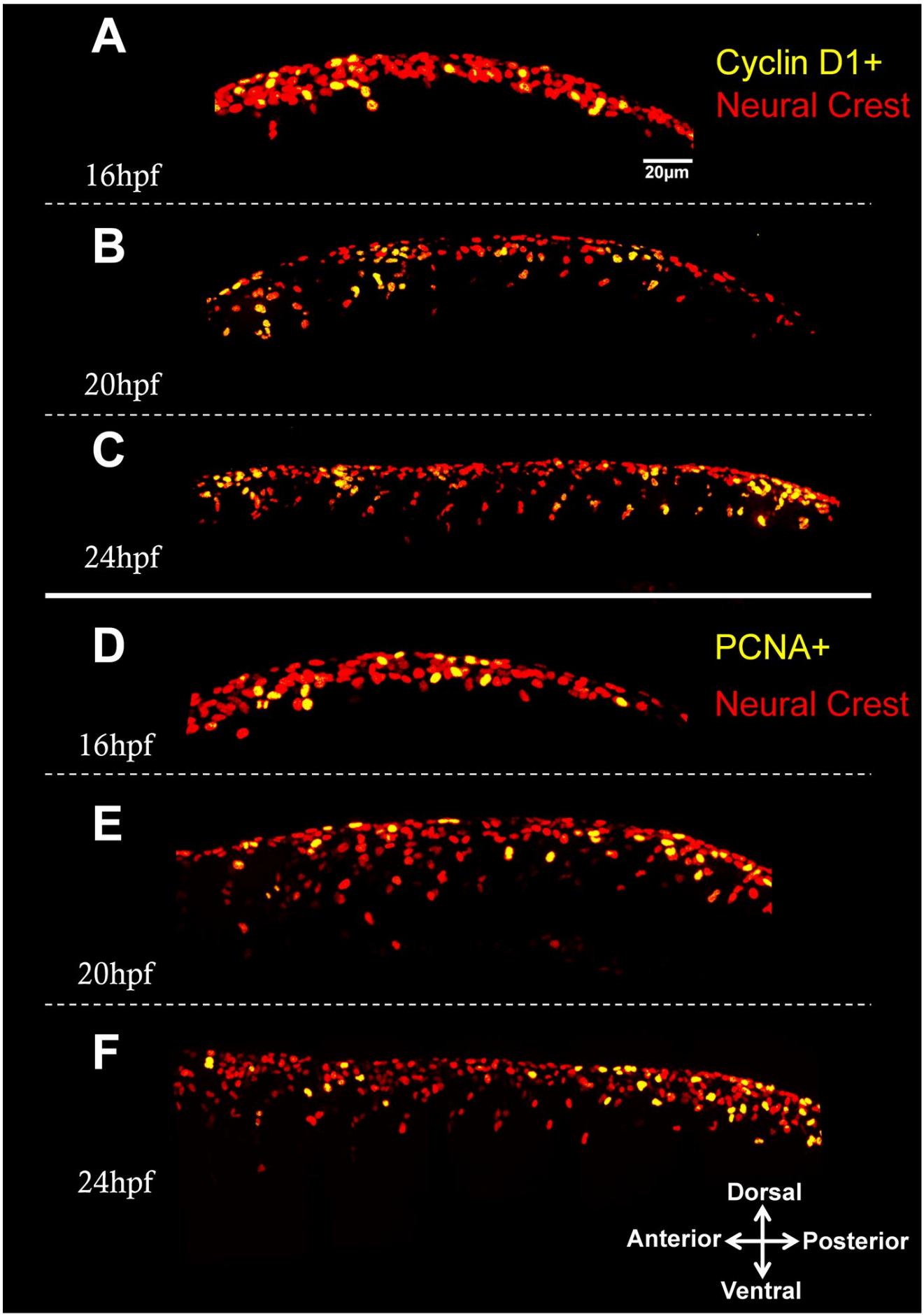
A
Cyclin D1+
Neural Crest
16hpf
20μm
B
20hpf
C
24hpf
D
PCNA+
Neural Crest
16hpf
E
20hpf
F
24hpf
Dorsal
Anterior
Posterior
Ventral

Figure 10: Cell cycle antibodies staining.
(A, B, C) Confocal images of Cyclin D1 antibody staining at **(A)** 16hpf, **(B)** 20hpf and **(C)** 24hpf embryos TNC in red and cyclin D1 in yellow; note that normally cyclin D1 is expressed in all G_1-phase cells of the embryo and not just in TNC as observed.
(D, E, F) Confocal images of PCNA antibody staining at **(D)** 16hpf, **(E)** 20hpf and **(F)** 24hpf ; note that normally PCNA is expressed in all S-phase cells of the embryo and not just in TNC as observed. Images show trunk region, anterior to the left, dorsal up.

1.5 Leaders and followers TNC progress through the cell cycle at different rates

Next, we decided to characterise whether leader and follower cells progress through the cell cycle at similar pace, and to establish whether there are differences in the total cell cycle length. Although, Sox10:FUCCI initially labels NC nicely, its expression diminishes after the first NC division, thus it can only be used to visualise a single cycle. Due to this problem and the fact that we are able to better resolve the different cell cycle phases using PCNA, we only utilised PCNA in all subsequent experiments.

Based on our earlier data, we hypothesised that leaders and followers differ in the total duration of the cell cycle and that this difference may explain their size differences. To this end, we measured the total duration of the cell cycle by measuring the time between two consecutive mitosis in PCNA-GFP injected Sox10:H2b-mCherry-Kalt4 embryos. To our surprise, we found no significant differences in the total span of the cell cycle between leaders and followers (13.6 ± 1.2 and 13.3 ± 1.4 hours respectively; Figure 13A). While the total duration of the cell cycle is similar between leaders and followers, it is possible that the durations of the cell cycle phases differ. Using the PCNA characteristic nuclear staining during the cell cycle phases, we quantified the duration of each phase from live imaging. We found that leader and follower cells show striking differences in the time they spend in G_1 and S-phases. Leaders present a short G_1 (3.2 ± 0.6 hours) and remain more than twice as long in S-phase (8.7 ± 1.3 hours),

while followers present the opposite distribution, remaining for almost twice as long in G_1 (7.4 ± 2.7 hours) than in S-phase (4.6 ± 2.8 hours; Figure 13B). No significant differences were observed in the durations of G_2 (1.6 ± 0.4 hours for leaders; 1.5 ± 0.3 hours for followers) or M phase (0.6 ± 0.1 hours for leaders; 0.5 ± 0.1 hours for followers; Figure 13B). Proportionally, leaders spend 23% of the cell cycle in G_1, 61% in S, 11% in G_2 and 4% in M; while followers spend 53% of the cell cycle in G_1, 33% in S, 11% in G_2 and 4% in M (Figure 13C). These data in turn explain the differences observed in the cell cycle phase at which leader and followers initiate migration. Follower cells divide in the premigratory area and have a long G_1 phase, hence they are more likely to initiate migration at G_1. In contrast, leaders have a longer S-phase and divide as they migrate, thus they are more likely to initiate migration at S-phase.

These data show that whereas G_2 and M phases are similar between leaders and followers, strikingly G_1 and S-phases exhibit an inversely proportional relationship between leader and follower cells, suggesting that cell cycle progression may play an important role in the identity acquisition process and/or the timing of migration initiation of TNC cells.

Figure 11

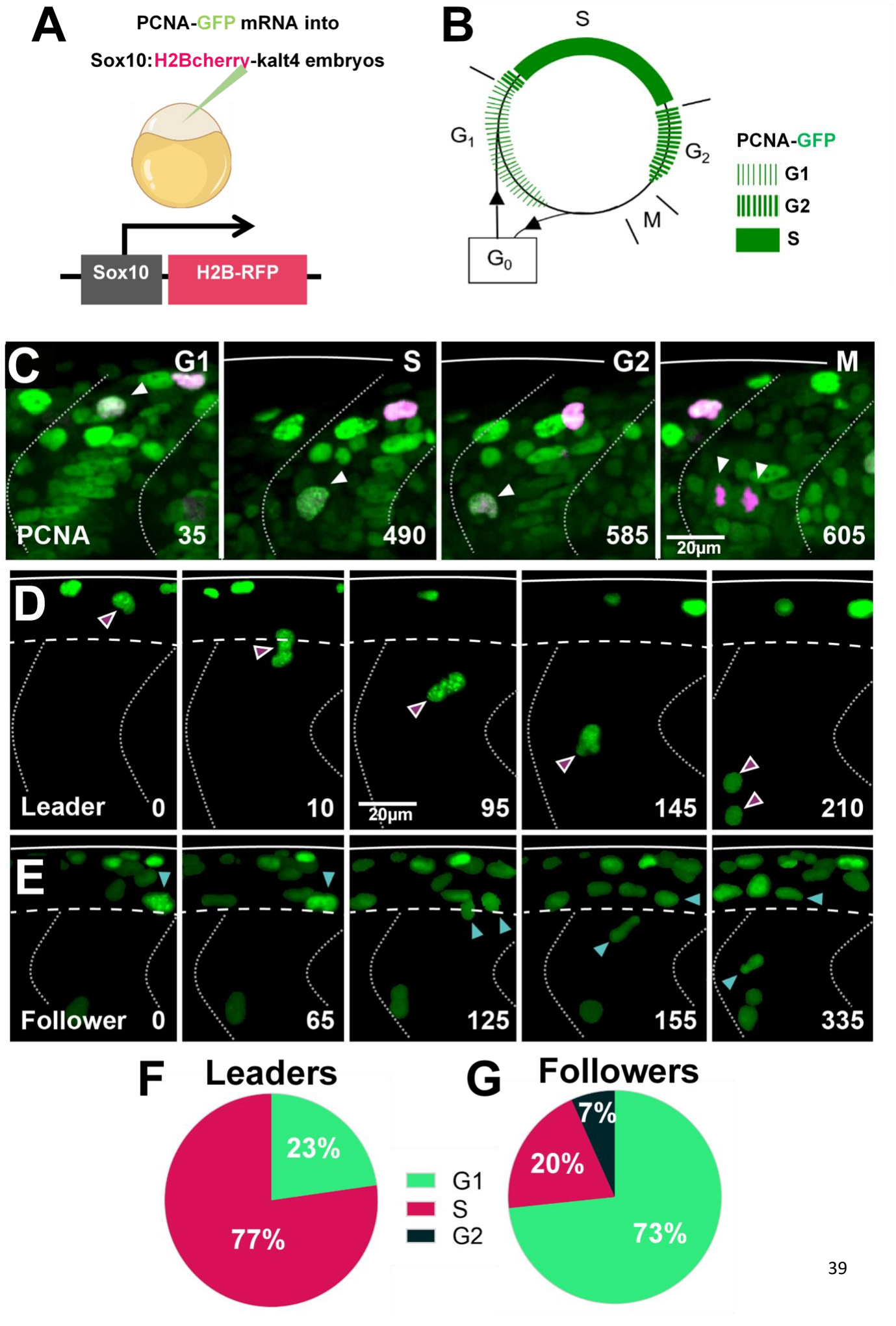
A
PCNA-GFP mRNA into
Sox10:H2Bcherry-kalt4 embryos
Sox10
H2B-RFP
B
S
G1
G2
M
G0
PCNA-GFP
G1
G2
S
C
G1
S
G2
M
PCNA
35
490
585
20μm
605
D
Leader
0
10
20μm
95
145
210
E
Follower
0
65
125
155
335
F
Leaders
23%
77%
G1
S
G2
G
Followers
7%
20%
73%

Figure 11: Leaders and followers initiate migration at different phases of the cell cycle (PCNA-GFP reporter).

(A) Schematic of the experimental procedure, PCNA mRNA was injected into one-cell stage of Sox10:Kalt4 transgenic embryos.

(B) Schematic of the oscillatory expression of PCNA during the cell cycle.

(C) Cyclical localization of PCNA-GFP in TNC. Selected frames from in vivo imaging of Sox10:Kalt4 embryos injected with PCNA-GFP mRNA between 16-28hpf. White arrow points to cycling TNC at the different phases. Note that PCNA-GFP is expressed in NC and non-NC cells.

(D) Leader cell initiates migration during S-phase and divides at the neural tube/notochord border. Selected frames from in vivo imaging of Sox10:Kalt4 embryos injected with PCNA-GFP mRNA, displaying PCNA localization in RFP labelled cells only.

(E) Follower cell divides in the premigratory area and initiates migration in G_1. Selected frames from in vivo imaging of Sox10:Kalt4 embryos injected with PCNA-GFP mRNA, displaying PCNA localization in RFP labelled cells only.

(F) Quantification of the cell cycle phase at the point of migration initiation for leader cells (n=22 cells in 10 embryos).

(G) Quantification of the cell cycle phase at the point of migration initiation for follower cells (n=45 cells in 10 embryos).

Solid lines indicate embryo dorsal border; dotted lines indicate somites borders; segmented line indicates the ventral border of the premigratory area. Time in minutes. Anterior to the left, dorsal up.

Figure 12

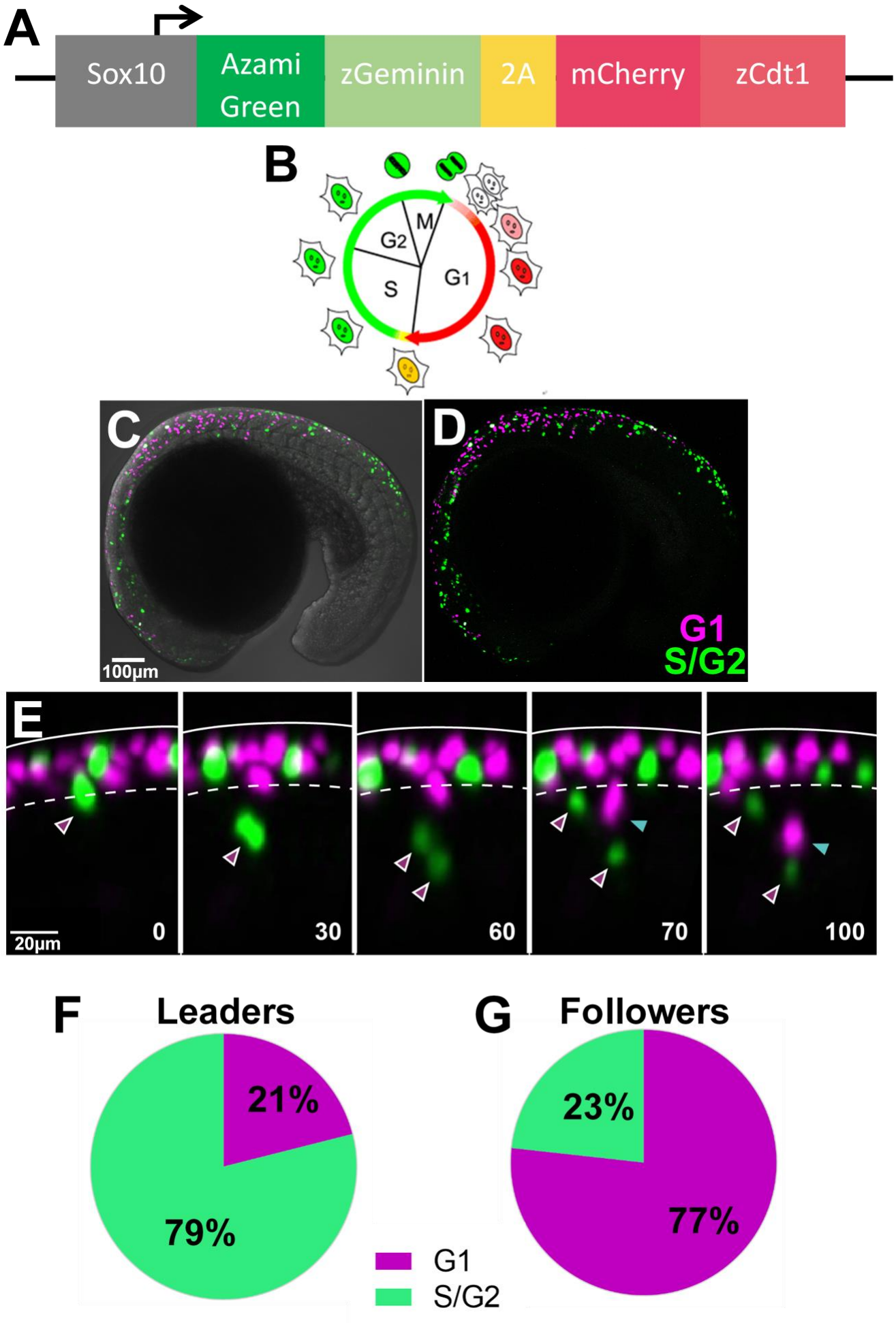
A
Sox10
Azami Green
zGeminin
2A
mCherry
zCdt1
B
M
G2
S
G1
C
100µm
D
G1
S/G2
E
20µm
0
30
60
70
100
F
Leaders
21%
79%
G
Followers
23%
77%
G1
S/G2

Figure 12: Leaders and followers initiate migration at different phases of the cell cycle (Sox10:FUCCI reporter).

(A) Schematic of the Sox10:FUCCI construct.

(B) Schematic of FUCCI expression across the cell cycle, where G_1 is marked with red florescence and S/G_2 are marked with green fluorescence; adapted from (Sakaue-Sawano et al., 2008).

(C-D) Confocal images of 18hpf Sox10:FUCCI embryo showing the cell cycle dynamics of TNC. **(C)** Bright field with fluorescence overlay. **(D)** Fluorescent channels only.

(E) Representative frames from Sox10:FUCCI time-lapse showing leader cell initiating migration in S-phase and subsequent division (purple arrowheads), and follower emigrating in G_1/S phase (turquoise arrowhead). Solid white line indicates the dorsal border of the embryo; dotted white line marks the edge of the premigratory area.

(F) Quantification of the cell cycle phase of migration initiation for leader cells (n=38 in 4 embryos).

(G) Quantification of the cell cycle phase of migration initiation for follower cells (n=43 in 4 embryos).

Figure 13

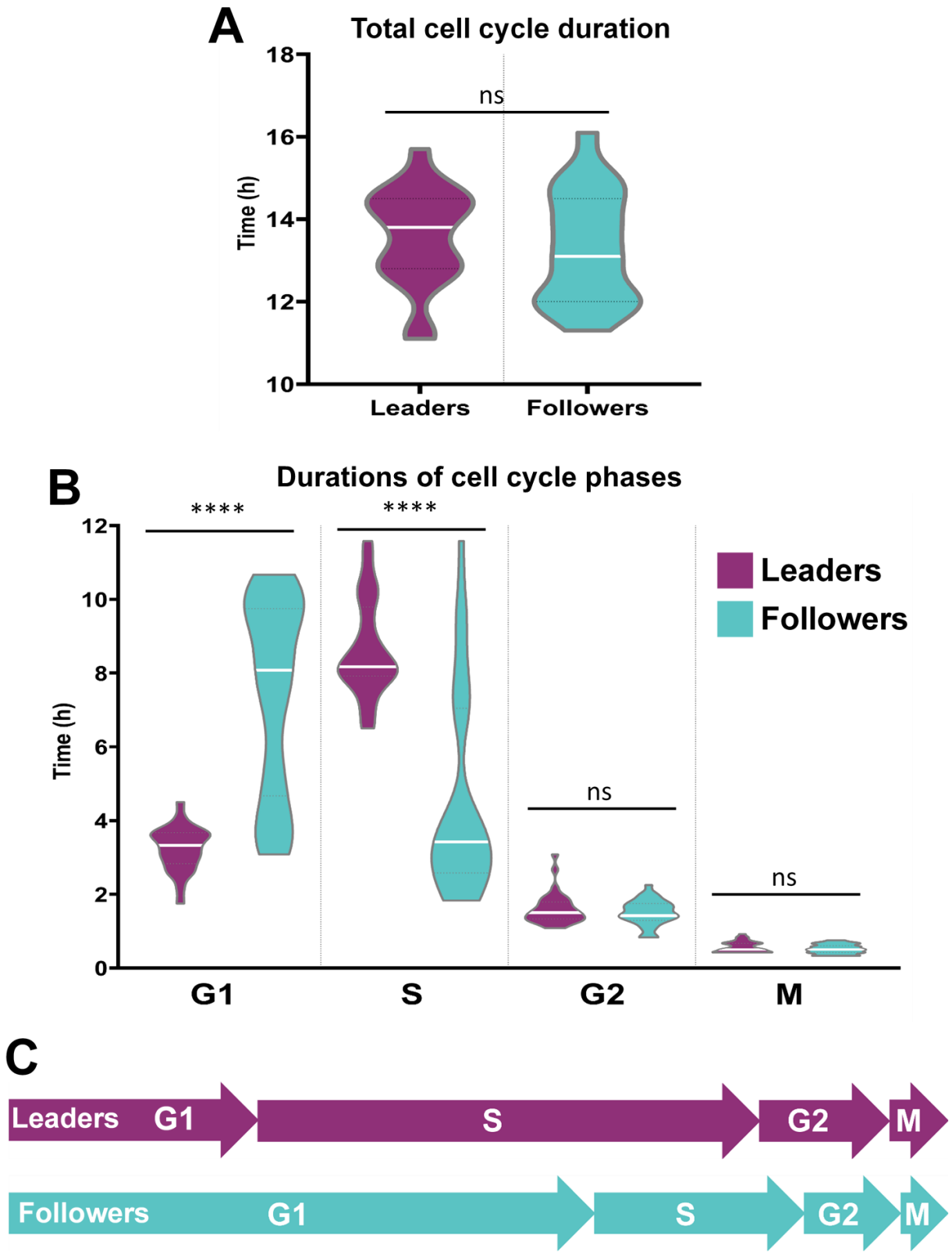
A
Total cell cycle duration
ns
Time (h)
18
16
14
12
10
Leaders
Followers
B
Durations of cell cycle phases
****
****
ns
ns
Time (h)
12
10
8
6
4
2
0
G1
S
G2
M
Leaders
Followers
C
Leaders
G1
S
G2
M
Followers
G1
S
G2
M

Figure 13: Cell cycle phases length in TNC cells.

The total duration of cell cycle is similar between leaders and followers but durations of G_1- and S-phases are inversely proportional.

(A) Quantification of the cell cycle total duration in leader (n=20 cells in 7 embryos) and follower cells (n=19 in 7 embryos; Unpaired t test, p=0.5240).

(B) Quantification of the cell cycle phases duration in TNC (leader cells G_1 n=25, S n=25, G_2 n=33 and M n=32 in 11 embryos; follower cells G1 n=27, S n=28, G2 n=33 and M n=34 in 11 embryos; Brown-Forsythe and Welch ANOVA tests, G_1 p<0.0001, S p<0.0001, G_2 p=0.9997, M p=0.9231).

(C) Schematic representation of the cell cycle phases durations.

Leaders in purple and followers in turquoise.

1.6 Establishment of a cell cycle arrest protocol in zebrafish embryos

Our previous data show that leader and follower cells initiate migration at different phases and progress through the cell cycle at different rates. Next, we sought to directly test whether progression through the cell cycle is required for TNC migration. First, we established a protocol for cell cycle arrest in zebrafish that: i) would not affect the cell cytoskeleton dynamics, as this would alter cell migration capacities; and that ii) could be timely controlled to arrest cell cycle without affecting early embryonic development including NC induction. We tested two chemical inhibitors of the S-phase, Aphidicolin (Aphi) and Hydroxyurea (HU; (Murphey et al., 2006; Zhang et al., 2008)); as well as two inhibitors of the G_2/M transition, Teniposide and Genistein (Geni; Figure 14A; (Murphey et al., 2006; Burstyn-Cohen and Kalcheim, 2002)). Using the transgenic line H2AFVA:H2A-GFP, in which all the nuclei are labelled with GFP ((Pauls et al., 2001); Figure 14B), we established the working concentration of each inhibitor by quantification of the number of mitotic figures in the neural tube within an area normalised to three somites length, using the length of the embryonic segment (somite) as a standard measurement allowed for normalization and direct comparison between embryos of different sizes. We found that 300µM of Aphi was sufficient to inhibit over 94.7 ± 4.5% of

mitotic figures (Figure 14B and C), while the combination of 300µM Aphi + 20µM HU did not improve the inhibition efficacy (not shown); 100µM of Geni was sufficient to inhibit over 90 ± 10 % of divisions (Figure 14C). On the other hand, Teniposide did not inhibit divisions and had no effect on arresting cell cycle even at high concentrations (Figure 14C), hence was not further used. Next, we established the time-course of action of each inhibitor to determine the optimal duration for each treatment. We found that Aphi reaches its peak activity within three hours of addition (Figure 14D), and combining it with HU had no effect on the timing of action. On the other hand, Geni exerts its maximum activity after six hours of treatment (Figure 14D).

1.7 TNC induction is not affected by cell cycle arrest

Since the cell cycle inhibitors were applied at early time point (11hpf) when NC induction may still be taking place, we sought to rule out the possibility that cell cycle arrest affects NC induction. We directly assessed TNC induction by analysing the expression of the neural crest marker Crestin at 16hpf before migration initiation. We found that the majority (>90%) of treated embryos showed a normal levels and pattern of Crestin expression (Figure 14E and F) and concluded that TNC induction takes place normally under these conditions.

Figure 14

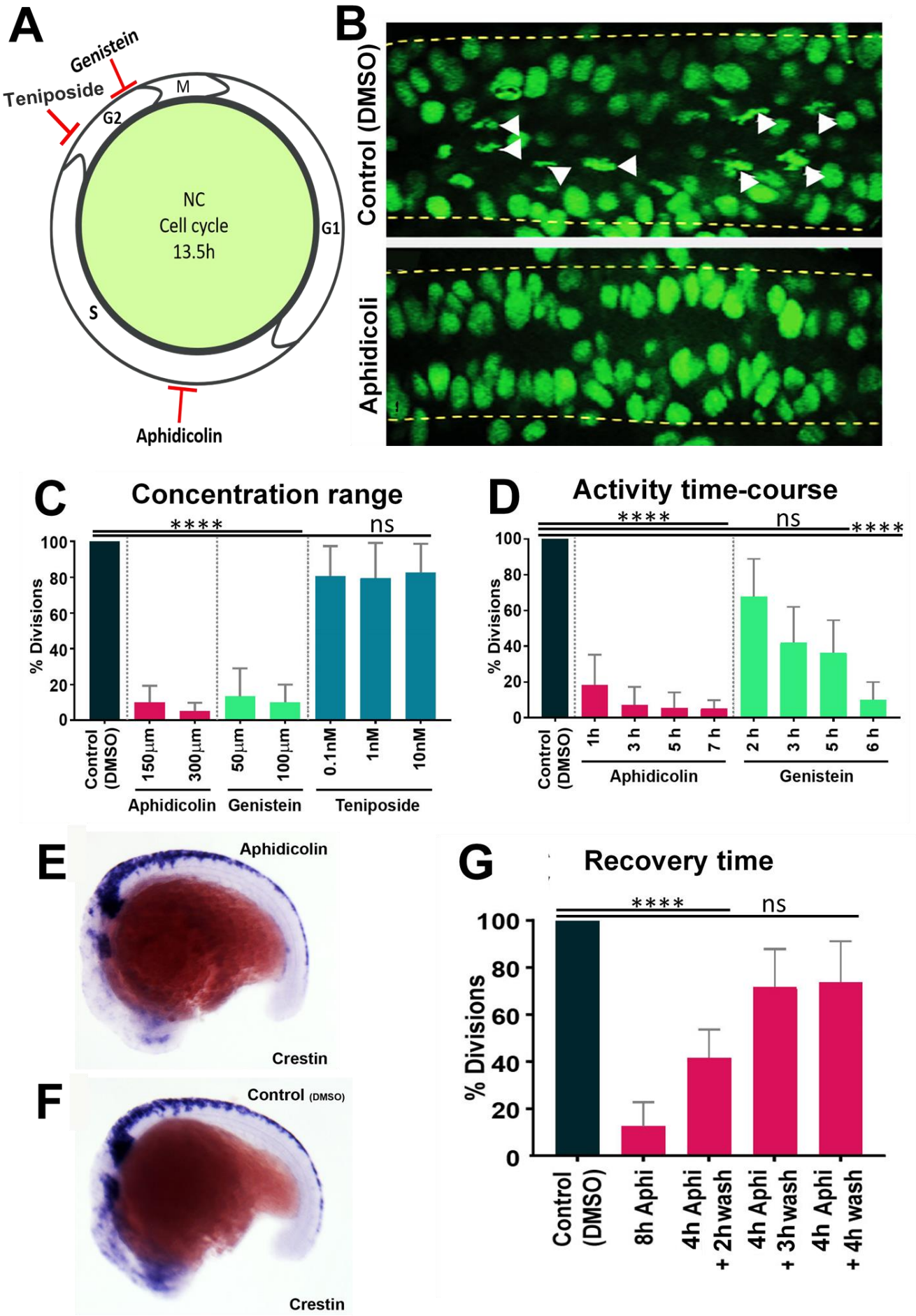
A
Genistein
Teniposide
M
G2
NC
Cell cycle
13.5h
G1
S
Aphidicolin
B
Control (DMSO)
Aphidicoli
C
Concentration range
****
ns
% Divisions
Control (DMSO)
150µm
300µm
50µm
100µm
0.1nM
1nM
10nM
Aphidicolin
Genistein
Teniposide
D
Activity time-course
****
ns
****
% Divisions
Control (DMSO)
1h
3 h
5 h
7 h
2 h
3 h
5 h
6 h
Aphidicolin
Genistein
E
Aphidicolin
Crestin
F
Control (DMSO)
Crestin
G
Recovery time
****
ns
% Divisions
Control (DMSO)
8h Aphi
4h Aphi + 2h wash
4h Aphi + 3h wash
4h Aphi + 4h wash

Figure 14: Aphidicolin and Genistein are potent inhibitors of the cell cycle in zebrafish.
(A) Diagram of aphidicolin, genistein and teniposide effects on the cell cycle.
(B) Confocal images of H2A:H2A-GFP embryo treated with DMSO (control) or aphidicolin. White arrowheads indicate mitotic figures; yellow dashed lines mark the neural tube borders. Dorsal view, anterior to the left.
(C) Quantification of cell cycle inhibitors efficacy. Percentage of dividing cells respect to the control at different drug concentrations (Kruskal-Wallis test, $p<0.0001$ for aphidicolin n=20 embryos and genistein n=32 embryos, teniposide $p>0.9999$ n=27 embryos).
(D) Quantification cell cycle inhibitors time-course of action. Percentage of dividing cells respect to the control at different drug concentrations (Kruskal-Wallis test, Control vs 1h Aphi $p=0.0007$, control vs 3h, 5h and 7h Aphi $p<0.0001$, control vs 2h, 3h and 5h Geni $p>0.0892$, control vs 6h Geni $p<0.0001$; for control n=15 embryos, Aphi n=35 embryos, Geni n=53 embryos).
(E, F) Whole mount in situ hybridisation of the NC marker Crestin in 16hpf upon **(E)** aphidicolin and **(F)** DMSO treatment from 11hpf. Anterior to the left, dorsal top.
(G) Quantification of cell cycle recovery times following aphidicolin removal (Aphi: Aphidicolin; for control n=21 embryos, 8 hours, n=14 embryos, 4+2h wash, 4+3h wash and 4+4h wash n=10 embryos; One-way ANOVA, Control vs 8h and 4+2h wash $p<0.0001$, control vs 4+3h wash and 4+4h wash $p>0.0851$).

1.8 Cell cycle progression is required for TNC migration

With an appropriate cell cycle arrest protocol at hand, we turned to answer the important question of whether cell cycle progression is required for TNC migration. To this end, we quantified the number of migratory chains at 24hpf after 12h treatment with Aphi, Geni, or DMSO as control. Inhibition of cell cycle progression at S-phase by Aphi treatment, resulted in a stark reduction in the number of migratory chains (control: 19 ± 2 chains, Aphi: 6 ± 2 chains; Figure 15A-D and G). Similarly, inhibition of the G_2/M transition by Geni treatment, caused a pronounced reduction in the number of migratory chains (Control: 19 ± 2 chains, Genistein 10 ± 3 chains; Figure 16A-D and G). Noticeably, not only the number of migratory chains formed was reduced upon cell cycle arrest, but the ventral advance of the chains that did form was diminished (Figure 15B and D; Figure 16B and D). Next, we sought to rule out the possibility

that the reduction in the number of migratory chains and ventral displacement was due to lack of cell motility. Time-lapse imaging of Aphi-treated embryos showed that individual TNC are motile and actively extend protrusions in the pre-migratory area but are unable to initiate migration, failing to advance ventrally and form chains. Instead, TNC cells moved abnormally along the anterior-posterior axis in the premigratory region; in contrast, DMSO control embryos migrate ventrally and from chains normally (Figure 15H and I; Supplementary movie S6). These data show that cell motility is not affected by cell cycle arrest, nevertheless cell cycle progression is required for the formation of TNC migratory chains.

It is possible that the applied cell cycle arrest treatments, may simply be affecting TNC permanently or disturbing surrounding cells, in which case the effect observed on migration would not be direct. Hence, we sought to investigate whether the effects on TNC migration upon cell cycle arrest were reversible once the inhibitors are removed. To this end, we first tested the recovery time required to reverse the inhibitors effect. H2AFVA:H2A-GFP transgenic embryos were treated for 4 hours, after which inhibitors were washed and embryos re-incubated and then imaged, at which point mitotic figures were quantified. We found that embryos recover from cell cycle arrest after 3 hours of inhibitors removal (Figure 14G).

After confirming that the inhibitors are reversible, we treated 12hpf embryos with a short pulse of Aphi (3h) or Geni (6h), after which the inhibitors were washed out and embryos incubated until 24hpf. Our data show that upon withdrawal of cell cycle progression inhibition, TNC re-initiate movement forming new migratory chains. On average, embryos treated with short pulse formed 3 chains more than the long pulse treatment (10 ± 3 chains for Aphi, Figure 15E-G; and 13 ± 3 chains for Geni, Figure 16E-G). Moreover, all chains that were formed before cell cycle inhibition, re-established migration upon withdrawal of the treatment, showing increased ventral advance compared with embryos treated for long pulses.

Taken together, our data show that cell cycle progression is required for TNC migration and that upon cell cycle reactivation, TNC migration recovers suggesting that cell cycle arrest blocks migration initiation.

Figure 15

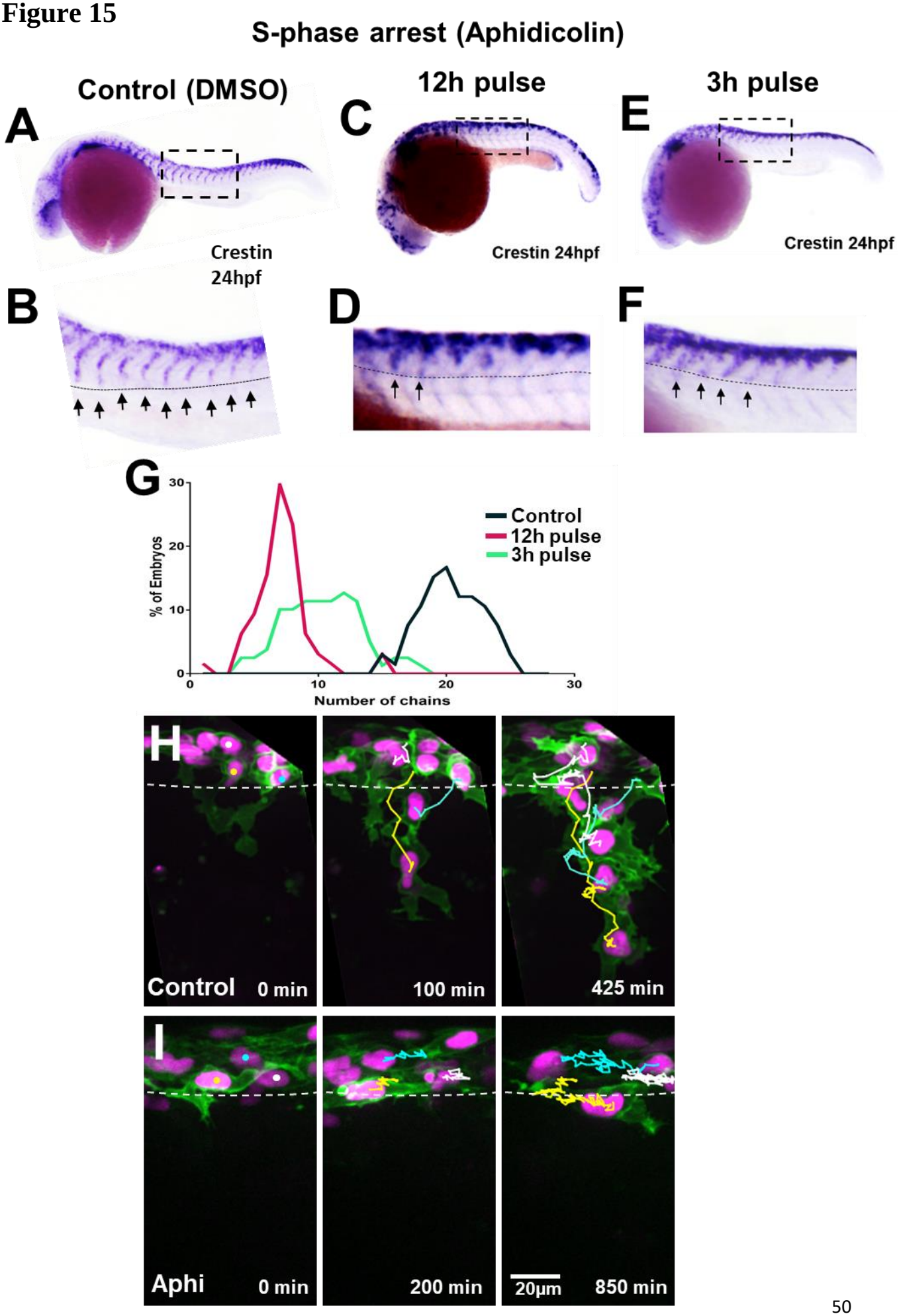
S-phase arrest (Aphidicolin)
Control (DMSO)
12h pulse
3h pulse
A
B
C
D
E
F
Crestin 24hpf
Crestin 24hpf
Crestin 24hpf
G
% of Embryos
Number of chains
Control
12h pulse
3h pulse
H
Control
0 min
100 min
425 min
I
Aphi
0 min
200 min
20µm
850 min

Figure 15: S-phase arrest by aphidicolin treatment halts TNC migration.

(A, B) Crestin in situ hybridisation of a 24hpf control embryo (treated with DMSO from 12-24hpf).

(C, D) Crestin in situ hybridisation of a 24hpf embryo treated from 12 to 24hpf with aphidicolin.

(E, F) Crestin in situ hybridisation of a 24hpf embryo treated for 3 hours with aphidicolin and re-incubated for 9 hours. In **(A-F)** boxes indicate enlarged areas, dotted lines mark TNC ventral advance and black arrows migratory chains. Anterior to the left, dorsal top.

(G) Frequency distribution of the number of migratory chains in control (DMSO) and aphidicolin treated embryos (DMSO n= 66 embryos, 12h pulse n= 64 embryos, and 3h pulse n=79 embryos).

(H, I) Selected frames from in vivo time-lapse of Sox10:mG embryo showing tracks of cells in **(H)** control imaged from 16hpf to 28hpf (DMSO) and **(I)** aphidicolin treated embryos imaged from 16hpf to 33hpf. White dashed line indicate the edge of the premigratory area; time in minutes.

Figure 16

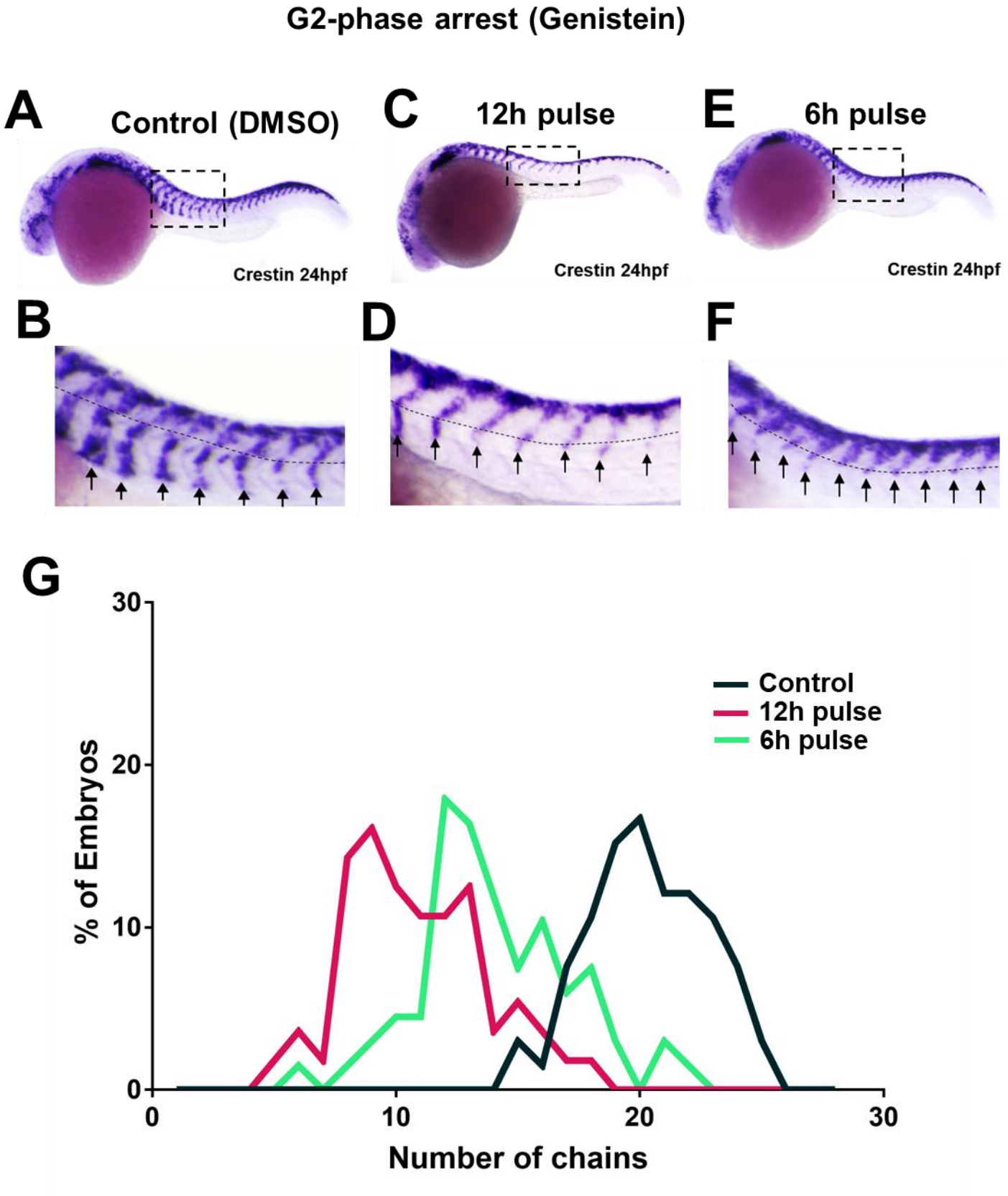
G2-phase arrest (Genistein)
A
Control (DMSO)
Crestin 24hpf
C
12h pulse
Crestin 24hpf
E
6h pulse
Crestin 24hpf
B
D
F
G
% of Embryos
Number of chains
Control
12h pulse
6h pulse
0
10
20
30

Figure 16: G_2-phase arrest by genistein treatment, delays TNC migration.
(A, B) Crestin in situ hybridisation of a 24hpf control embryo (treated with DMSO from 12-24hpf).
(C, D) Crestin in situ hybridisation of a 24hpf embryo treated from 12 to 24hpf with genistein.
(E, F) Crestin in situ hybridisation of a 24hpf embryo treated at 12hpf for 6 hours with genistein and re-incubated for 6 hours. In **(A-F)** boxes indicate enlarged areas, dotted lines mark TNC ventral advance and black arrows migratory chains. Anterior to the left, dorsal top.
(G) Frequency distribution of the number of migratory chains in control (DMSO) and aphidicolin treated embryos (DMSO n= 66 embryos, 12h pulse n= 56 embryos, and 6h pulse n=67 embryos).

1.9 Generation of transgenic lines for cell cycle progression alterations

Our cell cycle chemical inhibitors results show that cell cycle progression is required for migration, but it remains unclear whether these phenotypes are TNC autonomous or secondary effects due to alterations in the surrounding tissues. To investigate this question we generated stable transgenic lines harbouring genetic cell cycle inhibitors or accelerators that can be activated in NC only in a temporal controlled manner.

We took advantage of the UAS/Gal4 system, where Gal4 induces the expression of any protein downstream of the UAS regulatory sequence. We used two different cell cycle inhibitors, the dominant negative form of E2F (dnE2F) and the 15aa-MyoD; and the full length E2F (fl-E2F) that acts as cell cycle accelerator. The dnE2F causes a G_1 arrest by competing with endogenous E2F in biding to the retinoblastoma (RB) protein in an irreversible fashion (Burstyn-Cohen and Kalcheim, 2002), the 15aa-MyoD is a CDK-4 binding domain which prevents the phosphorylation of RB causing G_1 arrest (Zhang et al., 1999a; Zhang, et al., 1999b). On the other hand, the fl-E2F is predicted to accelerate the G_1/S transition (Figure 17F; (Helin et al., 1992)). These proteins were cloned into a double UAS vector where the UAS sequence drives expression of GFP from one strand and of the protein in question from the opposite strand (Figure 17A). Efficacy of the UAS cell cycle vectors was assessed by quantification of proliferating cells through BrdU staining (percentage of GFP+ cells expressing BrdU) in

hs:Gal4 embryos injected with these constructs (Figure 17D and E). Embryos were injected at one cell stage, heat shocked at 5hpf, and incubated for 3h with BrdU. Interestingly, we observed a drastic reduction in the number of GFP+ cells that express BrdU in embryos injected with the UAS:15aa-MyoD (a 60% reduction from 74 ± 5% BrdU+ cells in the GFP control to only 14 ± 12% BrdU+ cells; Figure 18A, A', B, B' and E). Similarly, there was a reduction in proliferation in dnE2F embryos (a 41% reduction from GFP control to only 33 ± 6% BrdU+ cells, Figure 18C, C' and E). While there was not significant change in the number of proliferating cells in embryos injected with the fl-E2F construct (68 ± 9% BrdU+ cells, Figure 18D, D' and E). While we did not observe the expected increase in proliferation for the latter construct, this may be due to limitations of BrdU staining and the fact that this was analysed in fixed samples. To define the effect of this constructs, it will be necessary to directly quantify the length of the cell cycle phases using the PCNA-GFP reporter.

Subsequently, the Cmlc:GFP cassette was incorporated in the UAS vectors, and these were injected into the inducible NC reporter line Sox10:H2B-mCherry-Kalt4ER. Injected embryos were grown, and founders selected (Figure 17B and C). However, due to the restricted access to the laboratory during the pandemic, we were unable to test the effect of genetic arrest or acceleration of the cell cycle on TNC migration. In conclusion, we have successfully generated inducible genetic cell cycle transgenic lines.

Figure 17

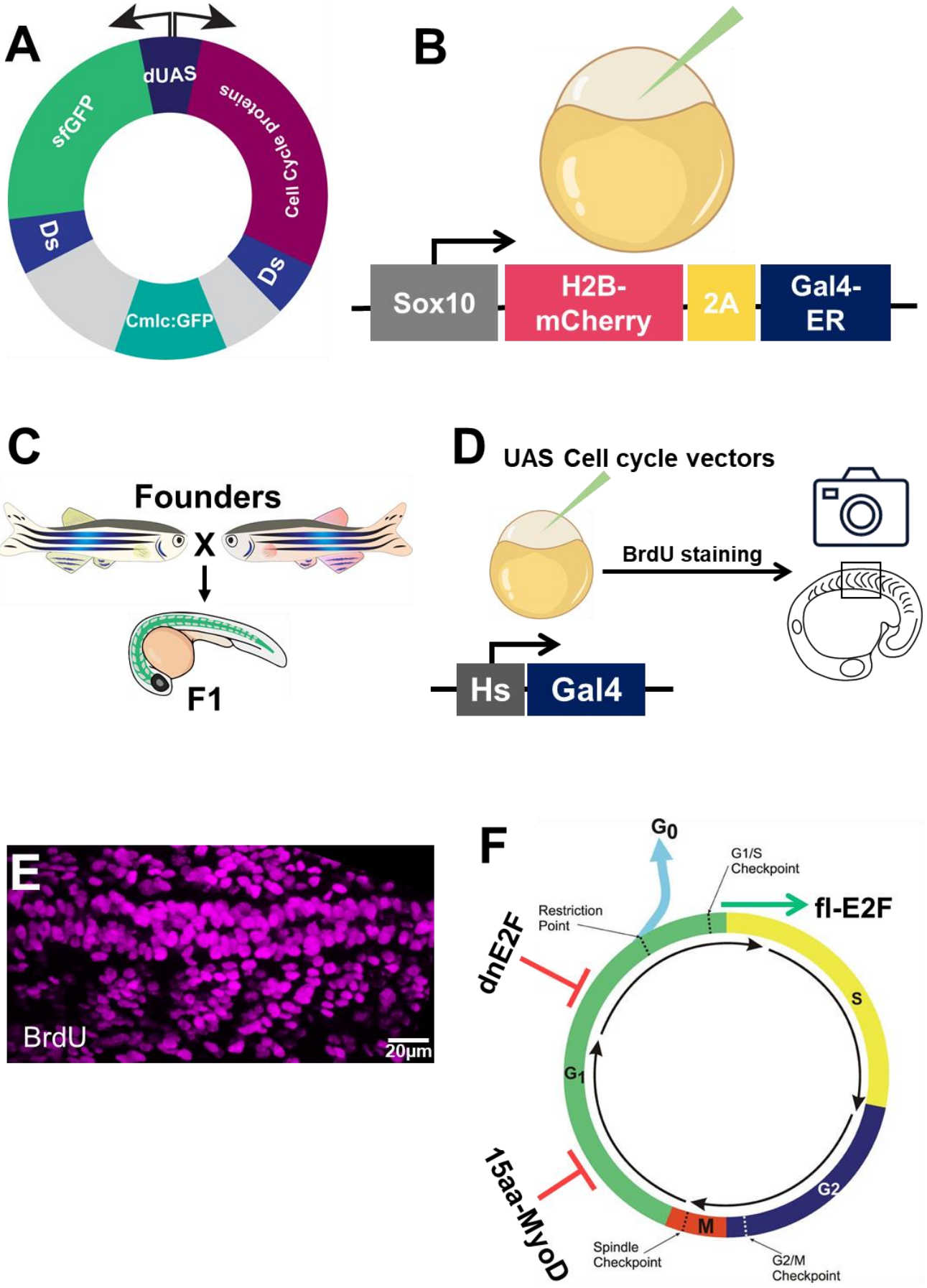
A
dUAS
Cell Cycle proteins
sfGFP
Ds
Ds
Cmlc:GFP
B
Sox10
H2B-mCherry
2A
Gal4-ER
C
Founders
X
F1
D
UAS Cell cycle vectors
BrdU staining
Hs
Gal4
E
BrdU
20μm
F
G0
G1/S Checkpoint
Restriction Point
fl-E2F
dnE2F
S
G1
G2
M
15aa-MyoD
Spindle Checkpoint
G2/M Checkpoint

Figure 17: Cell cycle inducible transgenic lines.

(A) Schematic of the used Ac/Ds dUAS:GFP vector. Double UAS sequence drives the bidirectional expression of super folded GFP from one direction and the cell cycle protein from the other one. The construct contains a transgenesis marker consisting of the cardiac myosin light chain promoter driving the expression of GFP in transgenic embryos.

(B, C) Schematic of the experimental procedure for transgenic line establishment. **(B)** Cell cycle constructs injected into one-cell stage Sox10:Kalt4 transgenic embryos and embryos grown to adulthood **(C)** Founder fish are selected and in-crossed get the first stable transgenic generation F_1.

(D) Schematic of experimental procedure to test constructs efficacy. UAS:cell cycle DNA constrcuts were injected at one-cell stage into Hs:Gal4 embryos, heat shock performed at 5hpf for 1h at 39°C and re-incubated for 3h with BrdU, fixed at 22hpf and processed by BrdU antibody staining and imaged.

(E) Confocal image of control BrdU stained embryo showing proliferating cells (nuclei in magenta).

(F) Schematic of the cell cycle depicting the phase at which the constructs arrest (dnE2F and 15aa-MyoD) or accelerate the cell cycle (fl-E2F).

Figure 18

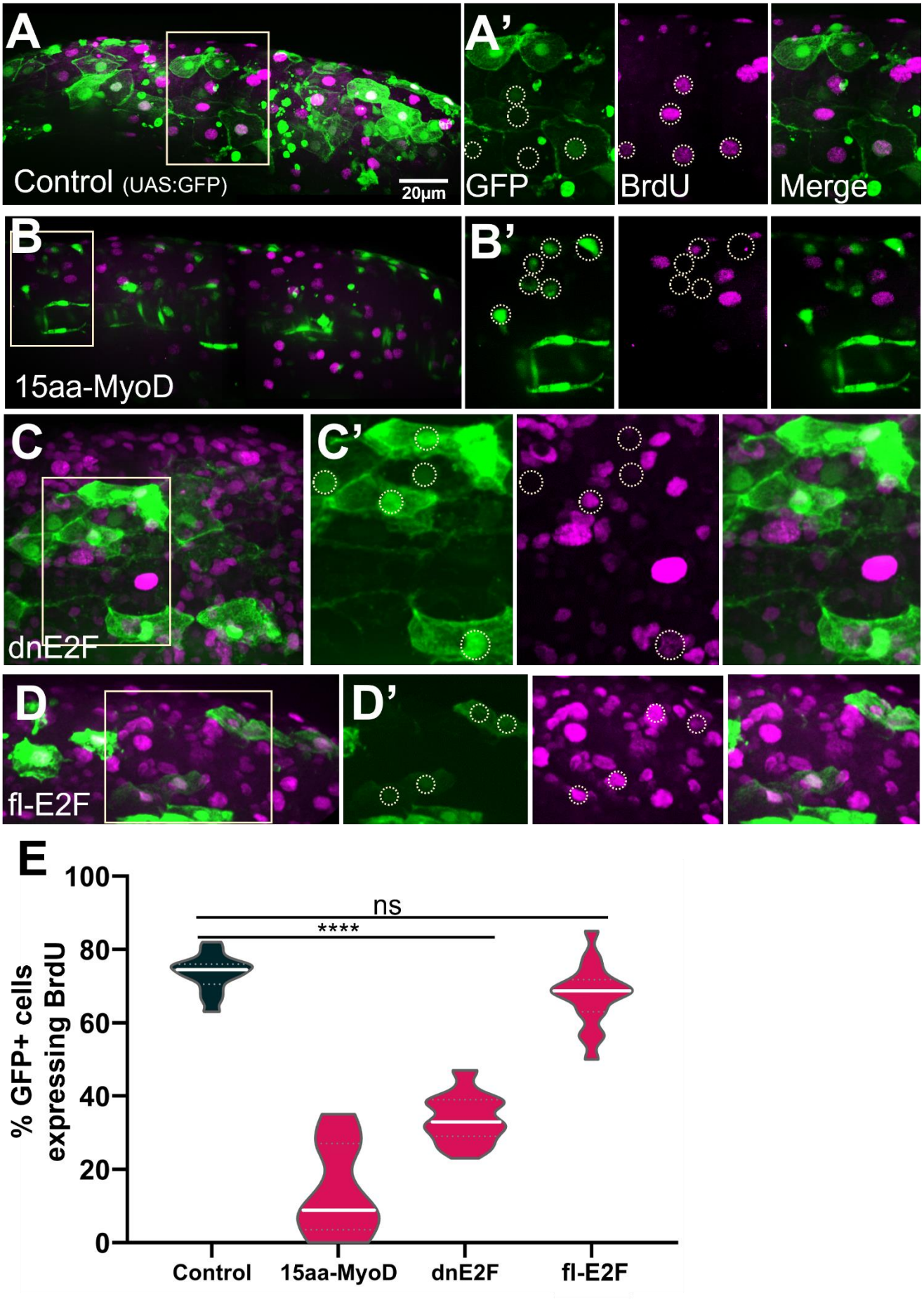
A
Control (UAS:GFP)
20μm
A'
GFP
BrdU
Merge
B
15aa-MyoD
B'
C
dnE2F
C'
D
fl-E2F
D'
E
% GFP+ cells expressing BrdU
100
80
60
40
20
0
ns
****
Control
15aa-MyoD
dnE2F
fl-E2F

Figure 18: Inducible cell cycle constructs arrest cell cycle progression.

(A-D) Confocal images of 22hpf hs:Gal4 embryo stained for BrdU after injection and heat shock as depicted in Figure 17D. **(A-A')** UAS:GFP (control), **(B-B')** UAS:15aa-MyoD, **(C-C')** UAS:dnE2F and **(D-D')** UAS:fl-E2F constructs. Boxes in A-D indicate enlarged areas in A'-D'; dotted circles mark cells co-labelled with the injected constructs and BrdU; anterior to the left dorsal top. BrdU in magenta and cell cycle construct expression in green.

(E) Quantification of cell cycle inhibition or acceleration efficacy for the different constructs, calculated as the percentage of GFP+ cells expressing BrdU (Brown-Forsythe and Welch ANOVA tests, MyoD and dnE2F $p<0.0001$, fl-E2F $p=0.1197$).

Chapter 1: Discussion

Leaders' progenitors divide asymmetrically

Asymmetric cell division (ASD) is an important mechanism of fate determination. A plethora of progenitor cells undergo ASD to produce daughter cells with different fates. *Drosophila* neuroblasts (Chia et al., 2008); sensory organ precursor cells (Schweisguth, 2015); angiogenesis and lymphatic vessels formation in zebrafish (Costa et al., 2016; Nicenboim et al., 2015); and germline and body axis formation in *C. Elegans* (Fickentscher and Weiss, 2017) all utilise ASD to produce distinctly fated daughter cells . This asymmetry can be observed by the generation of two equally size daughters that inherit different molecular components, or by the asymmetric positioning of the mitotic spindle that results in two daughter cells of different sizes (Li, 2013).

Our results reveal that one TNC progenitor cell per segment divide asymmetrically into two daughter cells of different sizes. The larger daughter will become the leader cell, while the smaller sibling migrates as a follower cell. The ASD of leaders' progenitor shares many similarities with the ASD of endothelial cells in zebrafish. Similar to TNC, endothelial cells present two migratory cell types, tip (leader) and stalk (follower) cells. Akin to the ASD of leaders' progenitor, endothelial tip cells undergo ASD giving rise to two daughter cells of different sizes and motilities (Costa et al., 2016). The presence of one leader progenitor cell per somite indicates that the main role of this cell is to generate the prospective leader cell that is required for TNC migration. On the other hand, the symmetrical division of the rest of the progenitors into prospective follower cells, suggests that these progenitors divide to ensure the presence of sufficient number of cells for chain migration.

Leaders and followers initiate migration at different phases of the cell cycle

Our data show that leaders and followers initiate migration at different phases of the cell cycle, leaders emigrating in S-phase and followers in G_1. This may be due to the fact that leaders spend the majority of the cell cycle in S-phase, while followers spend it in G_1. Thus probabilistically, it is likely for leaders and followers to initiate migration in these phases, and as such it may have no underlying function in TNC migration. However, cell cycle progression has been shown to regulate avian TNC migration initiation, where G_1/S transition is required for delamination resulting in avian TNC migrating in S-phase of the cell cycle. Molecularly, it has been shown that BMP4 positively regulates Wnt1 in TNC, which in turn induces the expression of cyclin D1 and driving the G_1/S transition (Burstyn-Cohen and Kalcheim, 2002). On the other hand, a different study shows that avian cranial NC delamination is not S-phase dependent (Théveneau et al., 2007, p.1). Avian cranial NC migrate as sheets, while TNC migrate as a large group of mesenchymal cells (Li et al., 2019). While it has not been proven that either of these populations present leaders and followers cells, it has been proposed that chick CNC may present few leader-like cells, termed trailblazers (McLennan et al., 2015a). These contrasting findings highlight differences between NC depending on the anteroposterior level of origin as well as the animal model utilised.

Leaders TNC undergo G1/S transition quicker than followers

Leaders and followers TNC exhibit different division patterns and initiate migration at different phases of the cell cycle which indicate differences in the timing of cell cycle phases. While there are no differences in the total duration of the cell cycle in leaders and followers, the durations of G_1 and S are inversely proportional. On average, TNC spend 13.5 hours in the cell cycle, which is consistent with measurements of the cell cycle duration in chick neural progenitors (Molina et al., 2020) and cranial NC (Ridenour et al., 2014; Paglini and Rovasio,

1994). Leaders TNC present a long S-phase and short G_1. This is similar to the observations in chick neural progenitors and zebrafish retina and hindbrain, where these cells spend over 50% of their cell cycle in S-phase and present a shorter G_1 (Molina et al., 2020; Leung et al., 2011).

Leaders TNC present short G_1 and undergo G1/S transition quicker than followers. This raises the question regarding the mechanisms that orchestrate the leaders' rapid G1/S transition. One such mechanism is the retinoblastoma (RB) dilution model. In G_1 phase, the RB protein inhibits cell cycle progression into S-phase via sequestering the transcriptional activator E2F, which is required for the transcription of S-phase genes. Hyperphosphorylation of RB by mainly cyclinD-CDK4/6 complexes results in the release of E2F and allows the progression into S-phase. This model proposes that even if the amount of RB protein is similar between cells of different sizes, the concentration of RB would differ, hence bigger cells would have lower concentration of RB by the virtue of their size. The further dilution of RB concentration as the cell grows results in the lack of enough RB to sequester all the E2F proteins allowing for initial transcription of S-phase genes which then facilitate the G1/S transition (Zatulovskiy and Skotheim, 2020). Also, it has been shown that the cell size at birth negatively correlates with the time cells spend in the G_1 phase of the cell cycle (Killander and Zetterberg, 1965). TNC leaders by virtue of their bigger size at birth, could dilute RB to critical levels in shorter time spans than followers, thus can undergo the G1/S transition quicker. On the other hand, it has been proposed that cells need to pass a size threshold in order to undergo G1/S transition (Facchetti et al., 2017), hence the small followers require longer time in G_1 to grow to that size threshold resulting in long G_1.

Another mechanism that could explain the different onset of G1/S transition in leaders and followers, links cell protrusions to cell cycle progression. Interestingly, a positive feedback loop has been described between levels of motility and G1/S transition. Migrating cells actively extend protrusions increasing actin branching at the leading edge. Actin

branching is promoted by Arp2/3 complexes, which are sensed by coronin1B that in turn can promote the the G1/S transition (Molinie et al., 2019). Leaders TNC are more elongated and protrusive than followers, suggesting that leaders could operate in a similar mechanism, which could explain the leaders' faster onset of G1/S transition.

Cell cycle progression is required for TNC migration

Our data reveal stark differences in cell cycle phase lengths between leaders and followers TNC, which prompted us to investigate the requirement of cell cycle progression for TNC migration. Both S- and G2-phases arrest halted TNC migration indicating that cell cycle progression is indeed required for TNC migration. Interestingly, it has been shown that cell cycle progression is required for zebrafish somite morphogenesis (Zhang et al., 2008) and that arresting the cell cycle at S or G2 halts the interkinetic nuclear movement in the zebrafish neuroepithelia (Leung et al., 2011). We observed a more drastic migratory phenotype upon S-phase arrest, which could be due to the longer time cells spend in S-phase and thus a higher probability of cell cycle arresting in that phase in contrast to the much shorter G2. The migratory aberrations observed following cell cycle arrest are not due to cytoskeleton alterations, as cells remain motile but are unable to undergo collective chain migration. TNC migratory defects upon cell cycle arrest could possibly be due to the arrest of the progenitors divisions, which give rise to leaders. Since leaders are required to direct the migration of TNC, the lack of leaders would lead to migration arrest. In cell cycle arrested embryos, only few anterior chains migrate, which could be due to the progenitors of these chains dividing at earlier time points before the cell cycle inhibitors exert their activity. The fact that S and G2 cell cycle arrest halts TNC migration, indicate that G1/S transition is not the limiting step for migration, but instead indicate the cell cycle progression and division are the important steps. Moreover, following removal of the cell cycle inhibitors, TNC reinitiate migration and form chains, demonstrating that active progression through the cell cycle is required for TNC

migration. In avian TNC, cell cycle arrest at G_1 results in halted migration since the G1/S transition is necessary for cell delamination, while S-phase arrest shows no effect on migration (Burstyn-Cohen and Kalcheim, 2002). This is in contrast to our results in which active cell cycle progression is required for TNC migration even following G1/S transition. This difference could be due to differences between avian and zebrafish TNC. Unlike zebrafish TNC, avian TNC do not consist of leaders and followers and do not form migratory chains but instead migrate as individual mesenchyme (Li et al., 2019).

Regulation of cell motility by cell cycle progression

Interestingly, cell motility has been shown to vary across the different phases of the cell cycle. Measurement of cell speed in murine fibroblast cell lines show that cells are faster in late G_1- and S-phases but exhibit a reduction of speed in early G_1 and G2 (Walmod et al., 2004). Interestingly, the activity of the GTPase Rac1, which is important for cell motility, is regulated throughout the cell cycle, being highest during S-phase when cells are most invasive, highlighting a link between cell motility and cell cycle (Kagawa et al., 2013).

Leader cells are faster, more directional, and present a significantly longer S-phase than followers; suggesting that there may be communications between cell cycle and cell motility. The inhibition of the GTPase Rac1 has been shown to decrease the probability of cells entering the S-phase and thus linking cell motility to cell cycle (Hirata et al., 2020). Moreover, a correlation between the duration of G_1 and migration persistence has been described, the longer cells remain in G_1 the less persistent they are, which may be in part responsible for the migratory behaviour of TNC followers, which show low persistence and long G_1 (Molinie et al., 2019). Together, the increased motility during S phase and decreased persistence in G_1, could explain the differences in migratory behaviour between leader and follower cells. In conclusion, our results suggest that asymmetric cell division and cell cycle differences play a role in distinguishing leaders from followers.

Chapter 2: Introduction

Notch signalling and mechanisms of fate allocation

Notch signalling is a cell-cell communication pathway that directly translates receptor activation at the membrane into gene expression changes. Notch receptors are activated by membrane-bound ligands of the Delta/Serrate/Lag2 family. Upon ligand binding, Notch receptors are cleaved by γ-secretases leading to the release of its intracellular domain (NICD). Subsequently, NICD translocates to the nucleus, binds the CBF1/Su(H)/Lag-1 complex and initiates transcription (Bray, 2016).

This pathway has been shown to control cell fate at many different stages of development and it is capable of generating different patterns within tissues depending on the mechanism of action. Two mechanisms have been characterised:

· Lateral inhibition. This mechanism allows for different cell fates to arise from an equivalence group, in which all cells are initially capable of adopting one of two fates. The process is commonly thought to act as a regulatory mechanism that limits the number of cells that will adopt one of the two fates (a 'primary' fate), leaving the majority of them to eventually adopt the other ('secondary') fate. Well known examples of lateral inhibition are the formation of neuroblasts in *Drosophila* (Chia et al., 2008) and of sensory hair cells in the inner ear of vertebrates (Daudet and Żak, 2020). Among Notch targets are genes of the Hes family. These encode transcriptional repressors able to antagonize the expression of cell fate determinants and Notch ligands. This mechanism generates a negative feedback loop in which cells that present high Notch receptor activity downregulate the expression of its ligands and cannot activate the pathway in their neighbours. Hence, adjacent cells interacting through the Notch pathway typically end up with either low or high levels of Notch activity and adopt distinct fates (Figure 5A and C; (Lewis, 1996)). The result is a salt-and-pepper pattern where

the Delta-expressing cells acquire the ‘primary’ fate (neuroblast or sensory cell in the examples above) and inhibits the surrounding cells from assuming this fate.

· Lateral induction. In contrast, it has been shown that Notch can positively regulate the expression of its ligands. In tissues where the cells acquire their fate through lateral induction, the resulting domain will be homogeneous with all cells adopting the same fate (Figure 5B). Some important examples of this process are the Notch-mediated boundary formation in the *Drosophila* wing or the induction of proneural domains in the eye, in *Drosophila* and vertebrates (Sjöqvist and Andersson, 2019).

Notch signalling has been implicated in cell migration (Leslie et al., 2007; Timmerman et al., 2004; Giniger, 1998) and promotes invasiveness during cancer progression (Reichrath and Reichrath, 2012). Interestingly, the lateral inhibition mechanism has been involved in the allocation of migratory identities during trachea formation in *Drosophila* (Affolter and Caussinus, 2008), in cell culture (Riahi et al., 2015) and during angiogenesis (Phng and Gerhardt, 2009). In hypoxic tissues, the secretion of growth factors and chemokines stimulate the sprouting of new blood vessels. Endothelial Growth Factor-A (VEGF-A) stimulates a cell in the existing vessels to become the tip cell, in turn, that cell will then leads the sprouting and suppresses the leader phenotype in its neighbours through Notch lateral inhibition, allowing them to become stalk cells. Whether Notch signalling plays a similar role in the context of mesenchymal cell migration is unknown. Notch signalling is required during NC induction (Cornell and Eisen, 2005) and its components and activity remain present in migrating NC (Liu et al., 2015; Rios et al., 2011), nevertheless, the role of Notch during NC migration remains controversial, Cardiac NC have been reported to develop normally under Notch loss-of-function conditions (High et al., 2007), however, using different genetic tools, it has been shown that both Notch gain- and loss-of-function lead to the lack of NC derivatives (Mead and Yutzey, 2012), moreover, in *Xenopus* embryos depletion of Notch effectors leads to aberrant NC migration (Vega-López et al., 2015). Whether these, seemingly

conflicting, results are due to differences in the animal models used or caused by methodological discrepancies remains to be addressed.

The Notch pathway has not only been implicated in cell fate allocation, but it is also important for cell proliferation. Depending on the cell context, Notch can inhibit (Patel et al., 2016; Nguyen et al., 2006; Devgan et al., 2005; Mammucari et al., 2005; Rangarajan et al., 2001; Ohnuma et al., 1999), or promote cell cycle progression (Fang et al., 2017; Zalc et al., 2014; Riccio et al., 2008; Carlson et al., 2008; Georgia et al., 2006; Park et al., 2005; Noseda et al., 2004). Indeed, among Notch target genes important cell cycle regulators are present, as CyclinD1, CDK2, p21 and c-MYC (Joshi et al., 2009; Guo et al., 2009; Campa et al., 2008; Palomero et al., 2006; Ronchini and Capobianco, 2001).

Due to its important role in identity specification and cell migration in many systems, we sought to investigate whether Notch regulates leader/follower identities and the migration of TNC.

Figure 5

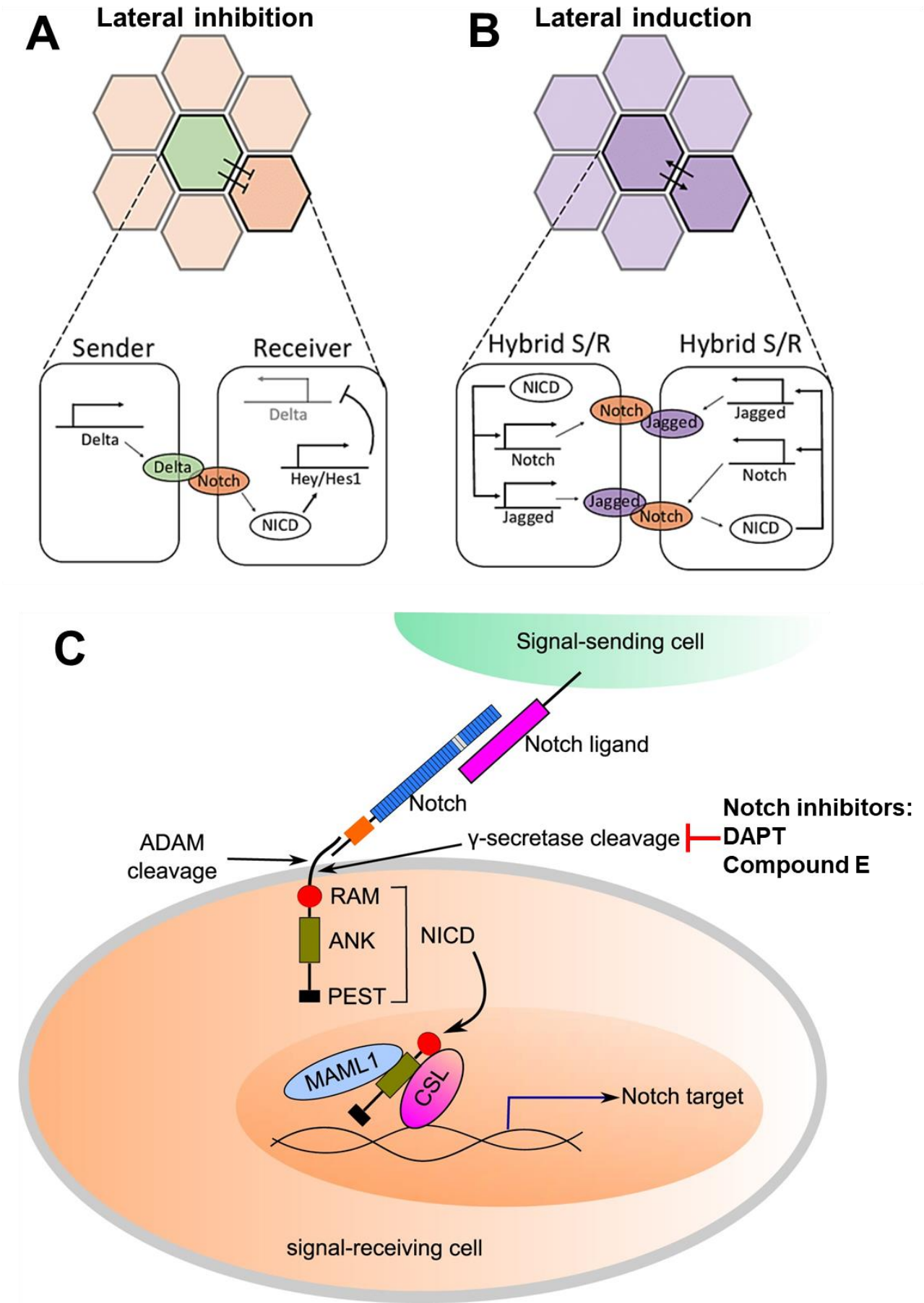
A
Lateral inhibition
Sender
Receiver
Delta
Delta
Notch
Delta
Hey/Hes1
NICD
B
Lateral induction
Hybrid S/R
Hybrid S/R
NICD
Notch
Jagged
Notch
Jagged
Jagged
Notch
Jagged
Notch
NICD
C
Signal-sending cell
Notch ligand
Notch
ADAM
cleavage
γ-secretase cleavage
Notch inhibitors:
DAPT
Compound E
RAM
ANK
PEST
NICD
MAML1
CSL
Notch target
signal-receiving cell

Figure 5: Notch signalling pathway.

(A) Schematic of Notch lateral inhibition; ligand-expressing cell (sender) signals to the receptor-expression cell (receiver) leading to the activation of Notch target genes such as Hey/Hes1 and downregulation of ligand expression such as Delta in the receiver cell.

(B) Schematic of Notch lateral induction; both cells express the receptor and the ligand (hybrid) such as NICD and Jagged and can signal to each other leading to both cells exhibiting the same fate. Adapted from (Bocci et al., 2020).

(C) Schematic illustrating mechanism of Notch signalling. Receptor-ligand contact between sender and receiver cells leads to the cleavage of the NICD, which translocates to the nucleus and in association with other factors drive the expression of Notch target genes. Also showing the proteins which Notch inhibitors inhibit.

NICD: Notch intracellular domain; CSL: CBF1, Suppressor of Hairless, Lag-1; MAML1: Mastermind Like Transcriptional Coactivator 1; ADAM: A Disintegrin And Metalloproteinase; RAM, ANK and PEST are NICD domains. Adapted from (Zhang et al., 2016).

Chapter 2: Results

Notch signalling regulates Trunk NC migration and cell cycle progression

2.1 Notch signalling is required for TNC migration

Notch components are expressed in the presumptive NC and are required for NC induction (Cornell and Eisen, 2005). To investigate Notch role in TNC migration and leader/follower identity acquisition, we first studied the expression of Notch receptors, ligands, and effectors at later developmental stages in NC. In situ hybridisation show that the expression of Notch receptor (Notch1a; Figure 19A-C), ligands (DeltaB and DeltaD; Figure 19D-I) and effectors (Her4; Figure 19J-L) is maintained in NC beyond induction and throughout migration. Next, we set to define the developmental stage at which NC induction becomes independent from Notch signalling in order to study the role of Notch in NC migration after induction. We inhibited Notch using the γ-secretase inhibitor DAPT (Richter et al., 2017) at different developmental stages, and NC induction was assessed by in situ hybridization for the NC marker Crestin at 18hpf. In these experiments Notch inhibition impairs NC induction up to 11hpf, thereafter NC formation is independent of Notch signalling (Figure 20A-D). To confirm these results, we tested the expression of other NC markers, FoxD3 and Sox10, in embryos treated at 11hpf and incubated until 15hpf, just before TNC migration initiation. In these experiments, Notch inhibition has no effect on the expression of any of these NC markers (Figure 20E-J). Hence, all subsequent manipulations were performed from 12hpf, avoiding any alteration to NC induction.

Figure 19

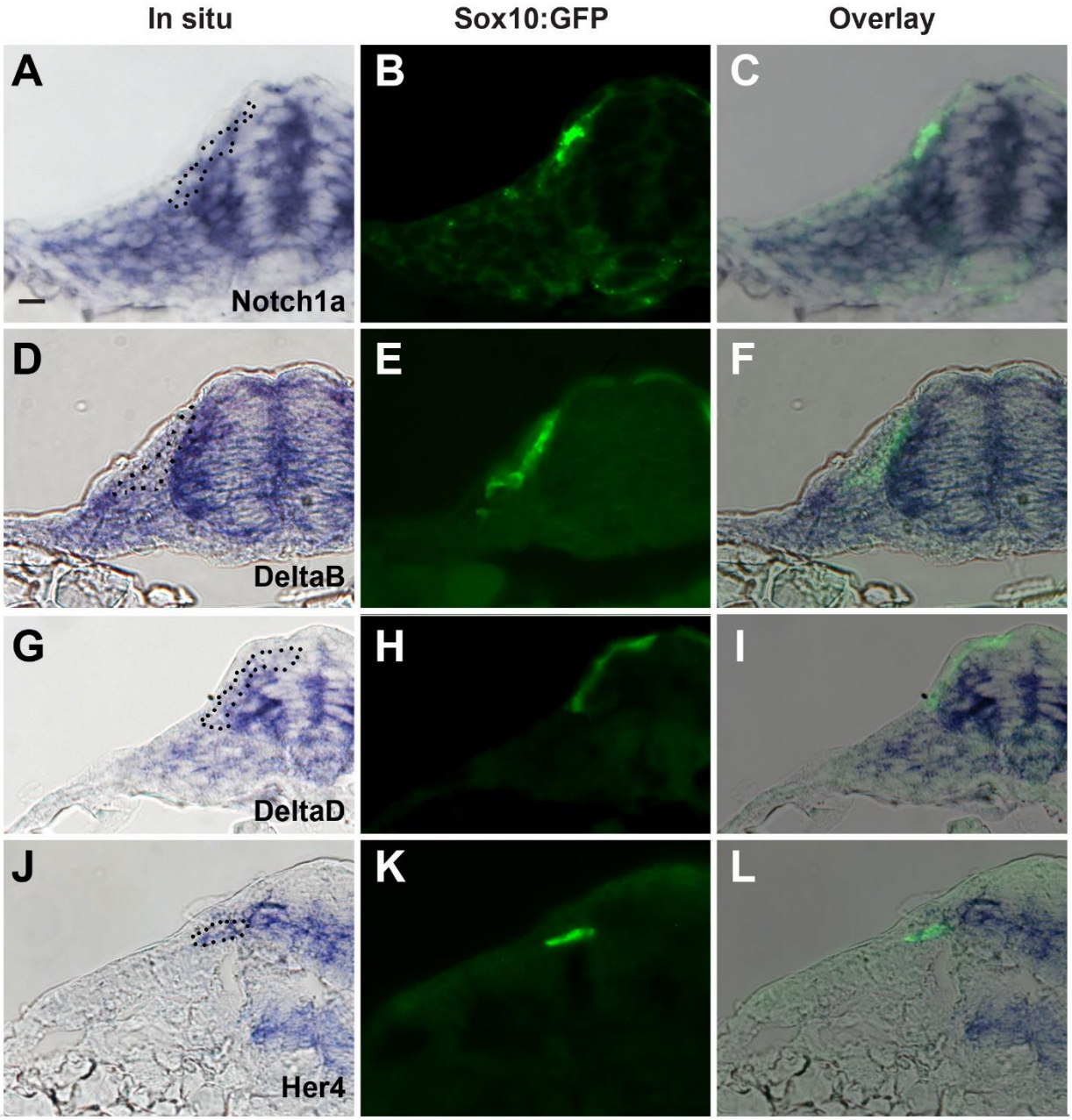

Figure 19: Expression of Notch components in TNC.

Transverse sections through the trunk of Sox10:GFP embryo showing **(A-C)** Notch1a, **(D-F)** DeltaB, **(G-I)** DeltaD and **(J-L)** Her4 expression. **(A, D, G and J)** bright field, **(B, E, H and K)** fluorescence and **(C, F, I and L)** overlay images. Dotted black line in the brightfield frames, indicate TNC seen in the fluorescent image. Data acquired by Tatiana Corveaux.

Figure 20

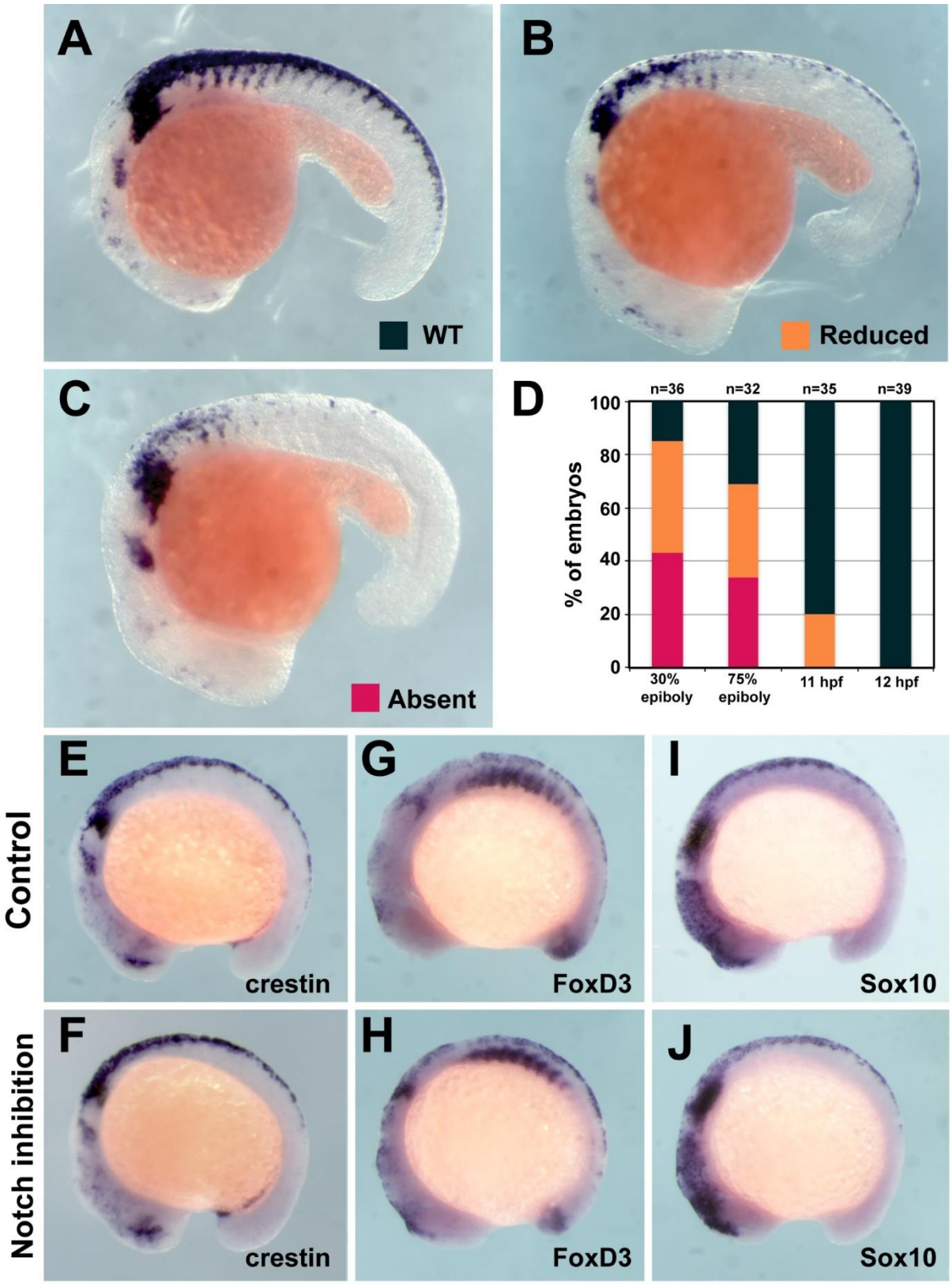
A
WT
B
Reduced
C
Absent
D
n=36
n=32
n=35
n=39
100
80
60
40
20
0
% of embryos
30% epiboly
75% epiboly
11 hpf
12 hpf
Control
E
crestin
G
FoxD3
I
Sox10
Notch inhibition
F
crestin
H
FoxD3
J
Sox10

Figure 20: TNC induction is independent of Notch signalling after 12hpf.
(A) Crestin whole mount in situ hybridisation in wildtype (WT) embryo at 18hpf.
(B-C) Crestin whole mount in situ hybridisation showing DAPT treatment phenotypes: **(B)** reduced or **(C)** absent TNC.
(D) Quantification of the different Crestin expression phenotypes observed upon DAPT treatment between 30% epiboly and 12hpf (black: WT as in A, yellow: reduced as in B and red: absent as in C; 30% epiboly n=38, 75% n=32, 11hpf n=35 , and 12hpf n=39).
(E-J) Whole mount in situ hybridisation for NC markers in control (DMSO) and DAPT treated embryos from 11-16hpf. **(E and F)** Crestin (DMSO n=32, DAPT n=38), **(G and H)** FoxD3 (DMSO n=16, DAPT n=35) and **(I and J)** Sox10 (DMSO n=27, DAPT n=29). Anterior to the left, dorsal top. Data acquired by Claudia Linker.

Next, we studied whether Notch inhibition affects the formation of TNC derivatives. We found that chemical (DAPT) and genetic inhibition (hs:dnSuH; (Latimer et al., 2005)) of Notch signalling impairs the formation of all TNC derivatives, including Schwann cell (Figure 21A and B), neurons (Figure 21C and D), and pigment cells (Figure 21E-F); suggesting that Notch signalling is required for TNC derivatives formation in a process prior to differentiation. Hence, we asked whether Notch inhibition affects TNC migration. Crestin expression shows that the number and ventral advance of TNC migratory chains are reduced when Notch is inhibited at 12hpf and embryos are analysed at 18hpf (Figure 22A-B), and 24hpf (Figure 22C-D), which explains the lack of TNC derivatives at later developmental stages.

Subsequently, we analysed whether the observed phenotypes are due to a delay or a halt of TNC migration. To this end, we performed a time course of Notch inhibition and analysed TNC migration by Crestin in situ in fixed embryos. Embryos were treated with DAPT at 12hpf, incubated for 6 to 12 hours and Crestin expression was used to quantify the number and ventral advance of TNC migratory chains. We observed a decreased number of migratory chains upon Notch inhibition at all analysed stages (18, 20 and 24hpf); nevertheless, the number of migratory chains increases in embryos fixed at later stages (Figure 22E). This shows that the lack of Notch

activity causes a delay in TNC migration and not a total lack of motility. Since the lack of Notch activity delays TNC migration, we hypothesised that Notch signalling might play a role in the timing of migration initiation, thus we studied the effect of Notch gain of function (GOF) expecting to observe an earlier onset of migration. Notch GOF was achieved using the inducible overexpressing Notch intracellular domain (NICD) only in NC through the addition of tamoxifen to Sox10:H2B-mCherry-Kalt4ER; UAS:NICD embryos. Surprisingly, we found that embryos with Notch overactivation show a very similar phenotype to Notch inhibited embryos, presenting a similar reduction of the ventral advance and the number of migratory chains (Figure 22F). Taken together, these data show that proper levels of Notch signalling are required for TNC chain migration.

Figure 21

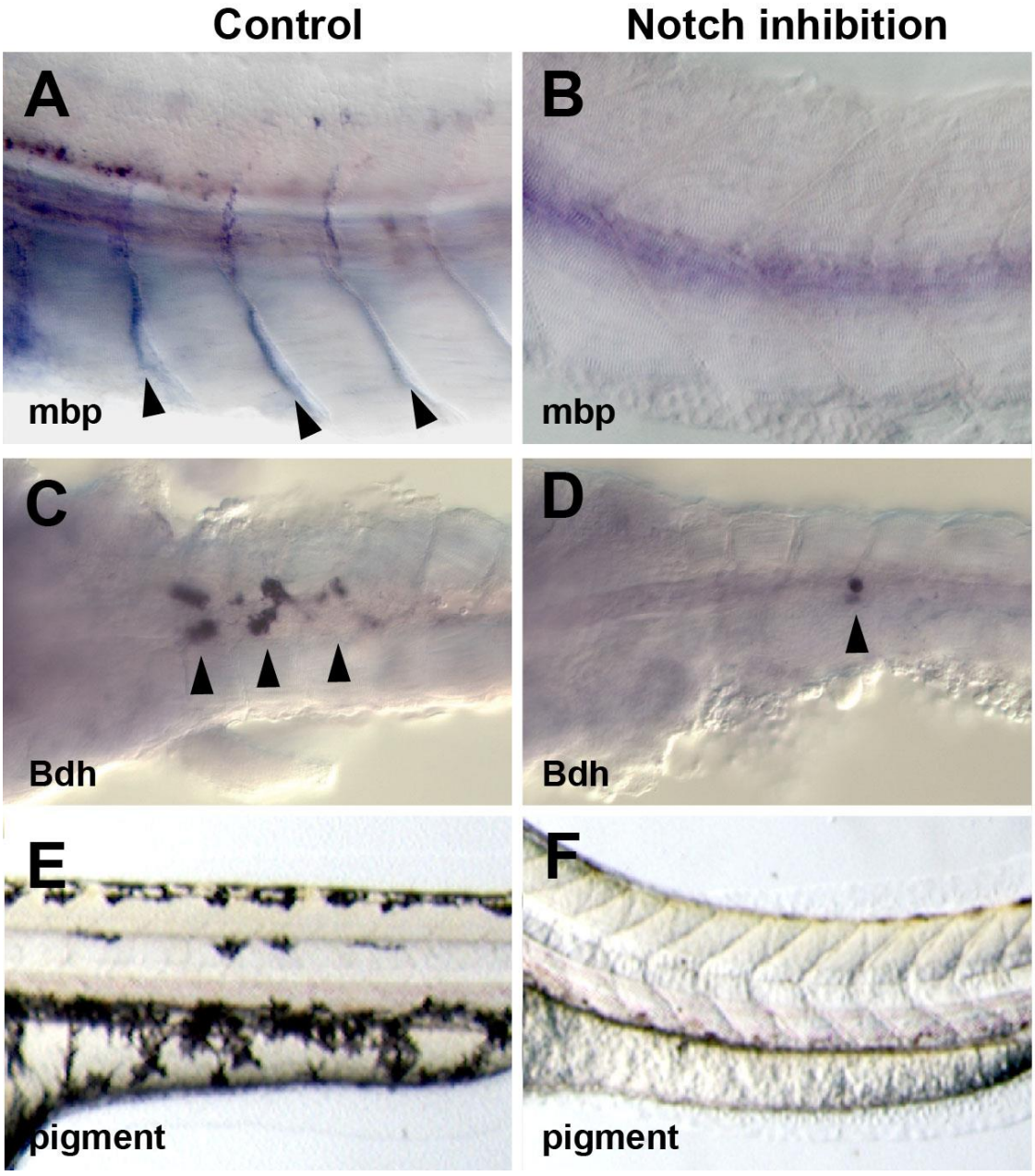

Figure 21: Notch inhibition impairs TNC derivatives development.

(A, B) In situ hybridisation for the Schwann cell marker mbp in **(A)** control (DMSO; n=15) and **(B)** DAPT (n=20) treated from 11 to 72hpf embryos; black arrowheads indicate Schwann cells. Anterior to the left, dorsal top.

(C, D) In situ hybridisation of the adrenergic neuronal marker Bdh in **(C)** control (DMSO; n=25) and **(D)** DAPT (n=18) treated 11 to 72hpf embryos; black arrowheads indicate Bdh expressing cells in the cervical ganglia. Anterior to the left, ventral view.

(E, F) Bright field image of pigment cells in **(E)** control (DMSO; n=40) and **(F)** DAPT (n=52) treated 11 to 72hpf embryos. Anterior to the left, dorsal top. Data acquired by Claudia Linker.

Figure 22

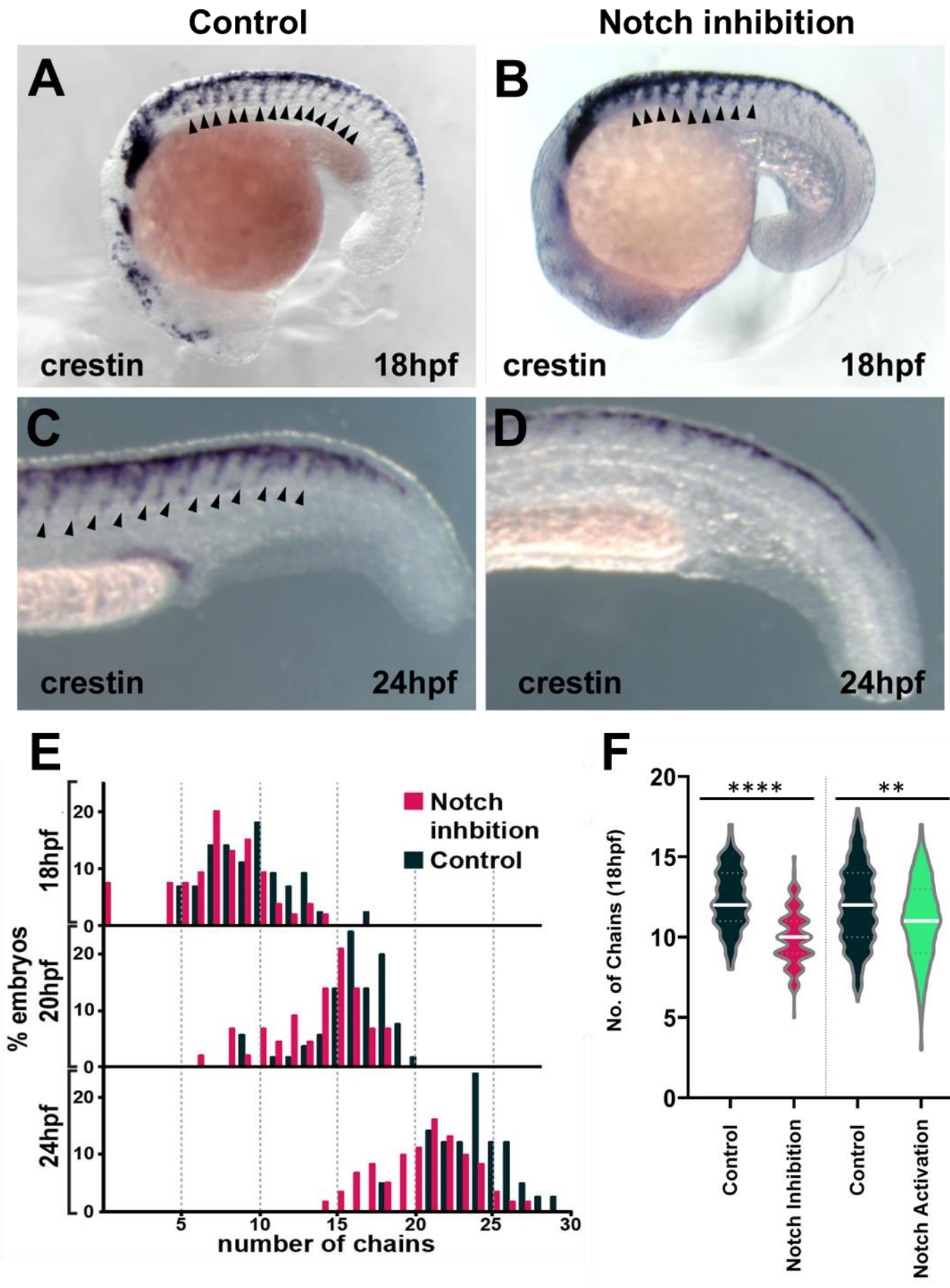
Control
Notch inhibition
A
crestin
18hpf
B
crestin
18hpf
C
crestin
24hpf
D
crestin
24hpf
E
Notch inhbition
Control
18hpf
20hpf
24hpf
% embryos
number of chains
F
No. of Chains (18hpf)
****
**
Control
Notch Inhibition
Control
Notch Activation

Figure 22: Notch inhibition delays TNC migration.
(A, B) Crestin whole mount in situ hybridisation of **(A)** control (DMSO) and **(B)** DAPT treated embryos from 12 to 18hpf.
(C, D) Crestin in situ hybridisation of **(C)** control (DMSO treated, n=42) and **(D)** DAPT treated embryo (n=61) from 12 to 24hpf.
Black arrowheads indicate migratory chains, anterior left, dorsal up.
(E) Quantification of migratory chain formation upon DMSO or DAPT treatment from 12-18hpf (DMSO n=98; DAPT n=126), 12-20hpf (DMSO n=111; DAPT n=109) and 12-24hpf (DMSO n=42; DAPT n=61).
(F) Quantification of migratory chain formation upon control (HS:Gal4 n=516 embryos), Notch loss- (HS:dnSu(H) n=220 embryos) or gain-of-function (HS:Gal4xUAS:NICD, n=142 embryos) from 12-18hpf. Mann-Whitney U test, Control vs inhibition $p<0.0001$, Control vs activation $p=0.0020$. Data acquired by Claudia linker and Jo Richardson.

2.2 Notch signalling is required for proper migratory identity allocation

Alteration of Notch leads to the loss of TNC derivatives and migratory defects, thus we asked whether these phenotypes are due to the loss of leader/follower identities, since Notch is known to regulate identity allocation in different systems. To this end, we analysed TNC migration *in vivo* under Notch inhibition conditions using the γ-Secretase inhibitor Compound E (CompE; (Richter et al., 2017)). Sox10:mG embryos were treated at 12hpf and time-lapse movies performed from 16hpf for 10-16h. Under these conditions, TNC remain motile and a single cell initiate chain migration, but contrary to control embryos, the leader cells are not able to retain the front position and are overtaken by one or several follower cells (Figure 23A and B). The overtaking follower cell in turn is not always able to retain the front position and can be overtaken by followers further behind in the chain. Whereas less than 3% of control leaders are overtaken more than once, 23% of CompE treated leaders are overtaken by followers (Figure 23E; compare the red bars). The lack of TNC chain coherence leads to a halt in ventral advance at the level of the neural tube/notochord border, where cells repolarise

and move anterior or posteriorly crossing somite boundaries or joining other migratory chains (Figure 23C and E). Measurements of the absolute ventral distance (Y distance in a straight line between the position of the cell a the first and last time points of the movie) and the total ventral distance (Y distance in a straight line between the dorsal edge of the embryo and the cell position at the last time point of the movie; Figure 24C), show that under Notch inhibited conditions, leaders and followers do not differ in their ventral displacement, both resembling the distance migrated by control followers (Figure 24A and B). Next, we analysed the migratory parameters of leader and follower cells. Characteristically, control leaders are faster and more direct than followers. However, upon CompE treatment leaders and followers migrate at similar speed (Figure 23D) and directionality to control follower cells (Figure 24D). Similar results were obtained when Notch inhibition was attained genetically, by inducing overexpression of the dominant negative Suppressor of Hairless (dnSuH) in the entire embryo through heat shock activation (hs:dnSuH transgenic; data not shown). Strikingly, whereas 89% of leaders migrate beyond the neural tube/notochord boundary (midpoint) in control, only 41% of leaders migrate past the midpoint upon Notch inhibition (Figure 24E). These results show that upon Notch inhibition migratory identity allocation is compromised and suggest that a homogeneous population of follower-like cells is established upon Notch signalling inhibition. Lack of leader cells formation under CompE treatment impairs the collective migration of TNC.

Figure 23

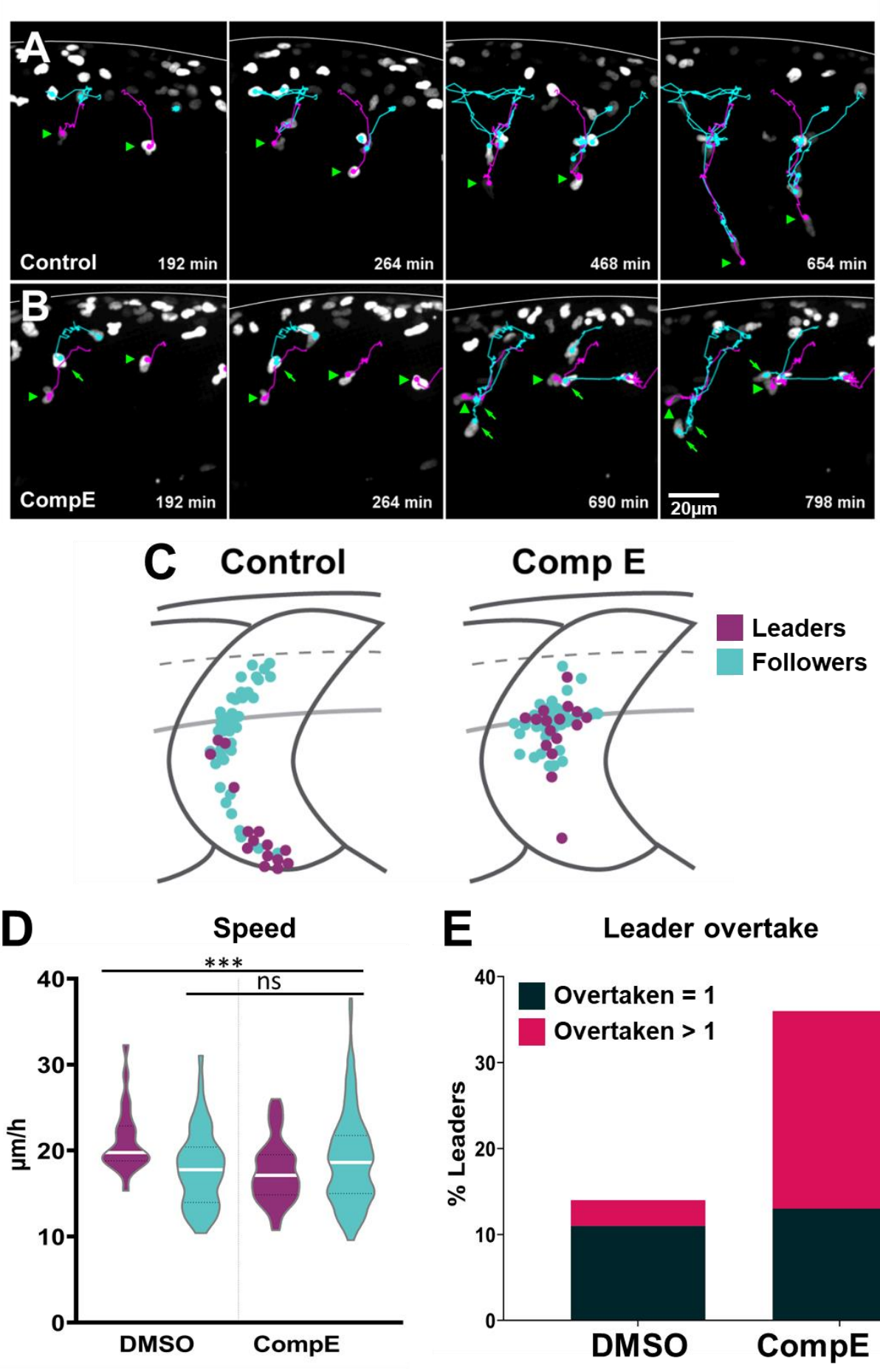
A
Control
192 min
264 min
468 min
654 min
B
CompE
192 min
264 min
690 min
20µm
798 min
C
Control
Comp E
Leaders
Followers
D
Speed
***
ns
µm/h
40
30
20
10
0
DMSO
CompE
E
Leader overtake
Overtaken = 1
Overtaken > 1
% Leaders
40
30
20
10
0
DMSO
CompE

Figure 23: Notch inhibition impairs TNC collective migration.

(A, B) Selected frames from in vivo imaging of Sox10:Kalt4 embryos under **(A)** control (DMSO) or **(B)** Notch inhibition conditions (CompE). Leader's track in magenta, follower's track in cyan; solid white lines indicate dorsal border of the embryo; green arrowheads indicate leader cells, green arrows follower cells overtaking leaders. Anterior to the left, dorsal top.

(C) Schematic of model embryo showing the migratory end positions of leader and follower cells under control (DMSO, leaders n=15, followers n=41, from 4 embryos) and Notch inhibition conditions (CompE, leaders n=16, followers n=39, from 5 embryos). Leaders and followers ventral displacement is arrested at the neural tube/notochord boundary in Notch inhibited conditions.

(D) Quantification of cell speed in control (DMSO, leaders n=22, followers n=50, from 5 embryos) and Notch inhibition conditions (CompE, leaders n=42, followers n=202, from 9 embryos). One-way ANOVA, DMSO leaders vs followers p=0.0002, CompE leaders vs followers p=0.4043, DMSO leaders vs CompE leaders and followers p=0.0001.

(E) Quantification of leader overtaken by follower cells. Only once (overtaken=1) or overtaken more than one time (overtaken>1) in control (DMSO) or Notch inhibition conditions (CompE). Overtaken once: DMSO 11% (n=4/38 cells from 8 embryos), CompE13% (n=5/39 cells from 8 embryos); overtaken>1: DMSO 3% (n= 1/38 from 8 embryos) and CompE 23% (n= 9/39 from 8 embryos).

Figure 24

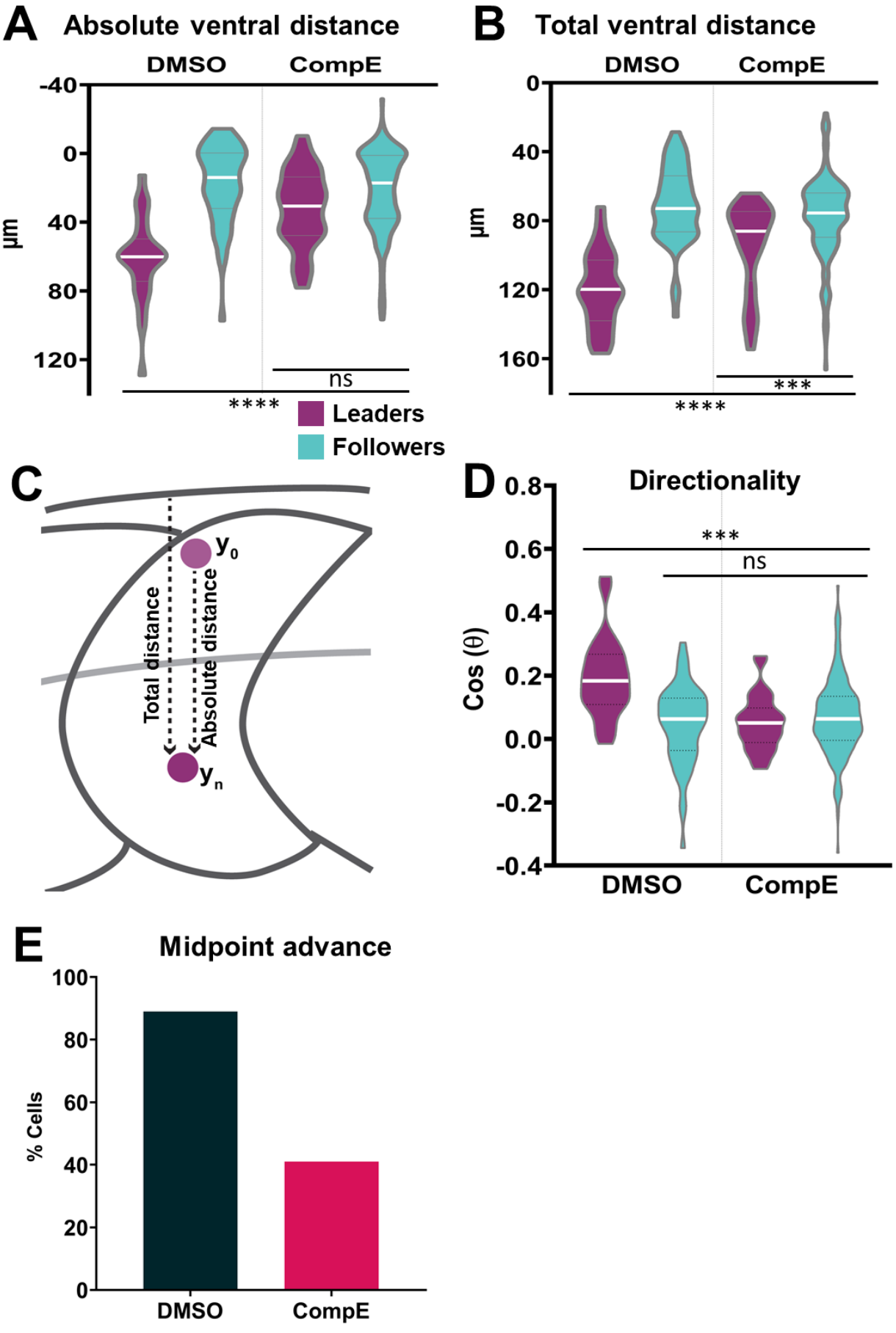
A
Absolute ventral distance
DMSO
CompE
-40
0
40
80
120
µm
ns
****
Leaders
Followers
B
Total ventral distance
DMSO
CompE
0
40
80
120
160
µm
***
****
C
y_0
y_n
Total distance
Absolute distance
D
Directionality
0.8
0.6
0.4
0.2
0.0
-0.2
-0.4
Cos (θ)
***
ns
DMSO
CompE
E
Midpoint advance
100
80
60
40
20
0
% Cells
DMSO
CompE

Figure 24: Notch inhibition reduces directionality and ventral advance of leaders and follower cells.

(A) Quantification of absolute ventral distance in control (DMSO; n=25 leaders, n=50 followers in 5 embryos) and Notch inhibited conditions (CompE; n=42 leaders, n=203 followers in 9 embryos). One-way ANOVA DMSO leaders vs all $p<0.0001$, CompE leaders vs followers $p=0.0601$.

(B) Quantification of total ventral distance under control (DMSO; n=25 leaders, n=50 followers in 5 embryos) and Notch inhibited conditions (CompE; n=42 leaders, n=203 followers in 9 embryos). One-way ANOVA DMSO leaders vs all $p<0.0001$, CompE leaders vs followers $p=0.0001$.

(C) Schematic of model embryo illustrating absolute and total ventral distance measurements.

(D) Directionality correlation quantification under control ((DMSO; n=25 leaders, n=50 followers in 5 embryos) and Notch inhibited conditions (CompE; n=42 leaders, n=203 followers in 9 embryos). Brown-Forsythe DMSO leaders vs all $p=0.0007$, DMSO followers vs CompE leaders and followers $p>0.9999$.

(E) Quantification of leader cells that advance past the neural tube/notochord boundary under control (DMSO; 32 out of 38 leaders in 8 embryos) and Notch inhibited conditions (CompE; n=16 out of 39 leaders in 8 embryos).

2.3 Somites and neural tissue are not altered by Notch inhibition

Somites and neural tissue act as substrate for TNC migration and are known to be patterned by Notch signalling, raising the possibility that the observed alterations of TNC migration upon Notch inhibition are secondary to abnormalities of surrounding tissues. To test this possibility, we analysed the formation and differentiation of TNC substrate under Notch inhibited conditions. Wild type embryos were treated with DAPT at 12hpf and fixed between 18 and 24hpf. In situ hybridization for the somite segmentation marker Cb1045 shows normal expression in segments 6-10 in which TNC were analysed. Moreover, segmentation of the most caudal somites is affected demonstrating that Notch signalling has indeed been inhibited (Figure 25A and B). Next, we studies somite anteroposterior pattern, by the expression of DeltaD (Figure 25E and F), and somite differentiation, by the expression of the muscle precursor marker MyoD (Figure 25C and D) or the presence of the heavy myosin protein (F59

immunostaining; Figure 25G and H). All of these markers show normal expression patterns under Notch inhibition, demonstrating that in segments 6-10, somite patterning and differentiation occur normally under these conditions. Finally, we established whether neural tube development was affected by this treatment. Analysis of the motoneuron marker Znp1 and the axon differentiation marker, acetylated tubulin (AC tub), show that neuronal development is not affected in the segments in which TNC are impaired by Notch inhibition (Figure 25I-L). Together, these results show that TNC substrate tissues are not affected by the performed Notch inhibition treatment, hence the phenotypes observed in TNC are most probably autonomous to this population.

Figure 25

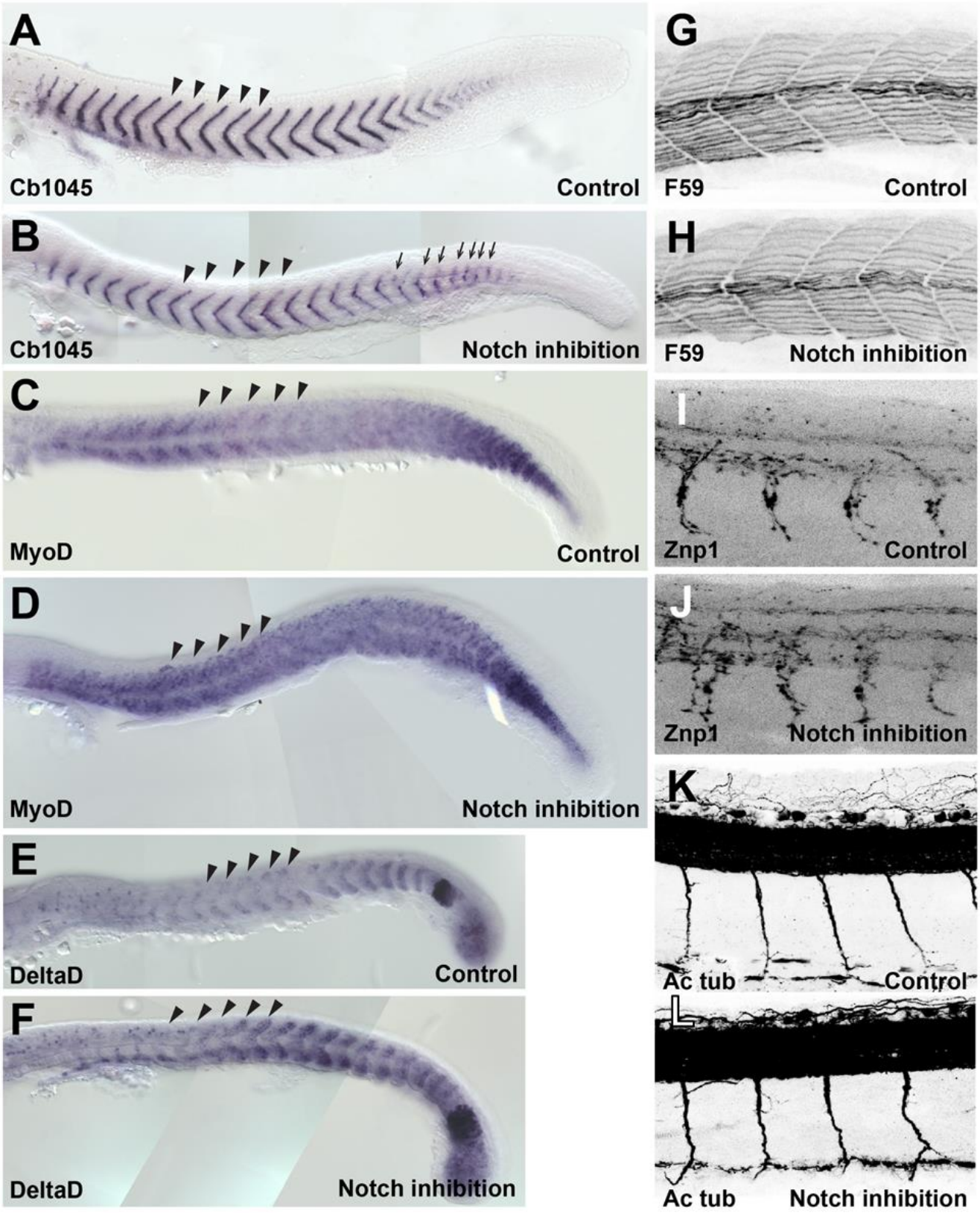
A
Cb1045
Control
B
Cb1045
Notch inhibition
C
MyoD
Control
D
MyoD
Notch inhibition
E
DeltaD
Control
F
DeltaD
Notch inhibition
G
F59
Control
H
F59
Notch inhibition
I
Znp1
Control
J
Znp1
Notch inhibition
K
Ac tub
Control
L
Ac tub
Notch inhibition

Figure 25: Somites and neural tissue are not altered by Notch inhibition.
(A, B) In situ hybridisation with the segmentation marker cb1045 in 24hpf embryos under **(A)** control (DMSO, n=23) and **(B)** Notch inhibition conditions (DAPT, n=30).
(C, D) In situ hybridisation with the muscles precursor marker MyoD in 24hpf embryos under **(C)** control (DMSO, n=47) and **(D)** Notch inhibition conditions (DAPT, n=45).
(E, F) In situ hybridisation for the Notch receptor DeltaD in 18hpf embryos under **(E)** control (DMSO, n=25) and **(F)** Notch inhibition conditions (DAPT, n=30).
(G, H) Antibody staining for heavy myosin (F59) in 24hpf embryos under **(G)** control (DMSO n=37) and **(H)** Notch inhibition conditions (DAPT, n=32).
(I, J) Antibody staining for the motoneuron marker Znp1 in 24hpf embryos under **(I)** control (DMSO n=35) and **(H)** Notch inhibition conditions (DAPT, n=42).
(K, L) Antibody staining for the axon marker acetylated tubulin (Ac. Tub) in 72hpf embryos under **(K)** control (DMSO n=20) and (H) Notch inhibition conditions (DAPT, n=27).
Black arrowheads indicate the anteroposterior level at which TNC migration was analysed that present normal expression of all the markers. Black arrows indicate segmentation defects of the caudal-most somites. Anterior to the left, dorsal top. Data acquired by Claudia Linker.

2.4 TNC autonomous inhibition of Notch signalling is responsible for migratory defects

Next, we directly analysed whether the migratory phenotypes described above were TNC autonomous. To this end, we took advantage of our inducible NC transgenic line Sox10:H2B-mCherry-Kalt4ER, in which all NC nuclei are fluorescently labelled and express the optimised Gal4ER. In these embryos tamoxifen addition induces the expression of any UAS driven sequence (Figure 26A). Analysis of target genes expression after tamoxifen addition showed that maximum levels of the UAS driven protein were attained within 1 hour of induction (100% Myc+ cells; Figure 26B). To attain Notch loss-of-function (LOF), we generated a new UAS driven dnSu(H) transgenic. The *Xenopus* sequence of dnSu(H) (Latimer et al., 2005) was cloned under the 5xUAS tandem sequence and a Myc-tag epitope was added for direct detection of the protein. The AcDs transposon vector, that includes GFP driven

under the control of the cmnl2 heart promotor, was used to generate the line (Chong-Morrison et al., 2018, p.); Figure 26C). With this tool on hand, we obtained inducible inhibition of Notch signalling exclusively in NC. In Sox10:Kalt4;UAS:dnSu(H) embryos, all NC express Gal4-ER and are fluorescently labelled by nuclear-RFP. Gal4-ER is maintained inactive in the cytoplasm in the absence of oestrogen, upon addition of tamoxifen it translocates to the nucleus activating transcription of the UAS:dnSu(H) transgene (Figure 26D; (Alhashem et al., 2021)). We found that although not all cells expressed the dnSuH protein to the same level in this transgenic (Figure 26E-G), it is a suitable tool to test the effect of Notch LOF on TNC migration and identity allocation.

Interestingly, we found that the autonomous LOF of Notch signalling exclusively in NC phenocopy the migratory defect observed in CompE treated embryos (Figure 27A-B). Leader cells are overtaken by followers (Figure 27E) and the ventral advance of the chains is arrested at the neural tube/notochord boundary with cells deviating in anterior or posterior paths (Figure 27C). Likewise, Notch inhibited leaders and followers present the characteristic migratory parameters of follower cells with reduced speed (Figure 27D), absolute and total ventral distance (Figure 28A and B), and directionality (Figure 28C). Also, leaders midpoint advance is severely affected under Notch LOF, with only 9% of leaders migrating beyond the midpoint compared to 86% of leaders in control condition (Figure 28D). These data show that Notch signalling is autonomously required in TNC for identity allocation. Upon loss of Notch signalling TNC develop as a homogeneous population of follower-like cells, which impairs collective chain migration.

Figure 26

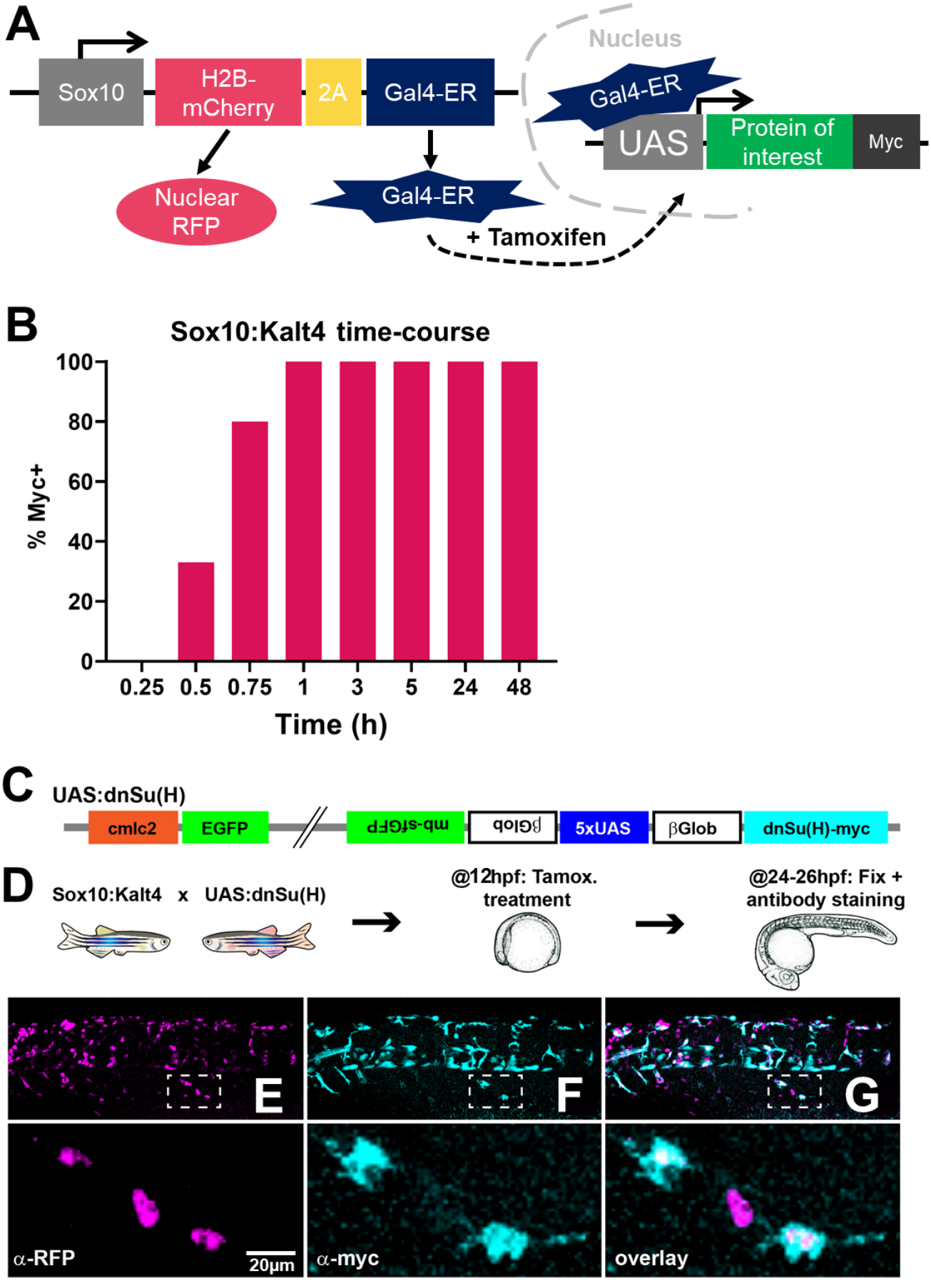
A
Sox10
H2B-mCherry
2A
Gal4-ER
Nuclear RFP
Gal4-ER
Nucleus
Gal4-ER
UAS
Protein of interest
Myc
+ Tamoxifen
B
Sox10:Kalt4 time-course
% Myc+
100
80
60
40
20
0
0.25
0.5
0.75
1
3
5
24
48
Time (h)
C
UAS:dnSu(H)
cmlc2
EGFP
mb-sfGFP
βGlob
5xUAS
βGlob
dnSu(H)-myc
D
Sox10:Kalt4 x UAS:dnSu(H)
@12hpf: Tamox. treatment
@24-26hpf: Fix + antibody staining
E
F
G
α-RFP
20μm
α-myc
overlay

Figure 26: Neural crest specific and time inducible gene expression system.

(A) Schematic of the Sox10:Kalt4ER construct showing Gal4ER expression under the control of the Sox10 promoter. Gal4ER is retained in the cytoplasm and only activated by nuclear translocation upon tamoxifen addition.

(B) Time-course Sox10:Kalt4ER induction of expression upon tamoxifen addition. All transgenic embryos express the UAS driven protein after 1h (0.25h n=20, 0.5h n=27, 0.74h n=25, 1h n=22, 3h n=18, 5h n=20, 24h n=14 and 48h n=10 embryos).

(C) Schematic of the UAS:dnSu(H) construct used to generate the transgenic line.

(D) Diagram of experimental procedure used for inducible Notch LOF in NC only.

(E, F, G) Confocal images of myc immunostaining in TNC after tamoxifen addition at 12hpf in Sox10:Kalt4ER X UAS:dnSu(H) 24hpf embryos. **(E)** RFP in magenta. **(F)** myc in cyan. **(G)** Overlay. White square marks the enlarged area. Anterior left, dorsal top.

Figure 27

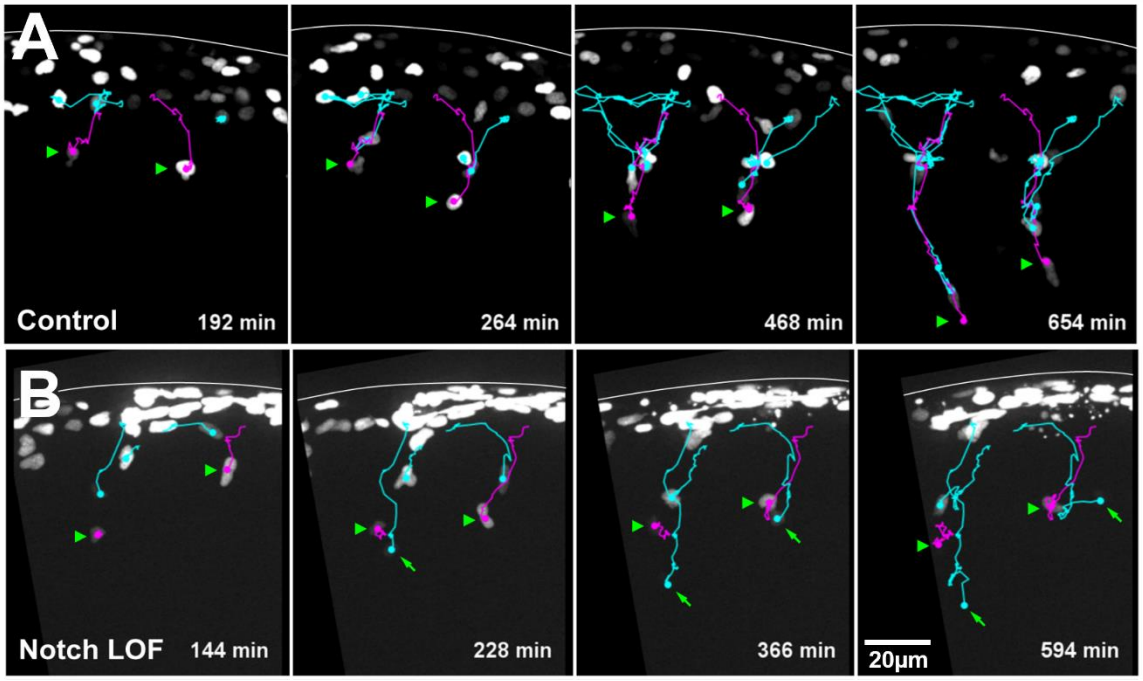
A
Control
192 min
264 min
468 min
654 min
B
Notch LOF
144 min
228 min
366 min
20µm
594 min

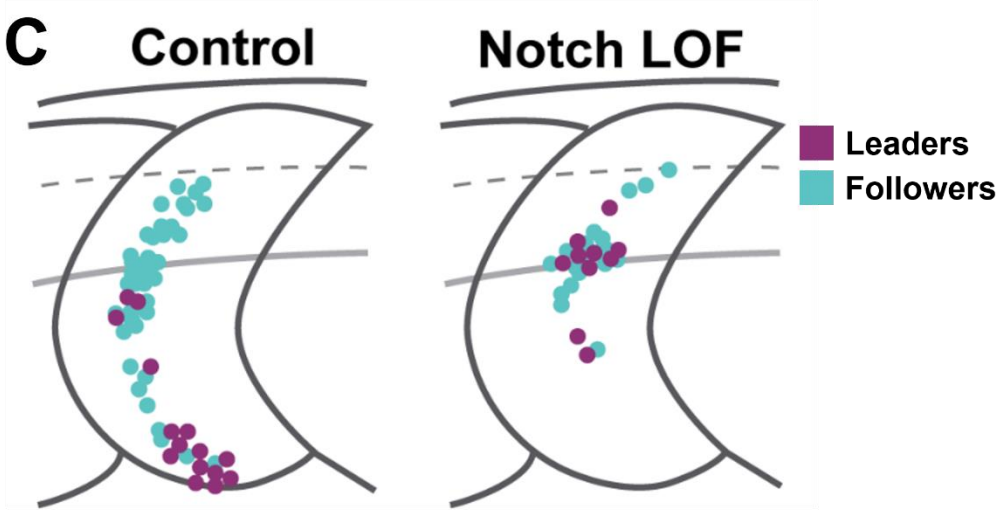
C
Control
Notch LOF
Leaders
Followers

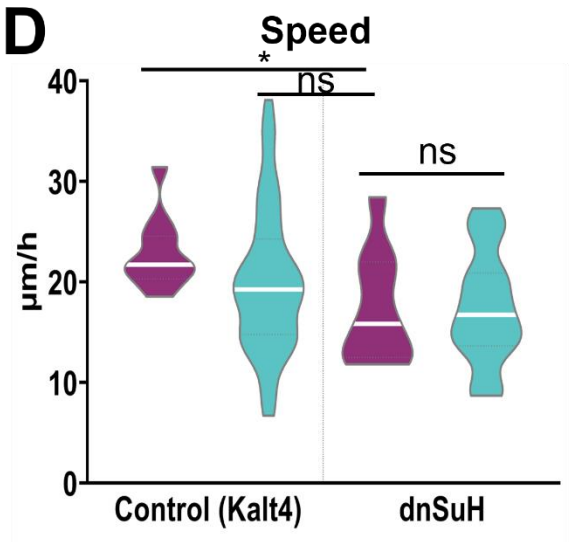
D
Speed
*
ns
ns
40
30
20
10
0
µm/h
Control (Kalt4)
dnSuH

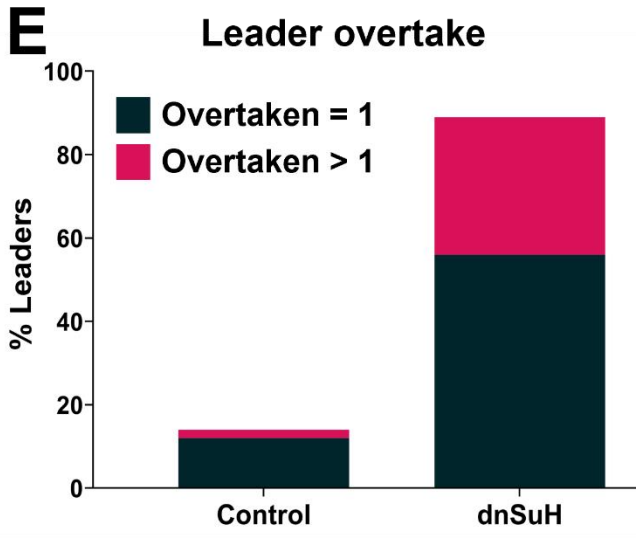
E
Leader overtake
100
80
60
40
20
0
% Leaders
Overtaken = 1
Overtaken > 1
Control
dnSuH

Figure 27: TNC autonomous Notch loos of function disrupt collective migration.

(A) Selected frames from in vivo time-lapse of control (Sox10:Kalt4) embryos from 16-26hpf.

(B) Selected frames from in vivo time-lapse of Notch LOF exclusively in NC (Sox10:Kalt4 xUAS:dnSu(H)) from 16-26hpf.

Leader tracked in magenta, followers in cyan. Solid white line indicates the dorsal border of the embryo. Green arrowheads indicate leader cells; green arrows indicate overtaking followers.

(C) Schematic of model embryo showing end positions of leader and follower cells under control (Sox10:Kalt4, leaders n=18, followers n=57, from 7 embryos) and Notch LOF conditions (Sox10:Kalt4 xUAS:dnSu(H), leaders n=10, followers n=19, from 5 embryos).

(D) Quantification of cell speed in control (leaders n=11, followers n=55, from 3 embryos) and Notch LOF conditions (leaders n=10, followers n= from 20, from 5 embryos. Unpaired t test, Control leaders vs Notch LOF leaders p=0.0142, control followers vs LOF followers p=0.2811, LOF leaders vs LOF followers p=0.9777.

(E) Quantification of leader overtaken by follower cells. Only once (overtaken=1) or overtaken more than one time (overtaken>1) in control (Sox10:Kalt4) and Notch LOF conditions (Sox10:Kalt4 xUAS:dnSu(H). Overtaken once: Sox10:Kalt4 12% (n=5/42 cells from 14 embryos), Sox10:Kalt4 xUAS:dnSu(H) 56% (n=5/9 cells from 5 embryos); overtaken>1: Sox10:Kalt4 3% (n= 1/42 from 14

Figure 28

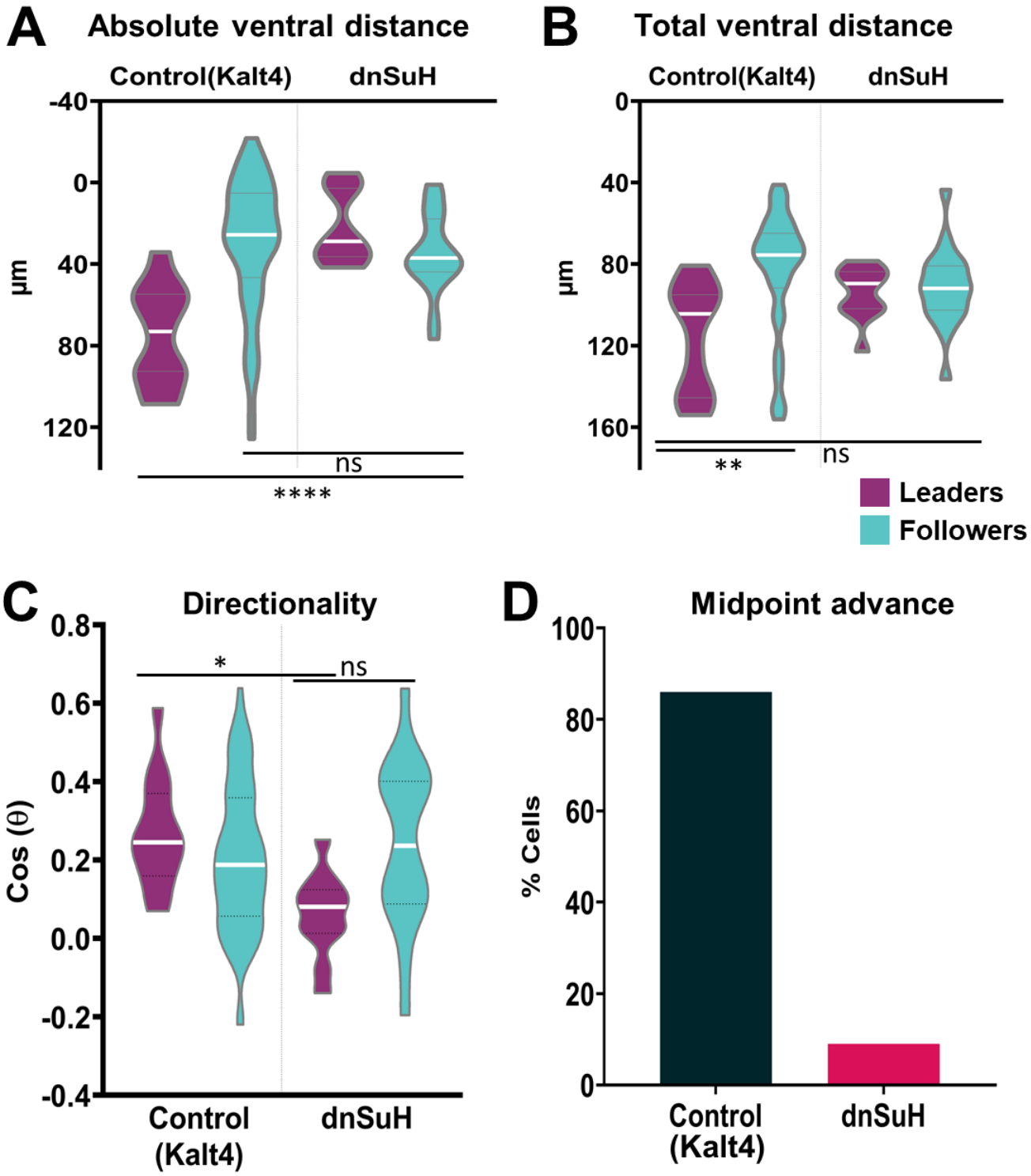
A
Absolute ventral distance
Control(Kalt4)
dnSuH
-40
0
40
80
120
µm
ns
****
B
Total ventral distance
Control(Kalt4)
dnSuH
0
40
80
120
160
µm
**
ns
Leaders
Followers
C
Directionality
0.8
0.6
0.4
0.2
0.0
-0.2
-0.4
Cos (θ)
*
ns
Control
(Kalt4)
dnSuH
D
Midpoint advance
100
80
60
40
20
0
% Cells
Control
(Kalt4)
dnSuH

Figure 28: TNC autonomous Notch LOF decreases directionality and ventral advance of leaders and followers.

(A) Quantification of absolute ventral distance under control (Sox10:Kalt4; leaders n=11, followers n=55 cells from 3 embryos) and Notch LOF conditions (Sox10:Kalt4 xUAS:dnSu(H); leaders n=11, followers n=19 from 5 embryos). One-way ANOVA, control leaders vs all $p<0.0001$, control followers vs dnSuH leaders and followers $p=0.8121$.

(B) Quantification of total ventral distance under (Sox10:Kalt4; leaders n=11, followers n=55 from 3 embryos) and Notch LOF conditions (Sox10:Kalt4 xUAS:dnSu(H); leaders n=11, followers n=19 from 5 embryos). One-way ANOVA, control leaders vs followers $p=0.0025$, control leaders vs dnSuH leaders and followers p=0.2409.

(C) Directionality correlation quantification under control (Sox10:Kalt4; leaders n=14, followers n=78 from 5 embryos) and Notch LOF conditions (Sox10:Kalt4 xUAS:dnSu(H); leaders n=11, followers n=19 from 5 embryos). Brown-Forsythe test, control leaders vs dnSuH leaders $p=0.0144$, dnSuH leaders vs followers $p=0.1327$.

(D) Quantification of leader cells that advance past the neural tube/notochord boundary under control (Sox10:Kalt4; 30/35 leaders in 11 embryos) and Notch LOF conditions (Sox10:Kalt4 xUAS:dnSu(H) n=1/11 leaders in 5 embryos).

2.5 TNC autonomous overactivation of Notch result in migratory alterations

Next, we tested the effect of Notch overactivation (GOF) on TNC migration. Using a similar strategy, Notch intracellular domain (NICD) was overexpressed only in NC by addition of tamoxifen to Sox10:H2B-mCherry-Kalt4ER; UAS:NICD embryos. Following Notch signalling overactivation, TNC initiate migration normally but, as in Notch LOF and inhibition conditions, leaders are overtaken by follower cells (Figure 29A, B and E). Also, TNC chain coherence is lost and the migration of many cells stalls at the neural tube/notochord boundary (Figure 29C). Under GOF conditions, both leaders and followers TNC present increased speed similar to the control leader cells (Figure 29D). Also, the absolute and total ventral distance (Figure 30A and B) covered by Notch GOF cells are similar to control conditions, albeit it takes GOF cells longer to reach their final sites due to

the loss of group coherence, leaders overtaking events and reduced directionality of followers (Figure 30C). Upon Notch GOF, leaders midpoint advance is impaired with only 61% of leader migrating past the midpoint, compared to 86% of leaders in control condition (Figure 30D). This shows that upon Notch overactivation in all TNC, these cells adopt a leader-like identity, which is the opposite of the observed effect under Notch LOF. Taken together, these results demonstrate that Notch signalling is autonomously required in TNC for identity allocation and collective chain migration. Cells presenting high levels of Notch activity show leader-like characteristics and cells lacking this signalling become follower-like. Alteration of Notch levels in the TNC population leads to the establishment of a homogeneous population of leaders or followers, and in both cases migration is impaired.

Figure 29

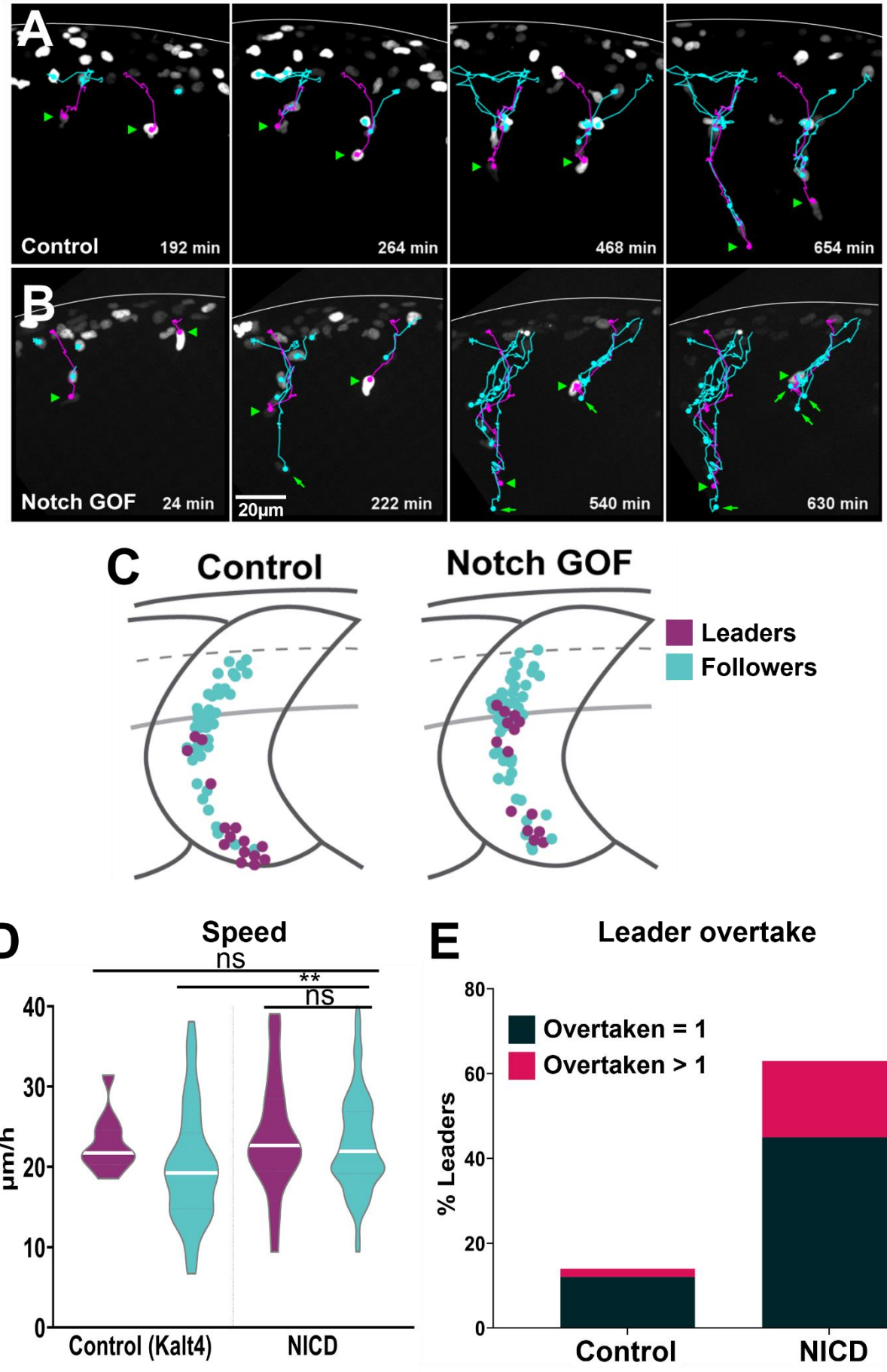
A
Control
192 min
264 min
468 min
654 min
B
Notch GOF
24 min
20µm
222 min
540 min
630 min
C
Control
Notch GOF
Leaders
Followers
D
Speed
ns
**
ns
µm/h
40
30
20
10
0
Control (Kalt4)
NICD
E
Leader overtake
Overtaken = 1
Overtaken > 1
% Leaders
80
60
40
20
0
Control
NICD

Figure 29: TNC autonomous Notch gain of function disrupt collective migration.

(A) Selected frames from in vivo time-lapse of control (Sox10:Kalt4) embryos from 16-27hpf.

(B) Selected frames from in vivo image of Notch GOF exclusively in NC (Sox10:Kalt4 xUAS:NICD) from 16-27hpf.

Leader tracked in magenta, followers in cyan. Solid white line indicates the dorsal border of the embryo. Green arrowheads indicate leader cells; green arrows indicate overtaking followers. Anterior left, dorsal top.

(C) Schematic of model embryo showing end positions of leader and follower cells under control (Sox10:Kalt4, leaders n=18, followers n=57, from 7 embryos) and Notch GOF conditions (Sox10:Kalt4 x UAS:NICD, leaders n=24, followers n=90 from 5 embryos).

(D) Quantification of cell speed in control (Sox10:Kalt4, leaders n=11, followers n=55, from 3 embryos) and Notch GOF conditions (Sox10:Kalt4 x UAS:NICD, leaders n=23 and followers n=114 from 5 embryos). Unpaired t test, control leaders vs Notch GOF followers p=0.9803, control followers vs GOF followers p=0.0074, GOF leaders vs GOF followers p=0.4960.

(E) Quantification of leader overtaken by follower cells. Only once (overtaken=1) or overtaken more than one time (overtaken>1) in control (Sox10:Kalt4) and Notch GOF conditions (Sox10:Kalt4 x UAS:NICD). Overtaken once: Sox10:Kalt4 12% (n=5/42 cells from 14 embryos), Sox10:Kalt4 xUAS:NICD 45% (n=10/22 cells from 9 embryos); overtaken>1: Sox10:Kalt4 3% (n= 1/42 from 14 embryos) and Sox10:Kalt4 xUAS:dnSu(H) 18% (n= 4/22 from 9 embryos). Data acquired by

Figure 30

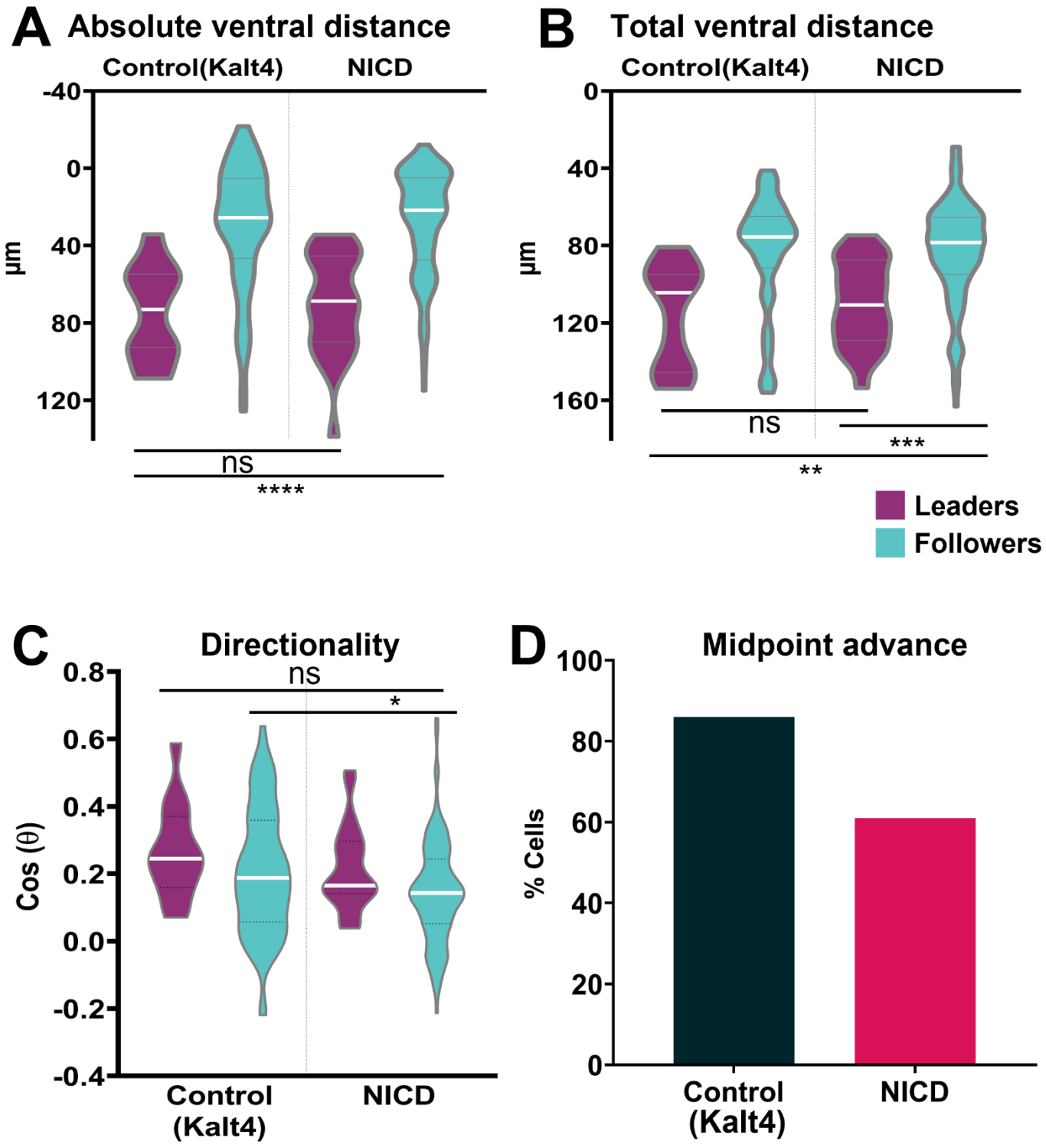
A
Absolute ventral distance
Control(Kalt4)
NICD
-40
0
40
80
120
µm
ns
****
B
Total ventral distance
Control(Kalt4)
NICD
0
40
80
120
160
µm
ns
***
**
Leaders
Followers
C
Directionality
ns
*
0.8
0.6
0.4
0.2
0.0
-0.2
-0.4
Cos (θ)
Control (Kalt4)
NICD
D
Midpoint advance
100
80
60
40
20
0
% Cells
Control (Kalt4)
NICD

Figure 30: TNC autonomous Notch GOF does not alter the ventral advance, but increases directionality of leaders and followers.

(A) Quantification of absolute ventral distance under control (Sox10:Kalt4; leaders n=11, followers n=55 from 3 embryos) and Notch GOF conditions (Sox10:Kalt4 xUAS:NICD; leaders n= 23, followers n=120 from 5 embryos). One-way ANOVA, control leaders vs control followers and NICD followers $p<0.0001$, control leaders vs NICD leaders $p=0.9756$.

(B) Quantification of total ventral distance under control (Sox10:Kalt4; leaders n=11, followers n=55 from 3 embryos) and Notch GOF conditions (Sox10:Kalt4 xUAS:NICD; leaders n= 23, followers n=120 from 5 embryos). One-way ANOVA, control leaders vs control followers and NICD followers $p=0.0010$, control leaders vs NICD leaders $p=0.9431$, NICD leaders vs followers $p=0.0001$.

(C) Directionality correlation quantification under (Sox10:Kalt4; leaders n=14, followers n=78 from 5 embryos) and Notch GOF conditions (Sox10:Kalt4 xUAS:NICD; leaders n=23, follower n=113 from 5 embryos). Welch's t test, control leaders vs Notch GOF leaders p=0.2356, control followers vs GOF follower p=0.0218.

(D) Quantification of leader cells that advance past the neural tube/notochord boundary under control 86% (Sox10:Kalt4; 30/35 in 11 embryos) and GOF Notch conditions 61% (Sox10:Kalt4xUAS:NICD

2.6 Interaction between Notch and the cell cycle regulate TNC migration

Our data show that communication through Notch signalling is required for leader and follower identity allocation, that cell cycle progression is necessary for migration, and that leader and follower cells progress through the cell cycle at different rates. Next, we asked whether Notch signalling and the cell cycle work in tandem or in parallel to define TNC identity allocation and migratory capacity. First, we analysed the cell division positions upon Notch signalling manipulation. In control conditions, the majority of leader cells divide midway through migration, at the neural tube/notochord boundary, while followers divide in the premigratory area (Figure 31A). Upon Notch LOF, follower cells divide during migration, mostly at the neural tube/notochord boundary (Figure 31B). While upon Notch overactivation, more leader cells divide in the premigratory or dorsal area of the somite than their control counterparts (Figure 31C). These data show that altering Notch signalling results in the loss of

the characteristic division positions of leaders and followers, suggesting that Notch might play a role in regulating cell cycle phase lengths and/or progression.

Figure 31

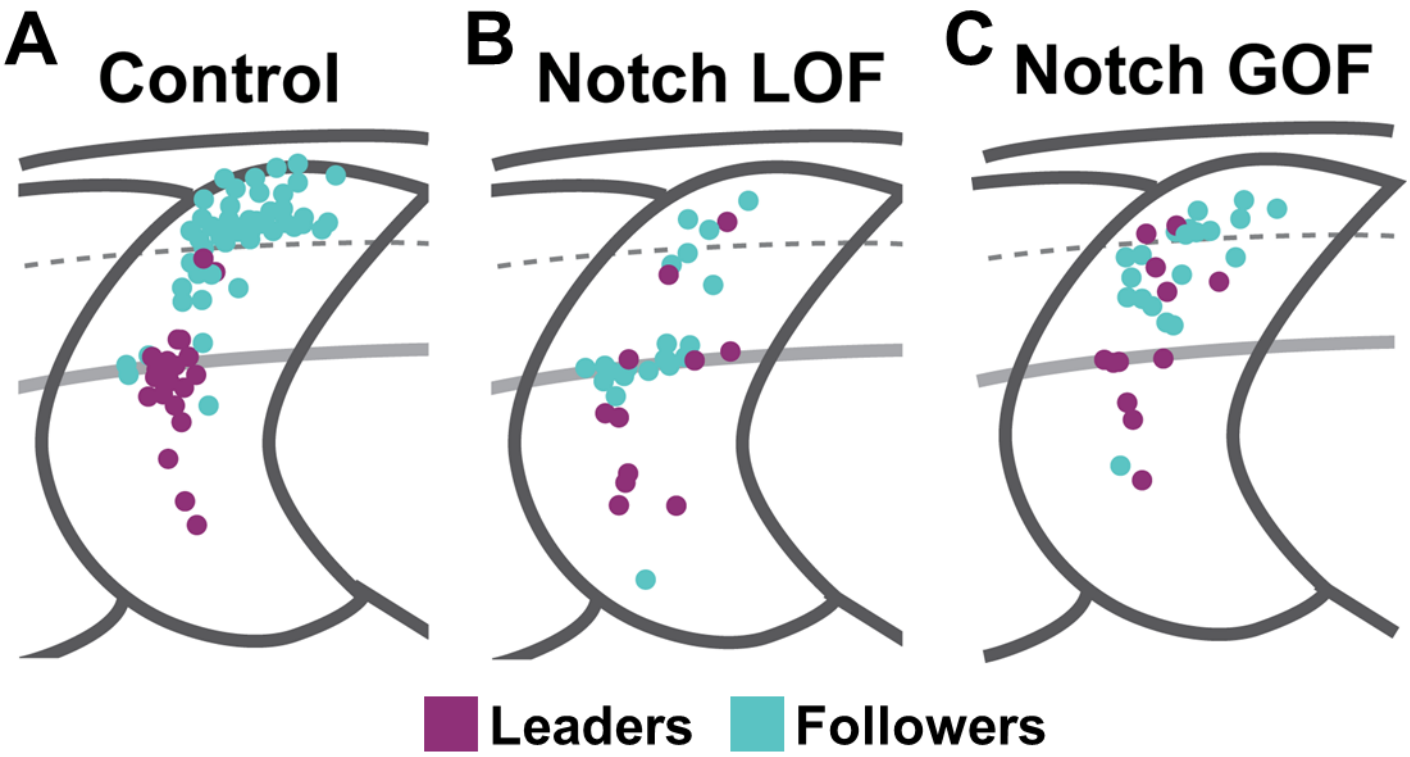

Figure 31: Notch inhibition and overactivation alter the position of leader and follower cell division.

(A, B, C) Schematic of model embryo showing the division positions of leaders (magenta) and followers (cyan) under **(A)** control (Sox10:mG, leaders n=21, followers n=56), **(B)** Notch inhibition (CompE, leaders n=28, followers n=38) and **(C)** Notch GOF conditions (Sox10:Kalt4xUAS:NICD, leaders n=11, followers n=20).

Next, we sought to directly test whether Notch regulates TNC cell cycle dynamics using DNA content analysis to define the number of cells in each phase of the cell cycle in control and Notch inhibition conditions. DNA content analysis measures the amount of DNA of each cell and thus it distinguishes cells in S and G2 from cells in G_1, as the latter present half of the DNA content than the former ((Verduzco and Amatruda, 2011); Figure 32C). To this end, the trunk region of 24hpf Sox10:H2B-Dendra2 embryos was dissected and dissociated into a single cell suspension ((Alhashem et al., 2021); Figure 32A). Cells were labelled with 7-AAD as a viability marker, and Hoechst 33342 was used to measure DNA content. Stained cells were analysed using Fluorescence-Activated Cell Sorting (FACS; Figure 32B), where a series of gates were used to separate viable cells and measure their DNA content. We first eliminated debris from the samples by looking at the size of the particles using the forward and side scatters (Figure 33A), then we gated for singlet cells by looking at the area and width of the side scatter (Figure 33B). This was followed by gating for viable cells using the 7-AAD marker, which does not stain live cells (Figure 33C). For increased scrutiny, a second singlet gating was subsequently performed by looking at the levels of Hoechst labelling, to retain only singlet DNA-stained cells (Figure 33D). Finally, DNA content was determined by quantifying the amount of stained DNA in each cell (Figure 33E). In a typical experiment, we processed between 50-100 embryos and obtained a total of less than 7000 viable cells. In control conditions, the total viable population present the expected cell cycle profile for embryonic cells (Verduzco and Amatruda, 2011): a large G_1 peak (68% of cells), a small G2 peak (10% of cells), and the S-phase being the area between the two peaks (22% of cells; Figure 33E). These data confirm that the dissection, cell dissociation and staining procedure did not affect the cell cycle results. Thereafter, we gated to separate GFP expressing TNC cells. This gating yielded less than 120 TNC cells per experiment (Figure 33F), which is an insufficient number of cells to obtain clear cell cycle profile and infer the

distribution of the cell cycle phases with any statistical significance, hence this analysis was inconclusive.

Figure 32

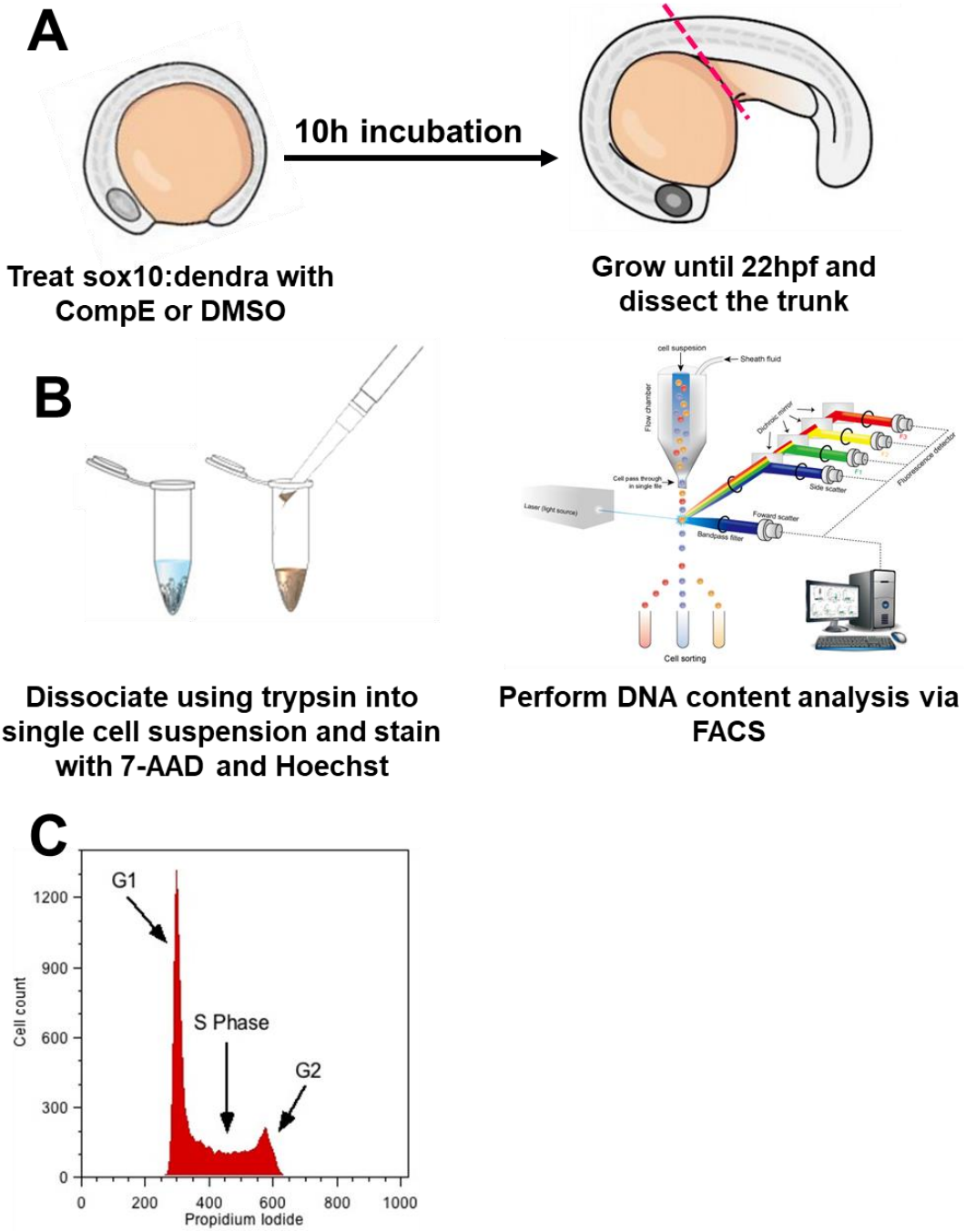

Figure 32: DNA content analysis by FACS procedure.

(A, B) Schematic of the experimental procedure of **(A)** embryo dissection and **(B)** embryo dissociation into single cells and analysis by FACS.

(D) Example graph of the distribution of cell cycle phases obtained by FACS DNA content analysis; adapted from Verduzco and Amatruda, 2011).

Figure 33

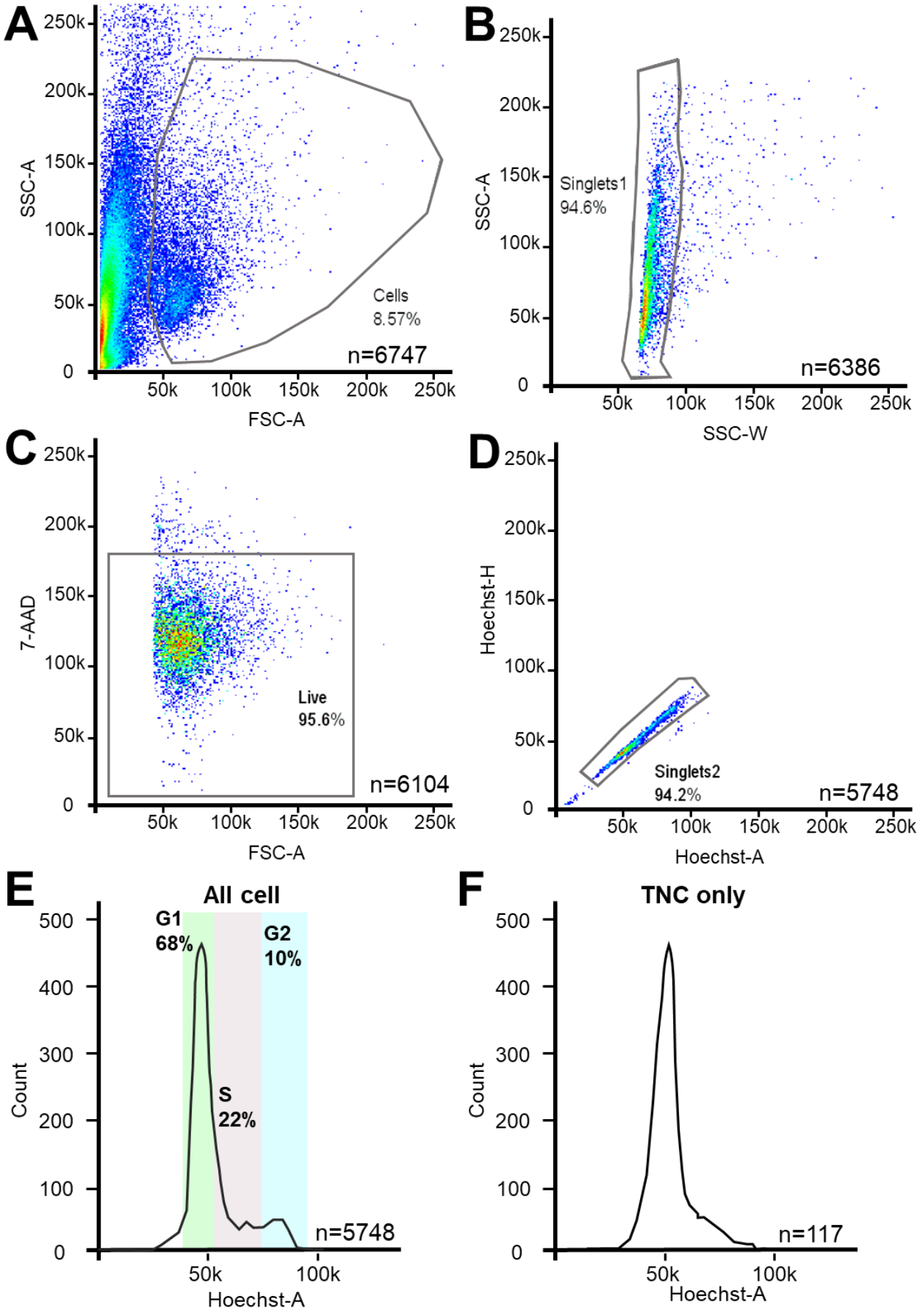
A
SSC-A
FSC-A
Cells
8.57%
n=6747
B
SSC-A
SSC-W
Singlets1
94.6%
n=6386
C
7-AAD
FSC-A
Live
95.6%
n=6104
D
Hoechst-H
Hoechst-A
Singlets2
94.2%
n=5748
E
All cell
G1
68%
S
22%
G2
10%
Count
Hoechst-A
n=5748
F
TNC only
Count
Hoechst-A
n=117

Figure 33: Isolation of TNC by FACS for DNA content analysis.

(A) First gate: cells size separates cells from debris.

(B) Second gate: isolation of singlets cells

(C) Third gate: isolation of live cells using the viability marker 7-AAD.

(D) Fourth gate: isolation of singlet cells stained for DNA with Hoechst.

(E) Distribution of cell cycle phases for all embryonic cells.

(F) Distribution of cell cycle phases for TNC.

FSC-A: forward scatter-area, SSC-A: side scatter-area; n is the number of cells in each gate; SSC-W: side scatter-width.

To solve this issue, we decide to quantify cell cycle progression *in vivo* using the expression levels and localization of the PCNA-GFP fusion protein (see Chapter 1.4). PCNA-GFP shows uniform GFP expression in G_1, intense GFP puncta in S and uniform GFP expression during G2 (Figure 11B and C). First, we analysed the cell cycle phase at which TNC initiate migration. In control conditions, the majority of leaders emigrate in S-phase (77%), while most follower cells initiating migration during G_1 (73%; Figure 34A). In contrast, under Notch inhibition (CompE), the majority of leaders (63%) initiate migration at G_1, while followers initiate migration randomly at different cell cycles phases, 53% of leaders emigrate in S phase, while 41% start movement while in G_1 (Figure 34B). Together these data suggest that Notch signalling regulate TNC cell cycle progression. We hence hypothesised that Notch inhibition may result in an alteration of the total cell cycle duration. Measurements of the time span between two mitotic events showed that the total duration of cell cycle is not altered by CompE treatment. In control embryos, the total cell cycle duration of leaders and followers is 13.6 ± 1.2 hours and 13.3 ± 1.4 hours respectively, which is not significantly different from CompE treated embryos, where leaders' cell cycle duration is 12.9 ± 1.7 hours, and followers' 12.7 ± 1.5 hours (Figure 34C).

We have shown that in control conditions, leader and follower cells progress through the cell cycle at different rates, hence we asked whether Notch inhibition has any effect on the durations of the cell cycle phases. Interestingly, we found that the characteristic profiles of cell cycle progression in leaders and followers are no longer observed under Notch inhibition. In CompE treated embryos, the leader and follower populations present similar distribution of cell cycle phase durations, showing a long G_1 (6.4 ± 1.2 hours for leaders, 6.5 ± 1.5 hours for followers) and a short S-phase (4.1 ± 1.2 hours for leaders, 4 ± 1.4 hours for followers), profiles that are indistinguishable from the control follower population (Figure 34D). The length of G2 and M phases were not significantly different between control and CompE treated leader and follower populations (Figure 34D).

One of the leaders' characteristics is that they present a bigger size than followers, thus we asked if Notch inhibition affects TNC cells size. To this end, we used area measurements as a proxy for cell volume, our logic was that if differences are found in the area of the cells in squared units, volume changes will be even bigger as these are in cubic units. Measurements of cell area under Notch inhibition show that whereas control leaders are bigger than followers (276 ± 52 µm2 and 192 ± 48 µm2 respectively), both Notch inhibited leaders and followers present similar sizes (217.6 ± 77 µm2 and 217 ± 62 µm2 respectively; Figure 34E and F). Together these data show that Notch signalling can regulate cell cycle phase durations in TNC cells and may influence cell size.

Figure 34

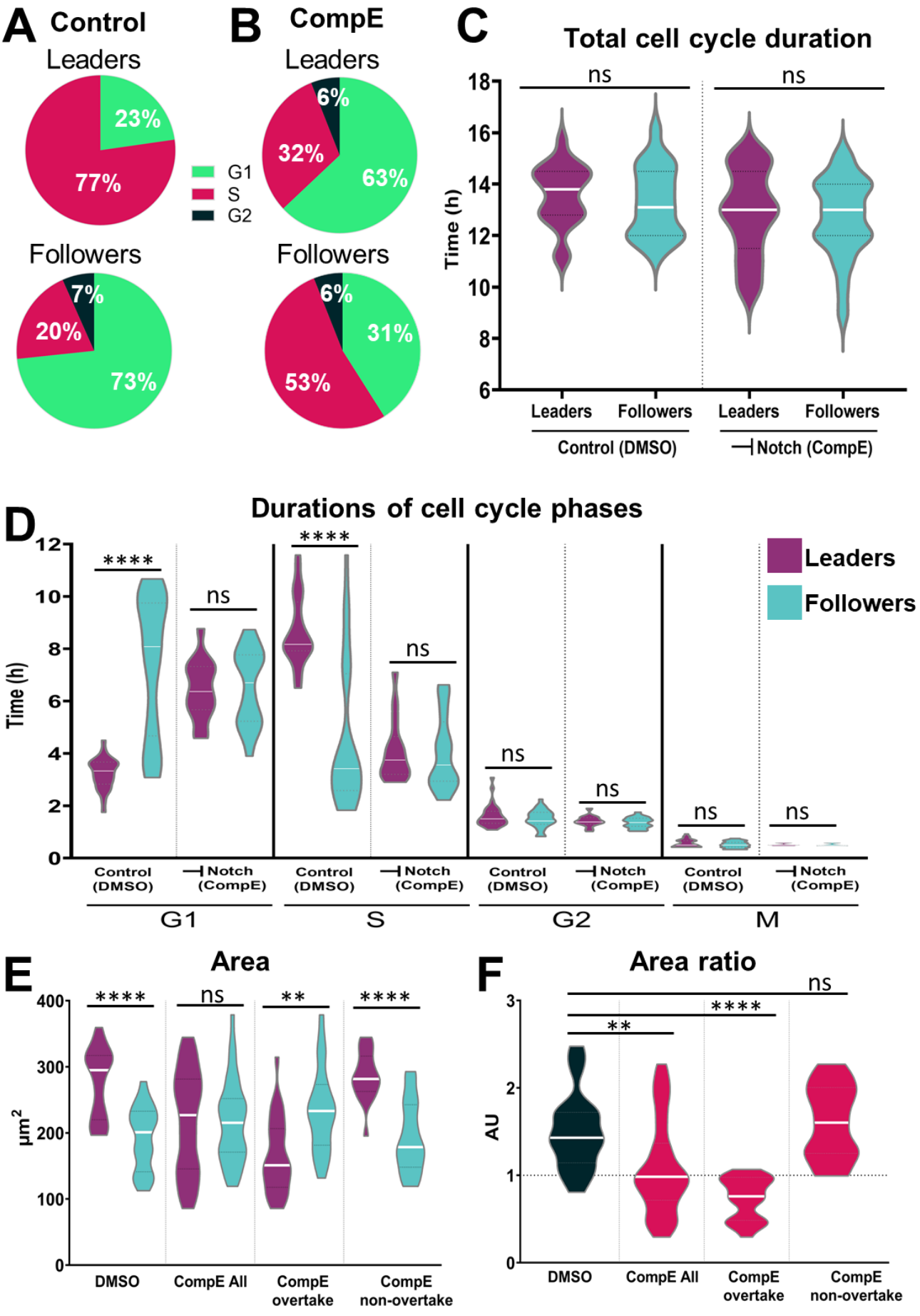
A Control
Leaders
23%
77%
Followers
7%
20%
73%
G1
S
G2
B CompE
Leaders
6%
32%
63%
Followers
6%
53%
31%
C
Total cell cycle duration
Time (h)
ns
ns
Leaders
Followers
Leaders
Followers
Control (DMSO)
Notch (CompE)
D
Durations of cell cycle phases
Time (h)
Leaders
Followers
****
ns
****
ns
ns
ns
ns
ns
Control (DMSO)
Notch (CompE)
G1
S
G2
M
E
Area
µm²
****
ns
**
****
DMSO
CompE All
CompE overtake
CompE non-overtake
F
Area ratio
AU
ns
****
**
DMSO
CompE All
CompE overtake
CompE non-overtake

Figure 34: Notch signalling regulates TNC cell cycle progression.

(A) Quantification of cell cycle phase migration initiation under control conditions (DMSO, leaders n=22, followers n=45).

(B) Quantification of cell cycle phase migration initiation under Notch inhibition conditions (CompE; leaders n=16, followers n=17).

(C) Quantification of total cell cycle length of under control (DMSO, leaders n=20, followers n=19) and Notch inhibition conditions (leaders n=17, followers n=22; one-way ANOVA, p=0.1939.

(D) Quantification of the duration of cell cycle phase length in control (DMSO, sample numbers and statistics are as described in Figure 13) and Notch inhibition conditions (CompE: leaders n=14, followers n=20; Brown-Forsythe and Welch ANOVA tests, all phases G_1, S, G_2 and M p>0.9999 between leaders and followers.

(E) Quantification of cell area in control (DMSO, leaders n=26, followers n=22) and Notch inhibition conditions (CompE, leaders n=44, followers n=41). Brown-Forsythe and Welch ANOVA tests, DMSO leaders vs followers p<0.0001, CompE All leaders vs followers p>0.9999, CompE overtake leaders vs followers p=0.0072, CompE non-overtake leaders vs followers p<0.0001.

(F) Quantification of cell area ratio leaders/followers in control (DMSO) and Notch inhibition conditions (CompE; sample numbers as in E). Brown-Forsythe and Welch ANOVA tests, DMSO vs CompE All p=0.0157, DMSO vs CompE overtake p<0.0001, DMSO vs CompE non-overtake p=0.9829.

2.7 Notch signalling selects more than one leader in the premigratory TNC population

From our migration and cell cycle analysis we concluded that communication between premigratory NC through Notch signalling results in the allocation of leader and follower migratory identities. Cells presenting high levels of Notch activity show leader-like identity (exhibiting high speed and persistence, and long S-phase), while cells with low Notch signalling acquire follower-like identity (lower speed and persistence, and extended G_1). Next, we analysed the frequency distribution of the durations of G_1 and S-phases upon control and Notch inhibited conditions. In control embryos, leader cells present a normal frequency distribution for the duration of G_1 and S-phase. Followers on the other hand, clearly show a bimodal distribution in both G_1 and S-phases with the durations minor median coinciding with the average expected for leader cells (Figure 35A and B). This result is indicative of the presence of two different populations within the follower cells. Quantification of this bimodal distribution shows that 25% of the cells present the characteristic phase duration of leader cells suggesting that one in every four cells in the body of the chain presents leaders' characteristics. Interestingly, upon Notch inhibition the bimodal distribution of G_1 and S-phases durations observed in control conditions is lost. Now leader and follower cells present a normal frequency distribution for G_1 and S-phases that coincides with the major median of the control follower population (Figure 35C and D). These results strongly suggest that Notch signalling between TNC select one leader cell for every three followers, making the body of the chain less homogeneous than previously thought.

Figure 35

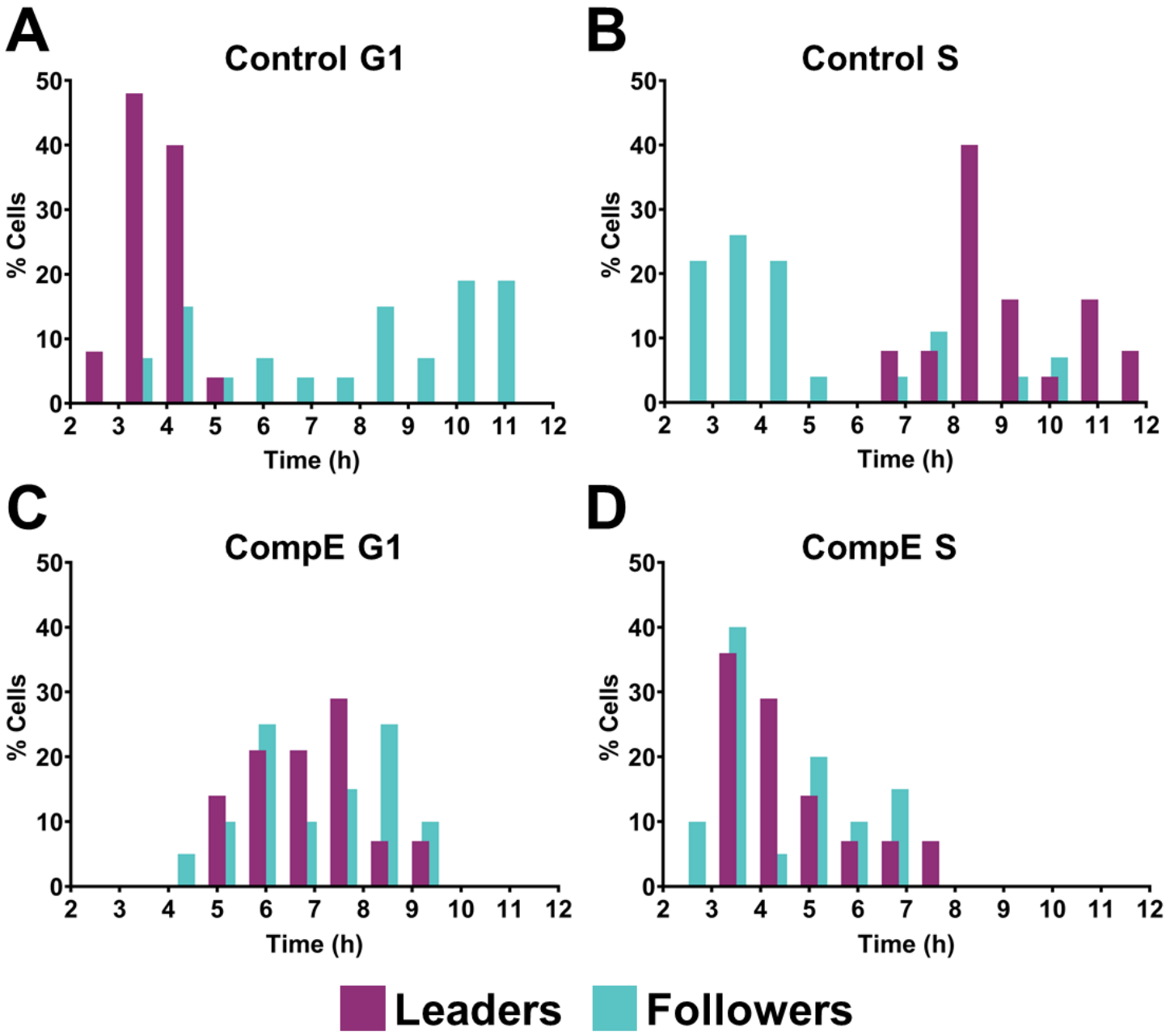

Figure 35: Followers TNC are heterogenous population of cells.

(A, B) Frequency distribution G1- and S-phases length in control conditions (DMSO, leaders: G_1 n=25, S n=25, followers: G_1 n=27, S n=28). Follower cells present a bimodal distribution, while leaders show a normal distribution.

(C, D) Frequency distribution G1- and S-phases length in Notch inhibition conditions (CompE, leaders: G_1 n=14, S n=14, followers: G_1 n=20, S n=20).

Chapter 2: Discussion

Notch regulation of TNC migration

Notch is a versatile and important signalling pathway implicated in tissue patterning, cell specification and differentiation during development and morphogenesis (Bocci et al., 2020; Sjöqvist and Andersson, 2019). Our data show that Notch components are expressed in TNC before and during migration. Using chemical and genetic alteration of Notch signalling, we show that it is required for TNC migratory identity allocation. Accumulation of Notch signalling results in cells acquiring leader-like identity, while cells with low Notch activity behave like followers. Furthermore, differences in Notch activity in leaders and followers influences cell cycle phase lengths.

In line with previous reports (McLennan et al., 2015a; Rios et al., 2011; Cornell and Eisen, 2005, 2002), our data show that Notch components are expressed in TNC prior and during migration. Moreover, Notch signalling is active and required during TNC induction and throughout differentiation (Wiszniak and Schwarz, 2019; Cornell and Eisen, 2005). Nevertheless, the role of Notch during NC migration remains poorly understood . In our work, we established that Notch inhibition leads to the loss of TNC derivatives. Moreover, Notch gain- and loss-of-function result in TNC migratory defects. In accordance, it has been shown that both Notch GOF and LOF lead to migration defects and the lack of cranial, cardiac and trunk NC derivatives in mice (Mead and Yutzey, 2012). However, using different genetic tools, murine cardiac NC have been reported to migrate normally, and only exhibit differentiation defects under Notch LOF conditions (High et al., 2007). These contradictory observations can be explained by differences in the degree of Notch inhibition obtained in the different transgenic models used in these studies. Mead and Yutzey, attained Notch inhibition through the deletion of the Notch1 receptor or the RBP-J protein. While deletion of Notch1 led to minor phenotypes, deletion of the RBP-J transcription factor resulted in the total

inhibition of Notch signalling and presented severe defects in NC migration. High et al, on the other hand, attained Notch signalling inhibition through the overexpression of the dominant negative form of the transcriptional coactivator MALM1 (dnMALM). dnMALM1 binds to the NICD-RBP-J complex but is unable to recruit transcriptional coactivators thus inhibiting transcription activation even in the presence of Notch signalling. Under these conditions cardiac NC migration and differentiation are only mildly affected, showing similar results to the deletion of Notch1 receptor. This strongly suggest that upon overexpression of dnMALM remanent levels of Notch signalling persist explaining the normal migration of cardiac NC. Interestingly, in *Xenopus* embryos inhibition of the Notch downstream component Hairy2, results in the lack of cranial NC migration (Vega-López et al., 2015). Moreover, Notch inhibition has also been shown to block chain invasion in wound healing assays and in cancer cell lines (Konen et al., 2017; Riahi et al., 2015). Taken together and in agreement with our results, these data suggest that appropriate levels of Notch signalling are required for TNC migration

Notch regulates migratory identity allocation

Trunk NC are a heterogenous population of cells consisting of leader and follower cells with different migratory capacity. Notch perturbations negatively affects TNC migration, thus we asked if the observed migratory defects are due to perturbations in leaders/followers identity allocation. Interestingly, we found that both Notch GOF and LOF cause identity allocation defects. Upon Notch GOF and LOF, followers are able to overtake leaders at the front of the group, a phenomenon that does not take place in control conditions indicating that Notch signalling alterations establish an homogeneous TNC population. Notch GOF results in all TNC exhibiting leaders' characteristics, while Notch LOF leads to all TNC becoming followers. These data show that Notch signalling is required for proper identity allocation in TNC.

Notch lateral inhibition is a main mechanism responsible for regulating identity allocation in different systems, from angiogenesis to inner ear patterning (Henrique and Schweisguth, 2019). This mechanism is characterised by the establishment of a negative feedback loop between its components. Activation of the Notch receptor leads to the downregulation of the expression of its ligands (Figure 5). Hence, cells that receive Notch signalling are unable to respond by activating Notch on their neighbours (Bocci et al., 2020; Sjöqvist and Andersson, 2019). An important example of Notch lateral inhibition can be seen in angiogenesis, where endothelial cells adopt either a leading/tip or trailing/stalk cell identities. VEGF signalling induces high expression of the Notch ligand Delta-like 4 in the tip cell, in turns this activates Notch signalling in neighbouring cells downregulating the transcription of the Notch receptors and impeding the activation of Notch signalling back in tip cells. In this manner, tip cells inhibit stalk cells from assuming a tip identity (Blanco and Gerhardt, 2013; Phng and Gerhardt, 2009). While recent studies recognise that intrinsic asymmetry of VEGF and other factors kick start identity allocation in endothelial cells, nonetheless, Notch has been shown to enforce and maintain these initial differences leading to endothelial cells with different identities (Page et al., 2019; Costa et al., 2016). Interestingly, in a similar manner, Notch1-Dll4 signalling combined with mechanical force have been shown to establish leader/follower cell identity allocation during collective cell migration in vitro (Riahi et al., 2015).

In stable epithelia, Notch lateral inhibition generates an alternating pattern of cells with low Notch activity surrounded by cells with high Notch levels. This is the case during inner ear (Daudet and Żak, 2020) and neural development (Bahrampour and Thor, 2020), where perfect mosaics of alternating fates are established. During angiogenesis, Notch lateral inhibition defines leader and follower cell fate (Phng and Gerhardt, 2009), nevertheless, the characteristic mosaic pattern of alternating fates seen in other tissues is absent. Leader cells are interspaced by multiple and varying numbers of followers. Different mathematical models

have been developed to explain this deviation from the classical Notch lateral inhibition mechanism. Some models incorporate Notch regulators that can slowdown fate selection, generating metastable partial leader/follower states (Venkatraman et al., 2016); while others consider initial heterogeneity of Notch receptor levels and the role of tension for signalling, in which case leaders can be interspaced by different number of follower cells (Konen et al., 2017). Similar mechanisms may be at play in TNC, which also deviate from the classical mosaic fate pattern, forming chains with one leader every three follower cells. The fact that Notch signalling is active during NC induction (Cornell and Eisen, 2005), together with the asymmetric division of the leader's progenitor, suggest that initial levels of Notch could vary among premigratory TNC. Moreover, cell migration generates forces that most certainly have an impact on Notch signalling. Together these factors may explain TNC deviation from the perfect alternating mosaic pattern expected from classical Notch lateral inhibition.

While our data show that Notch signalling regulates leader/follower identity acquisition in TNC, the most striking divergence from the classical lateral inhibition model is that leader identity is established by high Notch activity, instead of being induced by low Notch levels as expected. This configuration, in which leaders are defined by high Notch signalling and followers by low, presents a particular problem: it allows follower cells, which maintain Notch ligand expression, to remain in contact. In the classical lateral inhibition mechanism, communication through Notch between follower cells would exacerbate small differences and resolve with one cell presenting high Notch activity and the other low, which is not congruent with our results. Explanation of this conundrum may arise from several factors (Bocci et al., 2020):

(i) Dynamic interactions and regular neighbour exchange among premigratory TNC may minimize communication between follower cells, while variability in cell size and contact surface may further decrease follower-follower interactions (Bajpai et al., 2021).

(ii) Low or lack of Notch receptor expression in followers may result in negligible follower-follower communication via Notch.

(iii) The presence of Notch receptor-ligand pairs with different affinities and the inhibitory interaction of Notch receptors with their ligands within the same cell (cis-inhibition), can also alter the salt and pepper pattern predicted by classical lateral inhibition (Nandagopal et al., 2018; Bray, 2016; del Álamo et al., 2011). Interestingly, computational models show that initial variation in the levels of Notch components and the presence of cis-inhibition can result in the inversion of the expected salt and pepper pattern with the selection of a high Notch signalling cell every three cells with low Notch activity (Formosa-Jordan and Ibañes, 2014), a possibility that would explain all our observations. Differential segregation of Notch components between daughter cells may result from the asymmetric division of the leader's progenitor with the prospective leader sibling inheriting the majority of the Notch receptor, a mechanism that would generate a very clear imbalance and giving an advantage to the larger sibling to become the leader cell. TNC express different Delta and Jagged ligands, which raises the possibility of Notch cis-inhibition playing a role during TNC identity allocation. Also, based on frequency analysis of cell cycle profiles (discussed below), our data show that every three followers, there is a cell with a leader-like profile, which is in agreement with the earlier described computational models (Formosa-Jordan and Ibañes, 2014).

Whether any of these mechanisms are at play in TNC remains to be investigated and will require the direct visualisation of Notch activity at the single cell level in live embryos. Our analysis of existing Notch reporter lines (Moro et al., 2013; Yeo et al., 2007) has not been conclusive, due to strong signal emanating from the neural tube obscuring Notch activity in TNC (not shown). To overcome this issue, a llama-tag NC specific Notch reporter can be generated, where the anti-GFP nanobody sequence is inserted to the endogenous Notch receptor using CRISPR/Cas9 (Bothma et al., 2018). This transgenic line can then be crossed

to existing Sox10:GFP line (Carney et al., 2006). Transcription from the endogenous Notch locus would generate a Notch-tag protein that will bind cytoplasmic GFP, generating a membrane or diffuse fluorescent signal mirroring the receptor localization. Upon receptor activation, the cleaved NICD-tag bound to GFP will translocate to the nucleus, allowing for real-time quantification of nuclear-GFP accumulation in NC. Such system would provide a tissue specific quantitative Notch reporter and circumvent the problems encountered.

Notch regulation of cell cycle

Our results show that Notch signalling regulates TNC cell cycle phase lengths. Upon Notch inhibition all TNC present the characteristic cell cycle phase durations of follower cells. Notch has been shown to regulate proliferation in a cell context dependant manner. In many cases, through the transcriptional induction of Cyclin A and D, and transcriptional inhibition of the CKIs p^{21} and p^{27}. Using the human pancreatic cancer MIA PaCa-2 cell line, it was observed that RB expression was inhibited upon Notch overactivation (Zhang et al., 2018). Moreover, Notch stimulates early osteoblastic proliferation by upregulating cell cycle accelerators, such as cyclin D and cyclin E (Engin et al., 2008). Similarly, in cell lines, Notch induces the expression of cyclin D1 and CDK2, which promote S-phase entry (Ronchini and Capobianco, 2001). On the other hand, Notch inhibition in vitro and in xenografts reduce expression of cyclins D1, E1 and E2, while the cell cycle inhibitor $p21^{cip1}$ is upregulated, resulting in cell cycle arrest in G_1, suggesting that Notch is important to promote cell cycle progression (Tanaka et al., 2009). In breast cancer cells it has been shown that elevated levels of Jag1 directly induces Cyclin D1 transcription and thus promote G1/S transition (Cohen et al., 2010). In a different study of breast cancer cell lines, Notch activation stimulates proliferation and invasion, whereas Notch inhibition decreases Cyclin A and B1 expression causing cell cycle arrest in G2 (Rizzo et al., 2008). During mammalian lens differentiation, Notch LOF leads to low levels of Cyclin D1, D2 and $p27^{kip1}$ thus less cells in S-phase are

detected, while Notch GOF causes higher Cyclin D1 and 2 expression and increased proliferation is observed (Rowan et al., 2008). Likewise, in cardiomyocytes Notch activation induces proliferation by the induction of Cyclin D1 (Campa et al., 2008). In conclusion Notch signalling regulates the G_1/S transition in many systems, a mechanism that could be at play in TNC.

Our analysis of the frequency distribution of G_1 and S durations under control conditions reveals that followers TNC exhibit bimodal distribution where 25% of the cells show leaders' characteristic. Upon Notch inhibition, both leaders and followers show similar G_1 and S durations distribution, which resembles the distribution of control follower cells. This shows that followers are more heterogenous than previously thought and suggest that one every fourth cells in the body of the TNC chain present leaders' characteristics. The fact that the characteristic cell cycle distribution of leaders and followers is lost upon Notch inhibition, where all TNC adopt followers distribution, show that indeed Notch is implicated in regulating cell cycle. This also reinforces our earlier results showing that TNC present follower-like identity upon Notch inhibition.

Cell cycle regulation of Notch signalling

Remarkably, the response of cells to Notch signalling has been shown to be regulated throughout the cell cycle in *Drosophila, c. elegans* and chick embryos. Notch activity can be enhanced during G1/S transition, through the stabilization of NICD, and cells become refractory to signalling during G2/M, by active degradation of NICD (Carrieri et al., 2019; Nusser-Stein et al., 2012; V. Ambros, 1999). This mechanism limits the time window of Notch activity and coordinates cell cycle progression with fate specification (Hunter et al., 2016). Moreover, transcriptional analysis of cells in culture have shown that Notch signalling oscillates throughout the cell cycle (Boström et al., 2017). It may be possible that a similar mechanism generates a positive feedback loop between the cell cycle and Notch signalling in

TNC. Leader cells that are larger and may present higher levels of Notch signalling, would further increase Notch activity as they undergo the G1/S transition. It will be of interest to define whether such a feedback loop is at play in TNC cells.

Notch/cell cycle signalling model

Taken all together it is possible to propose the following scenario (Figure 36). Leaders arise from the asymmetric division of a progenitor cell (Figure 36A), being bigger and possibly inheriting higher Notch activity and/or Notch receptors than followers. Their size primes them to undergo the G1/S transition faster than follower cells, while communication through Notch lateral inhibition enhance their NICD levels (Figure 36B). In turn, Notch activity transcriptionally regulates CDKs, cyclins and CKIs, which further commit leaders to the G1/S transition. In turn the combined activity of CDKs, cyclins and small Rho-GTPases as cells approach S-phase, induce higher motility and increases directional movement. This generates a positive feedback loop as increased levels of branching actin reinforce the signals that activate G_1/S transition via Arp2/3 and coronin1B (Figure 36C). In turn, Notch activity is enhanced at the G1/S transition by stabilization of NICD through cyclins. Small follower cells on the other hand, are required to grow further to undergo the G1/S transition, hence remain in G_1 for longer periods. Moreover, follower cells would present low levels of Notch activity which further delays the G1/S transition. As consequence of being retained in G_1 for longer follower cells present less directional movement. In this way the interaction between Notch signalling and cell cycle progression, generate negative and positive feedback loops that define the identity and migratory behaviours of leader and follower cells, allowing them to migrate normally (Figure 36D and E).

Figure 36

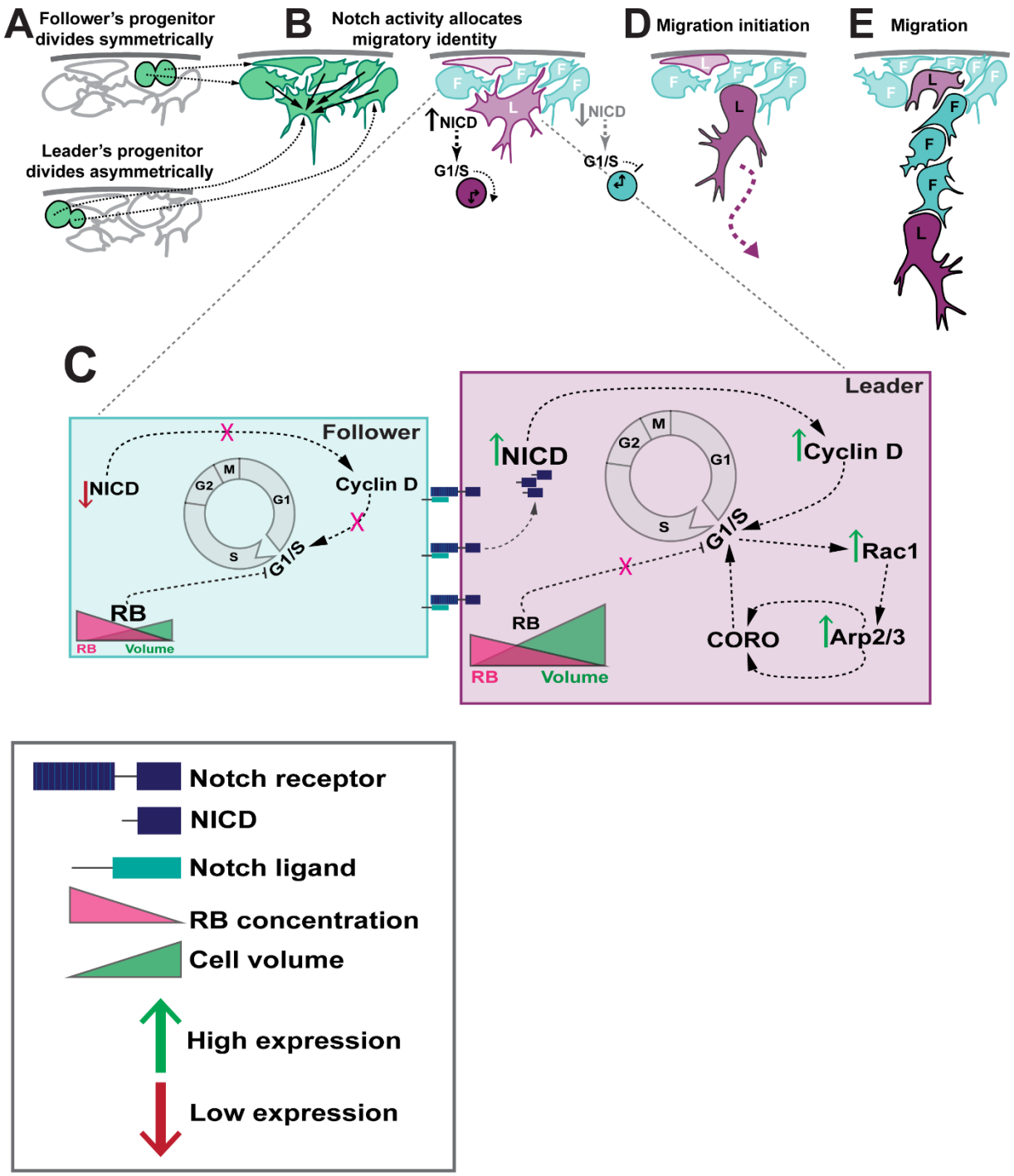

Figure 36: Notch/cell cycle signalling model.

Schematic of **(A)** Progenitor cells dividing in the premigratory area.

(B) Cell-cell communication via Notch fixes leader/follower identities.

(C) Possible mechanism of Notch and cell cycle interactions in leaders and followers.

(D) Leader cell polarising and initiating migration.

(E) Chain migration of TNC.

Progenitors in green, leaders in purple and followers in turquoise. L: Leader, F: Follower, NICD: Notch intracellular domain, Coro: Coronin1B, RB: Retinoblastoma protein.

Chapter 3: Introduction

Asymmetric cell division

Asymmetric cell division (ASD) is a main mechanism of fate determination and a fundamental mean of generating diversity. ASD leads to the formation of two daughter cells with different fates, developmental potentials, and in some cases different sizes. ASD can be extrinsic, whereas the two daughter cells are initially equivalent but acquire different fates as a result of contact with other cells in their environment as seen in the division of ovarian germline stem cells (Dunlop et al., 2014). It also can be intrinsic where the two daughter cells unequally inherit different fate determinants (e.g., RNAs, proteins) as observed in the division of neuroblasts (Gómez-López et al., 2014). Stem cells division is one of the best examples of ASD, in which a stem cell divides giving rise to a new stem cell with self-renewal capacity and a cell that commits to differentiation (Shahriyari and Komarova, 2013). In the *Drosophila* central nervous system, neuroblasts (NB) undergo many rounds of stem cell-like divisions giving rise to a large cell that retains a neuroblast identity, and a smaller cell called the ganglion mother cell (GMC), which divides giving rise to two terminally differentiating neurons (Gönczy, 2008).

ASD involves a large number of proteins that establish a cell polarity, position the spindle and direct the segregation of fate determinants (Chia et al., 2008). Neuroblasts delaminate from the neuroectoderm and assemble an apical complex consisting of Par3, atypical PKC and Par6, in turn this complex binds to an adapter protein, Inscuteable, which recruits a complex consisting of Pins, and G protein coupled subunits Gαi/βγ (Figure 6B; (Chia et al., 2008; Schaefer et al., 2000)). The assembly of these apical complexes establish the polarity of NB, regulating spindle positioning and segregation of determinants. Atypical PKC phosphorylate Numb, an important fate determinant that inhibits Notch signalling and directs its localisation to the basal side of the cell where it associates with other proteins such

as Pon and Miranda, complex that bind to determinants such as Prospero and Brat (Bowman et al., 2008). Together, these complex cascades of signalling result in asymmetric inheritance of determinants and the asymmetric positioning of the mitotic spindle, hence upon division there is a large apical and smaller basal cells. The apical cell retains a NB fate and continue to proliferate, while the basal daughter inherits basal fate determinants such as Numb, down regulates Notch signalling and becomes a GMC committed to differentiation (Gómez-López et al., 2014). The fact that cell polarity is established during interphase, while the segregation of fate determinants directed by the cell cycle kinases such as Aurora and Polo takes place during mitosis, suggest that cell cycle progression plays an important role in events leading to ASD (Wirtz-Peitz et al., 2008).

Many cell types undergo ASD to establish fate differences, including mammalian radial glia cells that generate differentiated neurons and basal progenitors (Noctor et al., 2008); the one-cell *C. elegans* embryo divides asymmetrically into a larger and smaller blastomeres, each with a different fate (Figure 6A; (Cowan and Hyman, 2004)) and the SOP in *Drosophila* (Figure 6C; (Schweisguth, 2015)). Interestingly, recent work has demonstrated that ASD can also play a role in collective cell migration. Endothelial tip cells divide asymmetrically generating two daughters of different sizes the largest of which is more motile. The ASD of the tip cell is mediated by the asymmetric positioning of the spindle which is shifted to the proximal side of the cell. The larger daughter becomes the leading tip cell inheriting higher levels of vegfr activity, which could explain its increased motility as upon inhibiting the pathway, this cell assumes stalk cell motility profiles These data demonstrate the role of ASD in defining the tip/stalk identities (Costa et al., 2016). Since TNC and endothelial cell migration share many common features, it is plausible that ASD may also play a role in the regulation of TNC differentiation.

Figure 6

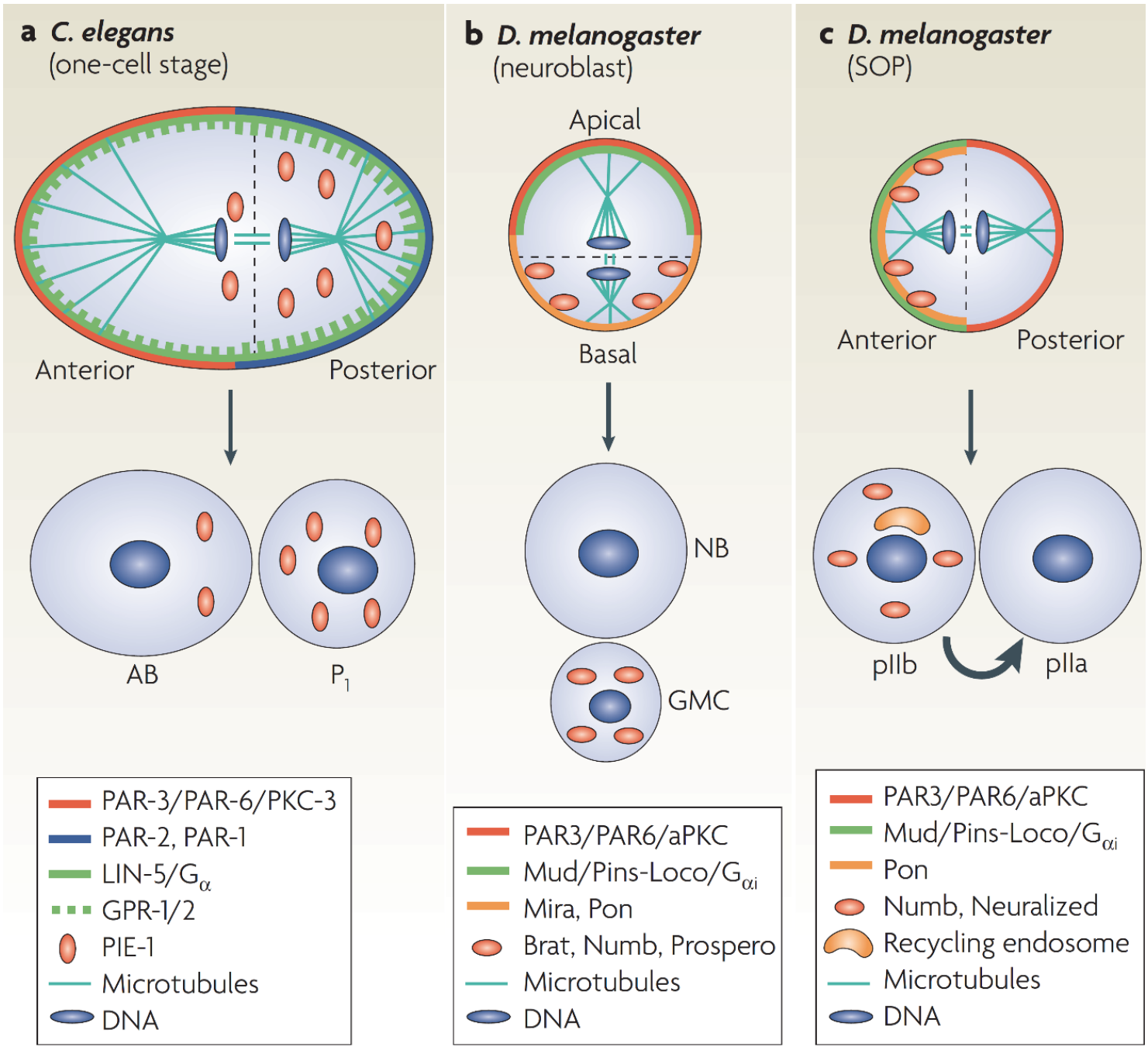
a C. elegans
(one-cell stage)
Anterior
Posterior
AB
P1
PAR-3/PAR-6/PKC-3
PAR-2, PAR-1
LIN-5/Gα
GPR-1/2
PIE-1
Microtubules
DNA
b D. melanogaster
(neuroblast)
Apical
Basal
NB
GMC
PAR3/PAR6/aPKC
Mud/Pins-Loco/Gαi
Mira, Pon
Brat, Numb, Prospero
Microtubules
DNA
c D. melanogaster
(SOP)
Anterior
Posterior
pIIb
pIIa
PAR3/PAR6/aPKC
Mud/Pins-Loco/Gαi
Pon
Numb, Neuralized
Recycling endosome
Microtubules
DNA

Figure 6: Asymmetric cell division.
Schematics of Asymmetric cell division in:
(A) The one cell stage *C. elegans* into AB and P1 cells. Mother cell depicted during anaphase at the top of the panel with proteins polarised to either sides. Polarity proteins PAR-1, PAR-2, PIE-1 and the spindle are positioned to the posterior of the cell, while PAR-3, PAR-6 and PKC-3 are located anteriorly. LIN-5 is present on the cell cortex and its distribution mirrors that of GPR-1/2.
(B) *Drosophila* neuroblasts into NB and GMC. Mira, Pon, Numb, Brat, Prospero as well as the spindle are localised basally, while PAR-3, PAR-6, aPKC and Mud are localised to the apical side. The GMC inherits Numb and its associated partners.
(C) *Drosophila* sensory organ precursor cells (SOPs) into pIIb and pIIa. The spindle is located medially, while Mud, Pon and Numb localised anteriorly and PAR-3, PAR-6, aPKC localised to the posterior of the cell. The anterior daughter pIIb inherits Numb and endosomes.
GMC: ganglion mother cell; NB, neuroblast. Adapted from (Gönczy, 2008).

Trunk neural crest derivatives

Zebrafish TNC that migrate through the medio-ventral route give rise to neurons and glia of the Dorsal Root Ganglia (DRG), Schwann Cells (SC) and neurons of the Sympathetic Chain Ganglia (SCG). The DRG is formed by migrating TNC that stop adjacent to the ventral side of the neural tube where they differentiate. Schwann Cells arise from TNC that migrate more ventrally, which envelop the motoneuron axons and stretch over the length of the somite. SCG is formed by NC that initiate migration first and migrate the longest paths, only stopping adjacent to the Dorsal Aorta (DA) and differentiating into neurons (Raible and Eisen, 1994; Raible et al., 1992).

A long-standing issue in developmental biology is the mechanism by which these diverse arrays of derivatives originate from the TNC. Studies in this field have produced two different models. The first, states that the NC are a multipotent population in which each cell can generate multiple cell-types according to local-cues (Harris and Erickson, 2007). Evidence supporting this theory arise from cell-culture studies of avian (Sieber-Blum and

Cohen, 1980) and mammalian (Shah, 1994; Stemple and Anderson, 1992) NC, which showed that single NC cells are able to generate multiple cell-types such as neurons, glia and pigment cells. Moreover, heterochronic and heterotopic chick-quail grafts experiments demonstrated that NCCs arising from the adrenomedullary region– which normally give rise to sympathetic neurons (SNs) – are capable of producing cholinergic neurons when transplanted into the vagal region (Lièvre and Douarin, 1975; Kalcheim and Le Douarin, 1986). Cell-lineage studies using lysinated rhodamine dextran (LRD) in avian (Bronner-Fraser and Fraser, 1991, 1989, 1988) and *Xenopus* embryos (Collazo et al., 1993) also demonstrate that single NCCs are capable of producing progeny of a variety of different cell-types. Interestingly, multipotent cells with self-renewal capacities have been identified in the adult tissues derived from NC, like the hair follicle in vitro (Sieber-Blum et al., 2004) and the sympathoadrenal (SA) cells of the adult bovine adrenal medulla (Ehrhart-Bornstein et al., 2010; Chung et al., 2009). However, the number of derivatives and self-renewal capacity of these cells have been shown to be reduced with time (Kruger et al., 2002; White et al., 2001). Importantly, recent studies in mouse have shown that NC maintain stem cell capacities during migration. Using the R26R-Confetti mouse model, Baggiolini et al showed that the vast majority of trunk NC are multipotent during both the premigratory and migratory stages (Baggiolini et al., 2015). Together these studies highlight the plasticity and large differentiation potential of NC in vivo.

Nevertheless, different evidence has led to propose that NC are a heterogeneous population of pre-determined cells capable of generating one or few cell-types. Early studies of NC in culture have shown that a major proportion of the NC consists of lineage-restricted cells soon after emergence from the neural tube (Henion and Weston, 1997). In vivo cell-lineage studies in avian (Krispin et al., 2010) and zebrafish (Raible and Eisen, 1994) embryos support previous analysis showing that the premigratory and early migratory NC populations are fate restricted and only capable of generating single cell-type derivatives. Moreover,

experiments in avian embryos suggest that the dorsolateral migratory-path, between the somites and the overlying non-neural-ectoderm, contains only NC specified as pigment cells (Erickson and Goins, 1995). Together these data has led to the proposition that early NC fate-restriction is the mechanisms that defines NC migratory path selection. However, this has been put into question by experiments suggesting that entry into a migratory route occur due to the time-sensitive removal of inhibitory signals and the presence of permissive environment (Leonard and Taneyhill, 2020; Jesuthasan, 1996).

Differences between the proposed models of NC fate determination may arise from the limitations of the techniques and the differences in the animal models used. Although cell-culture allows for cell-behaviour to be studied in a controlled environment, the culture medium is an artificial environment which may contain factors that bias NC differentiation and behaviour. While, in vivo studies are preferred, as cellular environments remain unperturbed, some of these also present limitations. In cell-lineage analysis only small numbers of cells can be labelled for study. As a result, the failure to observe NCCs which display multipotency may simply be due to the lack of labelling in that particular population. Therefore, it is necessary to study NC multipotency in vivo using alternative approaches.

Our data show that leaders and followers TNC exhibit different migratory capacities and sizes, divide at distinct positions in the embryo and progress through the cell cycle differently. It is clear that leaders and followers are starkly different, which raises an important question of whether these migratory identity differences result in differences in the differentiation capacities of these cells.

Figure 7

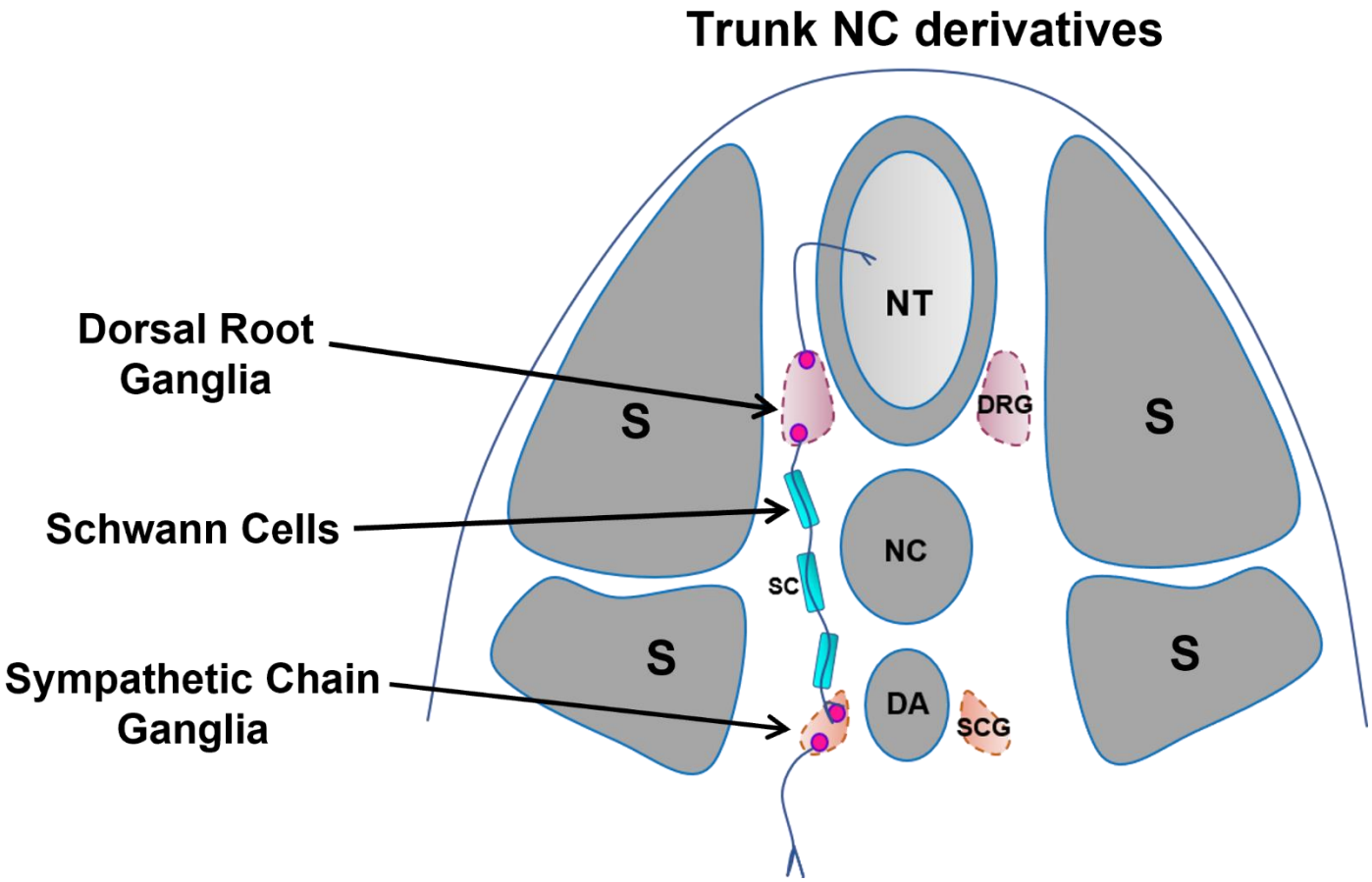

Figure 7: Trunk neural crest derivatives.

Illustration of a transverse section showing the derivatives medially migrating TNC contribute to and their axial level within the dorso-ventral axis.

NT: neural tube, DRG: dorsal root ganglia, NC: notochord, SC: Schwann cells, DA: dorsal aorta, SCG: sympathetic chain ganglia. S: somites

Chapter 3: Results

TNC divisions and long-term fate

3.1 Leaders TNC undergo asymmetric cell division

TNC migrate in coherent chains with leader cells retaining the front position of the group and followers forming the body of the chain. Interestingly, TNC undergo division while moving, which does not seem to alter the coherence of the group nor its migration. Here, we investigated how leader and follower cells divide as they migrate and what effect these mitotic events have on their collective movement.

In many tissues, cell division is characterised by cell rounding, where cells become spherical and push against their environment to create space for spindle formation (Taubenberger et al., 2020). Nevertheless, during angiogenesis tip cells retain polarisation upon cytokinesis, leading to an ASD event important for tip/stalk identity allocation (Costa et al., 2016). To define if this is the case in migrating TNC we performed live imaging of Sox10:mG transgenic embryos and analysed morphological and migratory parameters of dividing cells and their daughters.

First, we studied whether TNC undergo cell rounding upon division. Leader cells are extremely elongated during migration, sending long membrane protrusions in the direction of migration. Strikingly, this polarised morphology is retained throughout cytokinesis (Figure 37A). Follower cells on the other hand, present more typical morphologies upon division, undergoing cell rounding prior to cytokinesis (Figure 37B). Following leaders and followers divisions, we termed the daughter cell closest to the dorsal side of the embryo the Proximal cell, while the daughter closest to the ventral side of the embryo is termed the Distal cell. To quantify morphological differences, we measured the cell circularity of sibling cells after division as a shape descriptor. Circularity scale ranges from 0 to 1, where 0 is an elongated

polygon and 1 is a perfect circle. We found the leaders' Distal daughters to be more elongated than the Proximal ones, 0.45 ± 0.17 for the former and 0.60 ± 0.14 for the latter (Figure 38D). While followers' Distal and Proximal daughters presented similar circularity at 0.69 ± 0.16 (Figure 38E). These differences can be clearly observed when plotting circularity ratio (Figure 38F), and suggest that leader cells may undergo an ASD, while followers may divide symmetrically. Next, we analysed whether leader and follower cells differ in their angles of division. To this end we measured the angle of the mitotic plane with respect to the direction of migration. We found that the majority of leader cells divided perpendicular to the direction of migration (on average 106 ± 20°; Figure 37C), resulting in one front (Distal) and one rear (Proximal) daughters aligned in the direction of migration at birth . Follower cells show a distribution of division angles, mostly dividing parallel to the direction of migration (70% divided at an angle ≥143 ± 25°; Figure 37D), which results in the two daughter cells having similar positions in respect to the rest of the group.

Figure 37

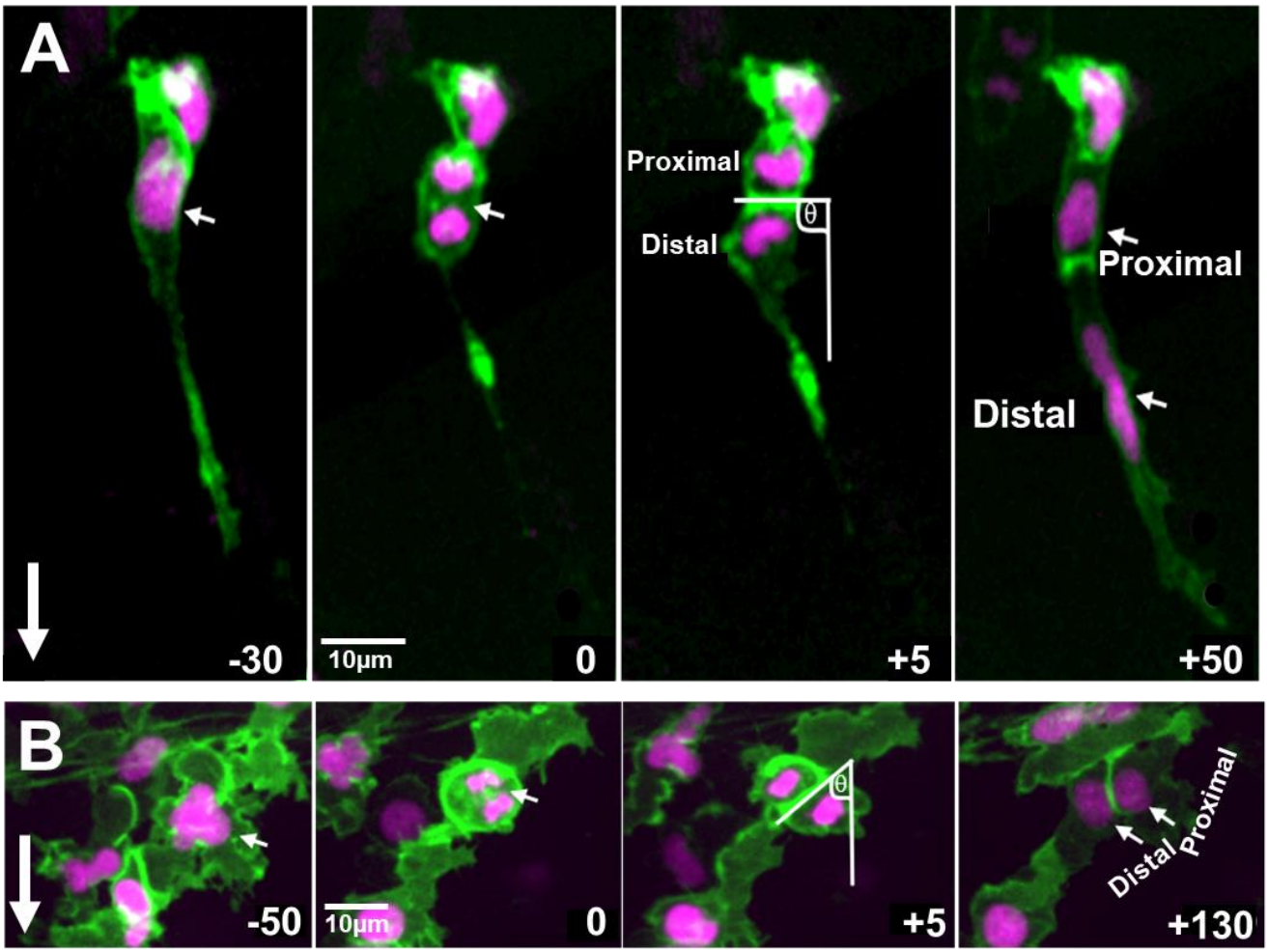
A
Proximal
Distal
θ
Proximal
Distal
-30
10μm
0
+5
+50
B
-50
10μm
0
θ
Distal
Proximal
+5
+130

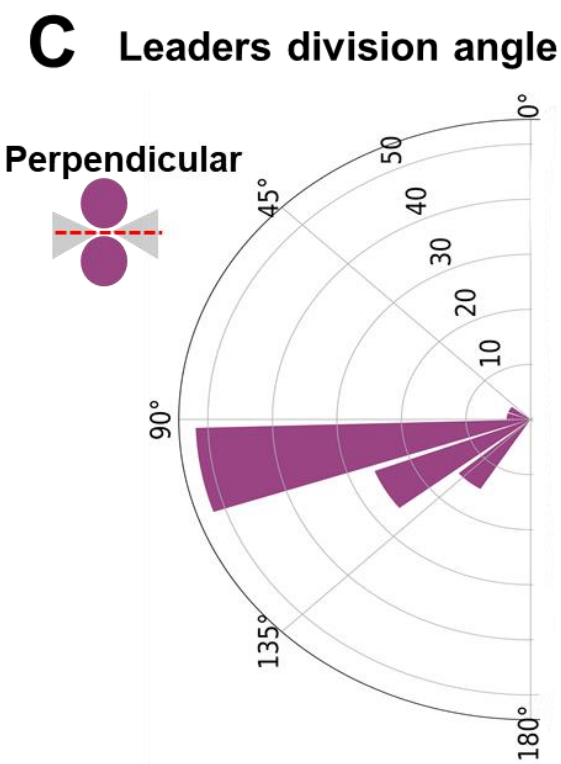
C Leaders division angle
Perpendicular
0°
45°
90°
135°
180°
10
20
30
40
50

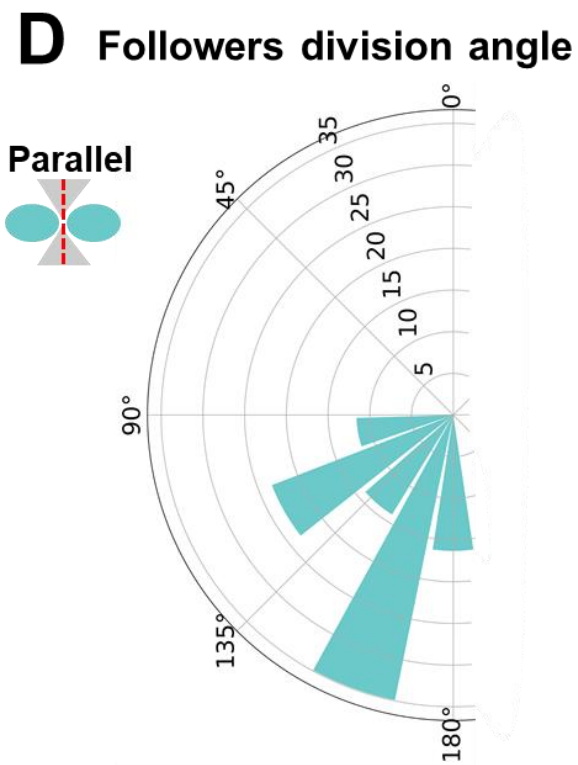
D Followers division angle
Parallel
0°
45°
90°
135°
180°
5
10
15
20
25
30
35

Figure 37: Leader cells retain an elongated morphology during mitosis, while followers round up before division.

(A, B) Confocal images of **(A)** leaders or **(B)** followers undergoing mitosis; small arrows point to leader or follower and their daughters; large vertical white arrow indicates the direction of migration; in the third frame the angel of the mitotic plane is depicted; time in minutes.

(C, D) Quantification of the division plane angles of **(C)** leaders or **(D)** followers measured (leaders n=27, followers n=43).

One characteristic of many asymmetric divisions is these result in two daughters of different sizes (Roubinet and Cabernard, 2014). As leader cells retain their polarized morphology during division and undergo cytokinesis perpendicularly to the direction of movement, we hypothesised that these behaviours may lead to the production of sibling cells of different sizes. To analyse this possibility, we measured the area of leaders' and followers' daughters immediately after cytokinesis. The average size of the leaders' Distal daughters is 130 ± 28 μm^2 , which is 30% bigger than leaders' Proximal daughters at 99 ± 23 μm^2 (Figure 38A). In contrast, followers' Distal and Proximal daughters present similar sizes (93 ± 26 μm^2 and 90 ± 25 μm^2 for Distal and Proximal cells respectively; Figure 38B). This is clearly observed when the area ratio is depicted (area of Distal daughter/ area of Proximal daughter). If both daughters are of equal size their ratio will be 1, if the Distal daughter is larger, the ratio will be >1, while if the Proximal daughter is larger, the ratio will be <1. The area ratio of the Leaders' daughters is 1.4 showing that the Distal Cell is bigger, while followers' area ratio is 1 showing that Distal and Proximal Cells have similar sizes (Figure 38C). Cell areas were measured in 2D, which is not trivial especially when cell membranes overlap making it difficult to assert where one cell start and the other ends. To confirm the area differences between the leaders' daughters after division, we measured cell volume of the leader before division and of their daughters after division. To this end, higher resolution images (1 µm Z-step) were obtained, and volumes were measured in 3D rendering of the cells (Figure 39A).

Leader cells have a volume of 978 ± 27 μm^3 before division and give rise to two daughters of smaller sizes after division (Figure 39B and C). Interestingly, the leaders' Distal cells is 3.8 times bigger than its Proximal siblings (500 ± 42 μm^3 compared to 298 ± 30 μm^3 ; Figure 39B and C). This result show that the volumes of Distal Cells are 3.8 times bigger than their area measurements, while the volumes of Proximal Cells are only 3 times bigger than their area.

Leaders' Distal and Proximal daughters present differences in cell size and shape at birth, we hypothesised that these differences may play a role in the allocation of migratory identity, with the Distal daughter retaining the leader's role, while the Proximal cells becoming a follower. Alternatively, siblings may not present inherited differences, and allocation of migratory identity may depend on interaction between the two siblings. In the former case differences in migratory behaviours (speed and directionality) will be evident immediately after division, in the latter, differences in migratory behaviours will only be observed after a lagging period while the cells define their identities. Previously, we have shown that leaders migrate faster and more directionally than followers (Richardson et al., 2016). Hence, we asked whether the leaders' Distal daughter is faster and more directional than its Proximal sibling, and how long after division are these differences established. Tracking analysis show that on average, the leaders' Distal daughters migrate faster (17.7 ± 4.3 μm/h) than their Proximal siblings (14.2 ± 4.3 μm/h; Figure 39D). Next, we analysed the directionality of migration of leaders' daughters. First, we analysed when these differences in directionality take place and whether these cells are persistent over time. To this end, we measured the directionality ratio, which is a measure of cells' directional persistence over time. We found that leaders' Distal daughters have a higher directionality ratio (0.34 ± 0.10) compared to the less persistent Proximal daughters (0.27 ± 0.11; Figure 39F), and this difference is observed immediately after division. Next, we measured the directional correlation, which compares the actual direction of a cell path to the ideal direction of migration (a straight vertical vector). Positive values indicate cells migrate ventrally in a

directed manner, values close to zero indicate the lack of directionality, while negative values signify that the cells displace but in the opposite direction, retracting dorsally. Leaders' Distal daughters exhibited higher positive directionality (0.1045 ± 0.09; Figure 39E), while proximal daughters show poor directionality with a slightly negative value, indicating this cell retracts dorsally after division (-0.0091 ± 0.10; Figure 39E).

Taken together, our results show that followers' divisions are symmetrical giving rise to daughters with similar characteristics. On the other hand, the leaders' division is an asymmetrical event, where the leaders' Distal daughter retain the leaders' traits while the Proximal cell show characteristics of a follower. Interestingly, the difference in migratory behaviour is observed without any temporal delay after division, suggesting that identity acquisition is immediate upon division.

Figure 38

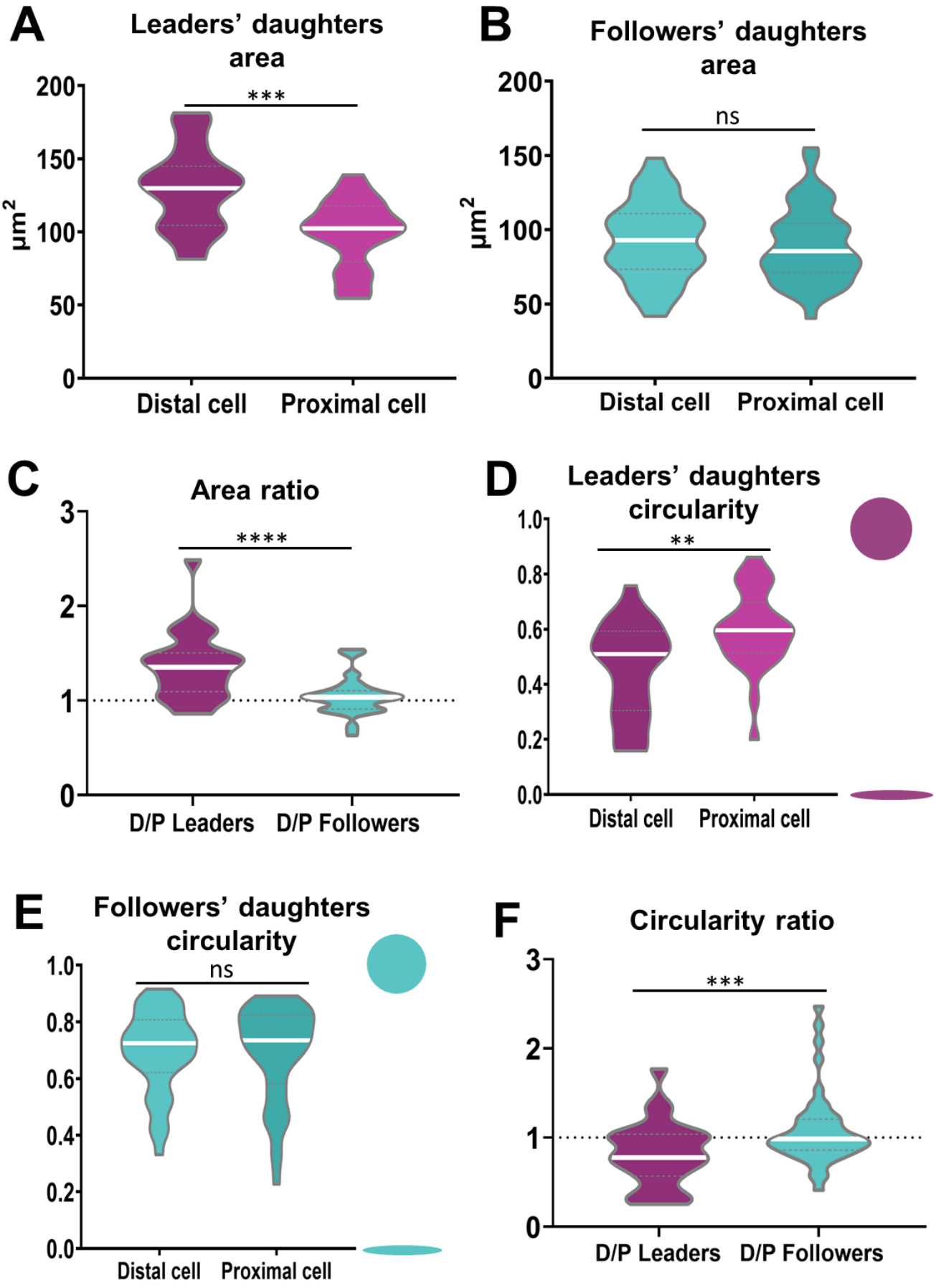
A
Leaders' daughters area
***
200
150
100
50
0
µm²
Distal cell
Proximal cell
B
Followers' daughters area
ns
200
150
100
50
0
µm²
Distal cell
Proximal cell
C
Area ratio
****
3
2
1
0
D/P Leaders
D/P Followers
D
Leaders' daughters circularity
**
1.0
0.8
0.6
0.4
0.2
0.0
Distal cell
Proximal cell
E
Followers' daughters circularity
ns
1.0
0.8
0.6
0.4
0.2
0.0
Distal cell
Proximal cell
F
Circularity ratio
***
3
2
1
0
D/P Leaders
D/P Followers

Figure 38: Leaders divide asymmetrically, while followers undergo symmetric divisions.

(A) Cell area of leaders' daughters quantified immediately after division (n=25; Unpaired t test, p=0.0001).

(B) Cell area of followers' daughters quantified immediately after division (distal n=44; Unpaired t test, p=0.5852).

(C) Distal/Proximal cells area ratio (leaders n=25, followers n=44; Unpaired t test, p<0.0001).

(D) Circularity of leaders' daughters quantified immediately after division. Value of 1 indicate a perfect sphere, 0 indicates an elongated polygon (n=25; Unpaired t test, p=0.0029).

(E) Circularity of followers' daughters quantified immediately after division (n=44; Unpaired t test, p=0.9089).

(F) Distal/Proximal circularity ratio (leaders n=25, followers n=44; Unpaired t test, p=0.0002).

Figure 39

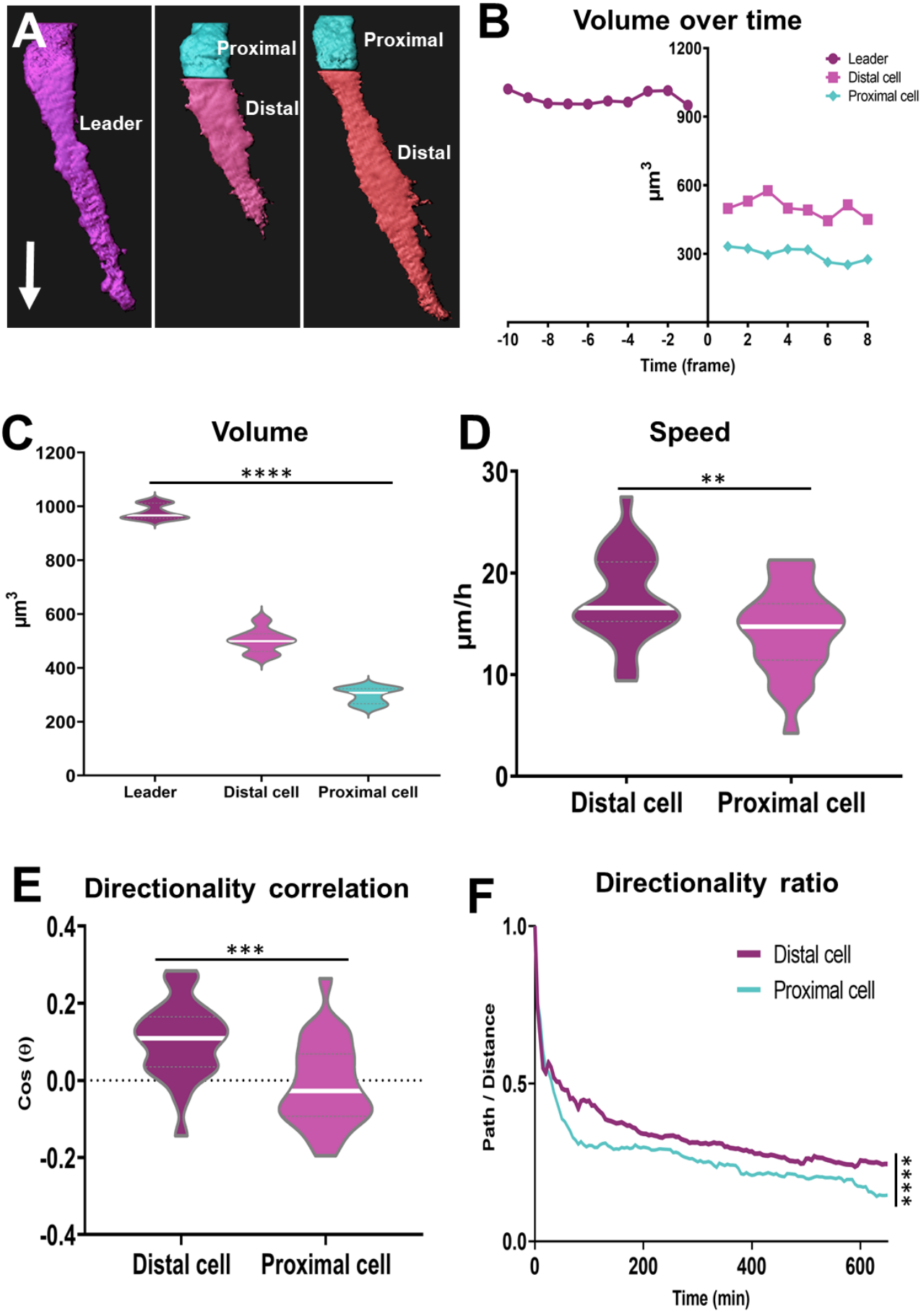
A
Leader
Proximal
Distal
Proximal
Distal
B
Volume over time
Leader
Distal cell
Proximal cell
µm3
1200
900
600
300
-10 -8 -6 -4 -2 0 2 4 6 8
Time (frame)
C
Volume
****
µm3
1200
1000
800
600
400
200
0
Leader
Distal cell
Proximal cell
D
Speed
**
µm/h
30
20
10
0
Distal cell
Proximal cell
E
Directionality correlation
***
Cos (Θ)
0.4
0.2
0.0
-0.2
-0.4
Distal cell
Proximal cell
F
Directionality ratio
Distal cell
Proximal cell
Path / Distance
1.0
0.5
0.0
0
200
400
600
Time (min)
****

Figure 39: Distal leader's daughter retains migratory parameters characteristic of leader cells.
(A) 3D rendering of a leader before and after division (white arrow indicates direction of migration).
(B) Cell volume over time of a representative leader before and after division.
(C) Quantification of cell volume of leaders and its daughters (n=10; Brown-Forsythe and Welch ANOVA tests, $p<0.0001$).
(D) Quantification of leaders' daughters speed (n= 25; Unpaired t test, $p=0.0072$).
(E) Directionality correlation of leaders' daughters (n= 25; Unpaired t test, $p=0.0004$).
(F) Directionality ratio of leaders' daughters (n= 25; Unpaired t test, $p<0.0001$).

3.2 Leaders and followers give rise to different derivatives

Leader and follower cells exhibit different characteristics in terms of morphology, cell cycle progression and mode of division, leading to the question of whether these traits translate into divergent differentiation capacities.

Trunk neural crest migrating into the ventro-medial pathway give rise to neurons and glia of the Dorsal Root Ganglia (DRG), Schwann Cells (SC) and neurons of the Sympathetic Chain Ganglia (SCG). To assess the contributions of leaders and followers to the different TNC derivatives, we aimed to mark individual cells and track their fate over time. To this end, we used Sox10:H2B-dendra2 transgenic line (Figure 40A), in which all NC cells express nuclear-Dendra2 and in which single TNC can be labelled by photo-conversion when illuminated with UV laser (Alhashem et al., 2021). Upon photo-conversion, NC nuclei change fluorescent emission from GFP to RFP (Figure 40B). Using this tool, we photo-converted single leader or follower cells before differentiation (22hpf), re-incubated the embryos and imaged these individually every 24 hours (Figure 40C-E). Although, the RFP signal from photo-converted NC was strong initially, we were not able to clearly distinguish photo-converted cells after 24 hours (Figure 40F and G). Thus, this method was not suited for long term tracking of cells up to differentiation stages. To overcome this issue, we performed long term live imaging of Sox10:mG embryos, tracked leader and follower cells throughout migration to their final

destinations and inferred their fates according to their positions and expression of differentiation markers. TNC originating from somites 7-10 initiate migration around 16hpf, reach their final destinations between 24hpf and 26hpf, and express specific differentiation markers hours or days later, depending on their fate. TNC broadly maintain their relative positions within the migratory chain. Leader cells, that initiate migration first and remain at the front of the chain reach the ventral-most location, halting movement lateral to the dorsal aorta (DA). As leader cells stop their movement, the advance of the cells behind is halted. Follower cells retain their respective positions, and often divide before differentiating (Figure 41A). This behaviour is analogous to a conga line, where each member of the line stops remaining in place when the first person stops.

Figure 40

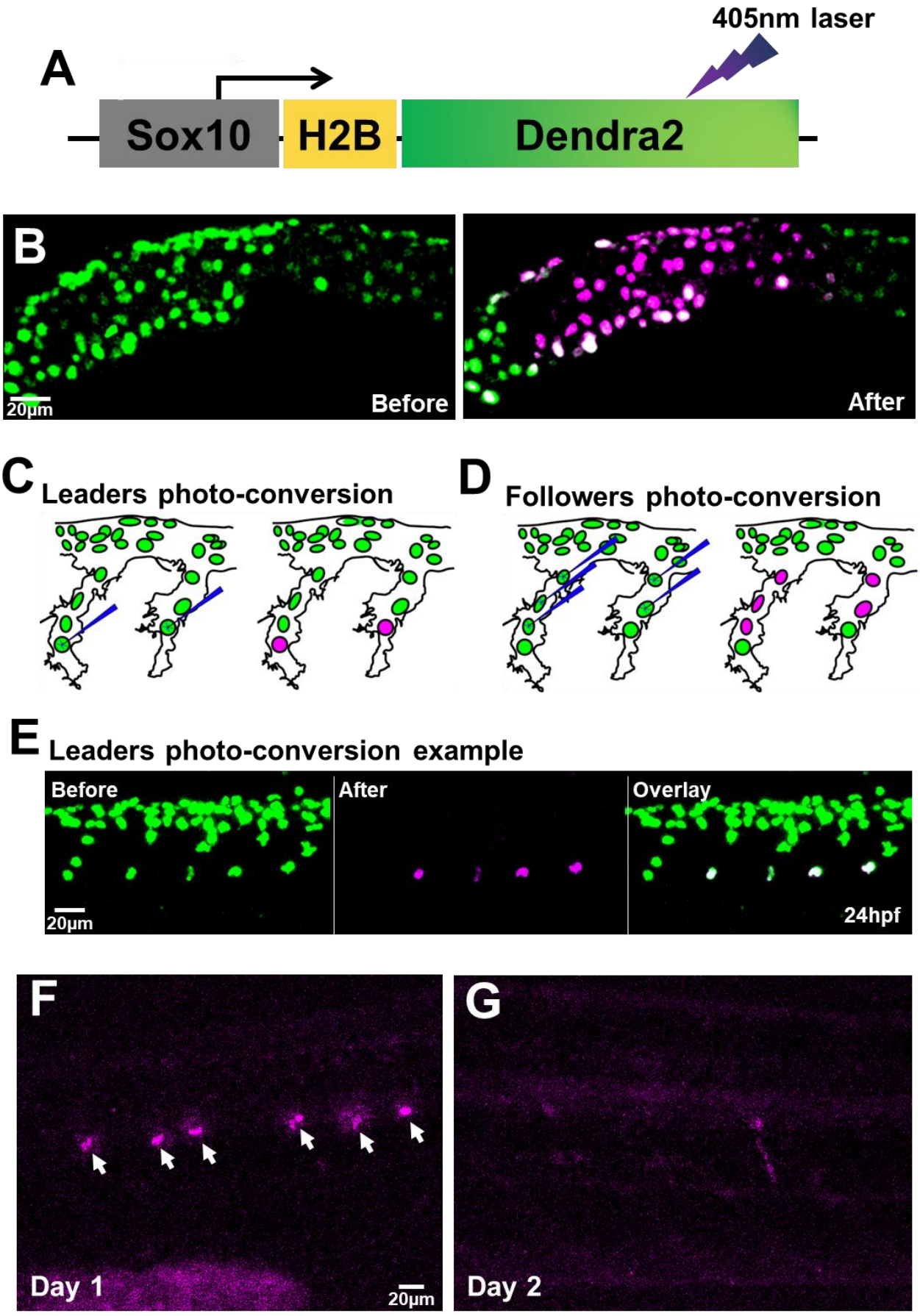
405nm laser
A
Sox10
H2B
Dendra2
B
20µm
Before
After
C
Leaders photo-conversion
D
Followers photo-conversion
E
Leaders photo-conversion example
Before
After
Overlay
20µm
24hpf
F
Day 1
20µm
G
Day 2

Figure 40: Red fluorescence persist for 24 hours after photoconversion in Sox10:Dendra transgenic embryos.

(A) Schematic of Sox10:H2B-Dendra2 construct.

(B) Confocal images of H2B-Dendra2-expressing TNC cells before and after photoconversion showing the spectral change from GFP to RFP.

(C, D) Schematic of the photoconversion strategy of individual **(C)** leader or **(D)** follower cells.

(E) Confocal images of representative leader's photo-conversion experiment.

(F, G) Confocal images of photoconverted leaders showing **(F)** strong RFP signal day 1 after photoconversion, **(G)** but very diminished signal 2 days after photoconversion (white arrows indicate photoconverted leaders).

Anterior to the left, dorsal up.

Our previous results show that leader cells divide asymmetrically during migration giving rise to a Distal daughter that becomes the new leader, and to a Proximal sibling that becomes a follower. Next, we determined whether the leaders' asymmetric division results in siblings acquiring distinct fates. Tracking analysis show that the leaders' Proximal daughter stretches across the migration path and slightly retracts dorsally, connecting the first follower's distal daughter at the entrance of the DRG, with the leaders' Distal cell (Figure 41A-B and 43A). The leader Distal daughter continues to migrate ventrally reaching its target site by 24hpf, adjacent to the DA where the SCG will form. The leader Distal cell is the only cell that reached this ventral position and is not joined by any other TNC during the length of our movies (up to 3 days). The leader Distal cell retain this position without differentiating but undergoing division for 3 days (Figure 43C and E). The fact that leaders' Distal cell retains the SCG position and divides in the absence of any other TNC, strongly suggest that the SCG is formed clonally by the leaders' distal daughter (Figure 43A and B).

In most embryos, two Schwan cells (SC) connect the SCG to the DRG. SCs arise from the daughters of the leaders' Proximal cell and first follower or originate exclusively from the first follower daughters. The most ventral SC originates from the leaders' Proximal daughter

(60% cases; Figure 43B-D), or from the first follower Distal daughter in 40% of cases. The dorsal SC, on the other hand, is formed in all cases from the first follower Distal daughter (Figure 41C). Both of SC present an elongated morphology and envelope the motor axons tracks marked by the neuronal reporter neurogening1:GFP ((McGraw et al., 2008); Figure 43C and D).

The DRG is exclusively formed from followers 1-3, which migrate short distance and coalesce ventral to the neural tube (Figure 41A and B). The first follower cell (F1) can differentiate as part of the DRG or give rise to a SC. We found two different situations: i) in a small number of cases F1 does not undergo division and give rise only to a SC enveloping the motor axon; ii) F1 undergoes one division, in which case the most Distal daughter differentiates as a SC and its Proximal sibling joins the DRG (Figure 41C). The second and third followers (F2 and F3) migrate ventrally reaching the prospective DRG location and divide before starting differentiation by 32hpf. Morphological changes become first apparent by 30hpf, DRG cells show smaller sizes and a low cytoplasmic/nuclear ratio (Figure 41A), thereafter expression of neural markers such as neurogenin1 are detected (Figure 41D). Using neurogenin1:GFP reporter embryos, we found that one cell at the caudal edge of the DRG, exhibiting neuronal morphology, becomes clearly GFP labelled by 36hpf (Figure 42B and C) and concomitantly reduces Sox10 expression (Figure 42A and C), demonstrating its neuronal differentiation. The surrounding cells do not express neurogenin1, but retain FoxD3 expression, which is a glial marker at these developmental stages ((Lukoseviciute et al., 2018); Figure 42D-F). These data show that only follower cells give rise to the DRG, wherein one cell differentiates as a primary neuron surrounded by followers that mostly give rise to DRG glial cells.

In conclusion, our data show that leaders divide asymmetrically into two distinct daughter cells, which end up giving rise to different derivatives. On the other hand, followers divide symmetrically and differentiate into DRG and some SC (Table 1).

Table 1: Leaders and followers derivatives

	DRG	SC	SCG
Follower 3	**100%**	**0%**	**0%**
Follower 2	**100%**	**0%**	**0%**
Follower 1	**60%**	**40%**	**0%**
Leaders' Proximal	**0%**	**100%**	**0%**
Leaders' Distal	**0%**	**0%**	**100%**

Figure 41

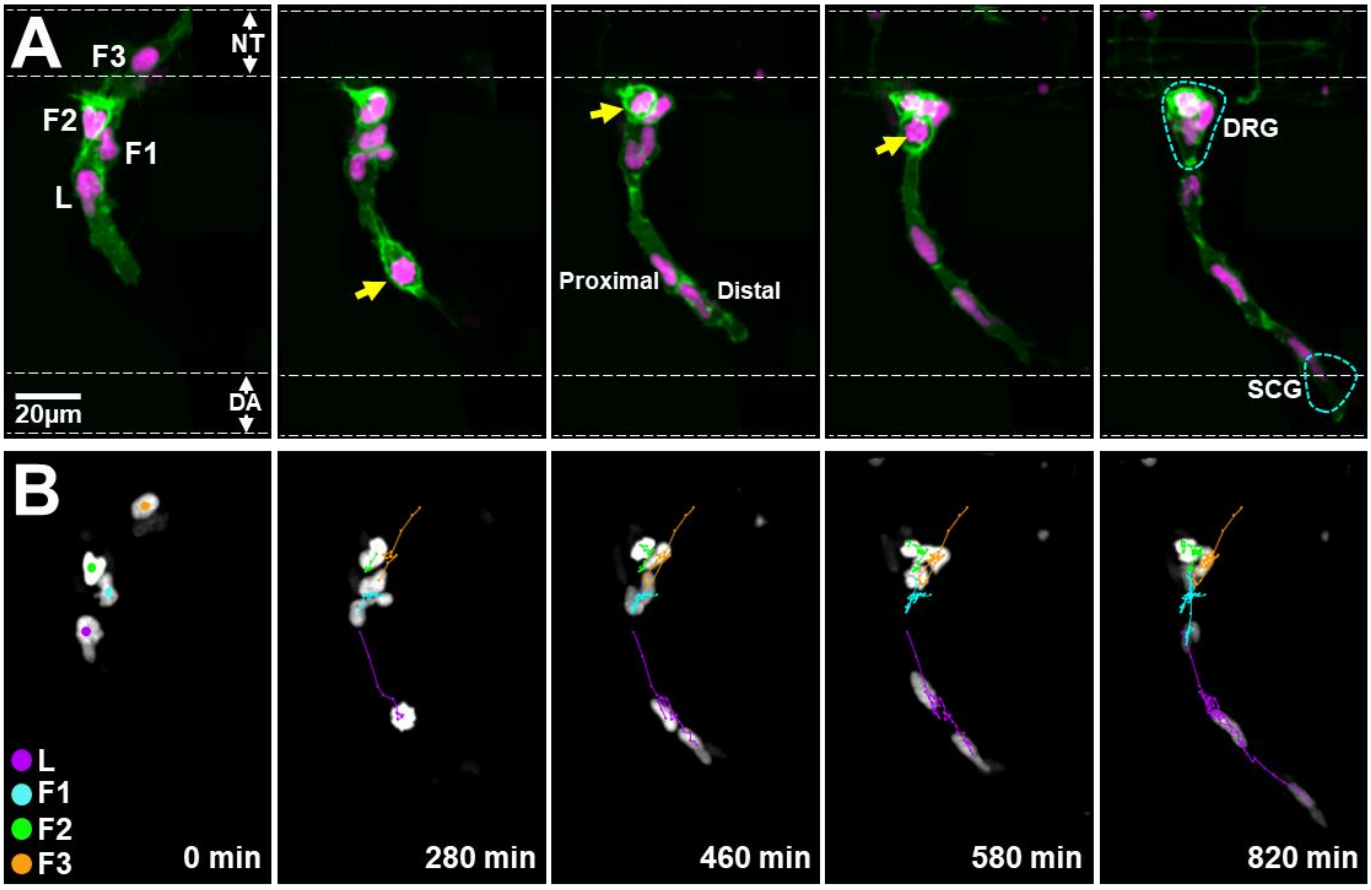
A
F3
NT
F2
F1
L
20μm
DA
Proximal
Distal
DRG
SCG
B
L
F1
F2
F3
0 min
280 min
460 min
580 min
820 min

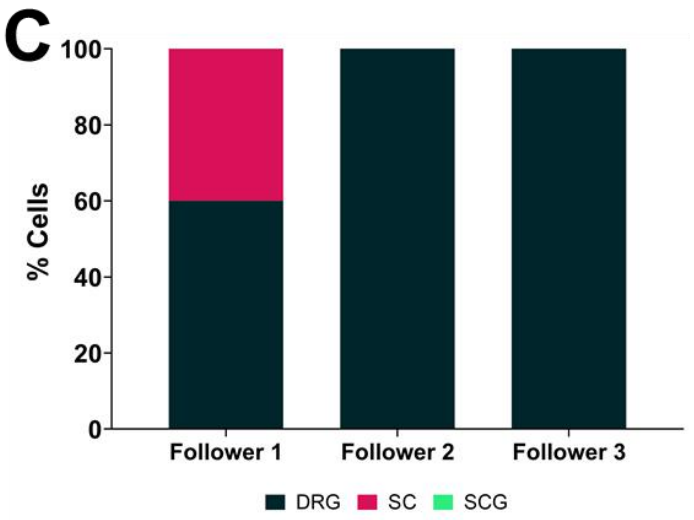
C
100
80
60
40
20
0
% Cells
Follower 1
Follower 2
Follower 3
DRG
SC
SCG

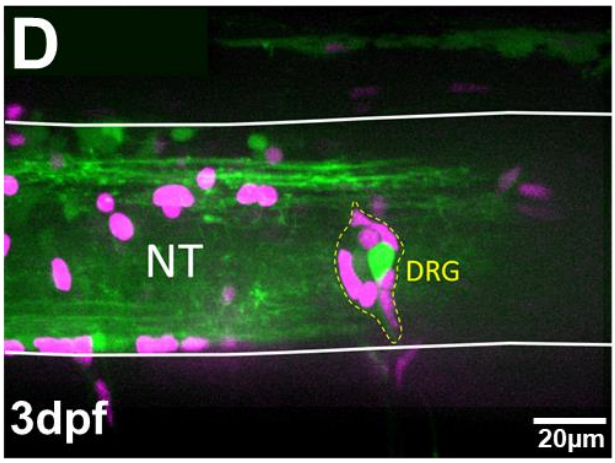
D
NT
DRG
3dpf
20μm

Figure 41: Followers TNC give rise to the Dorsal root ganglia.

(A, B) Selected frames of TNC from segment 9 Sox10:mG live imaging from 22-36hpf. **(A)** RFP and GFP channels **(B)** tracking of cells in **(A)** (yellow arrows indicate mitosis, white dotted lines and white arrowheads indicate the boundaries of the neural tube (NT) or dorsal aorta (DA); cyan dotted lines indicate the position of the dorsal root ganglia (DRG) or sympathetic chain ganglia (SCG); L: leader, magenta track; F1: first follower, cyan track, F2: second follower, green track; F3: third follower, orange track).

(C) Quantification of follower cells contribution to TNC derivatives (SC: Schwann cells; n=10 for F1, F2 and F3).

(D) Confocal image of a DRG at 3dpf from Sox10:Kalt4 x nrg1:GFP transgenic embryo (TNC nuclei labelled in magenta, neurogenin1 in green; white solid lines indicate the neural tube borders; yellow dotted line indicate the DRG).

Anterior left, dorsal top.

Figure 42

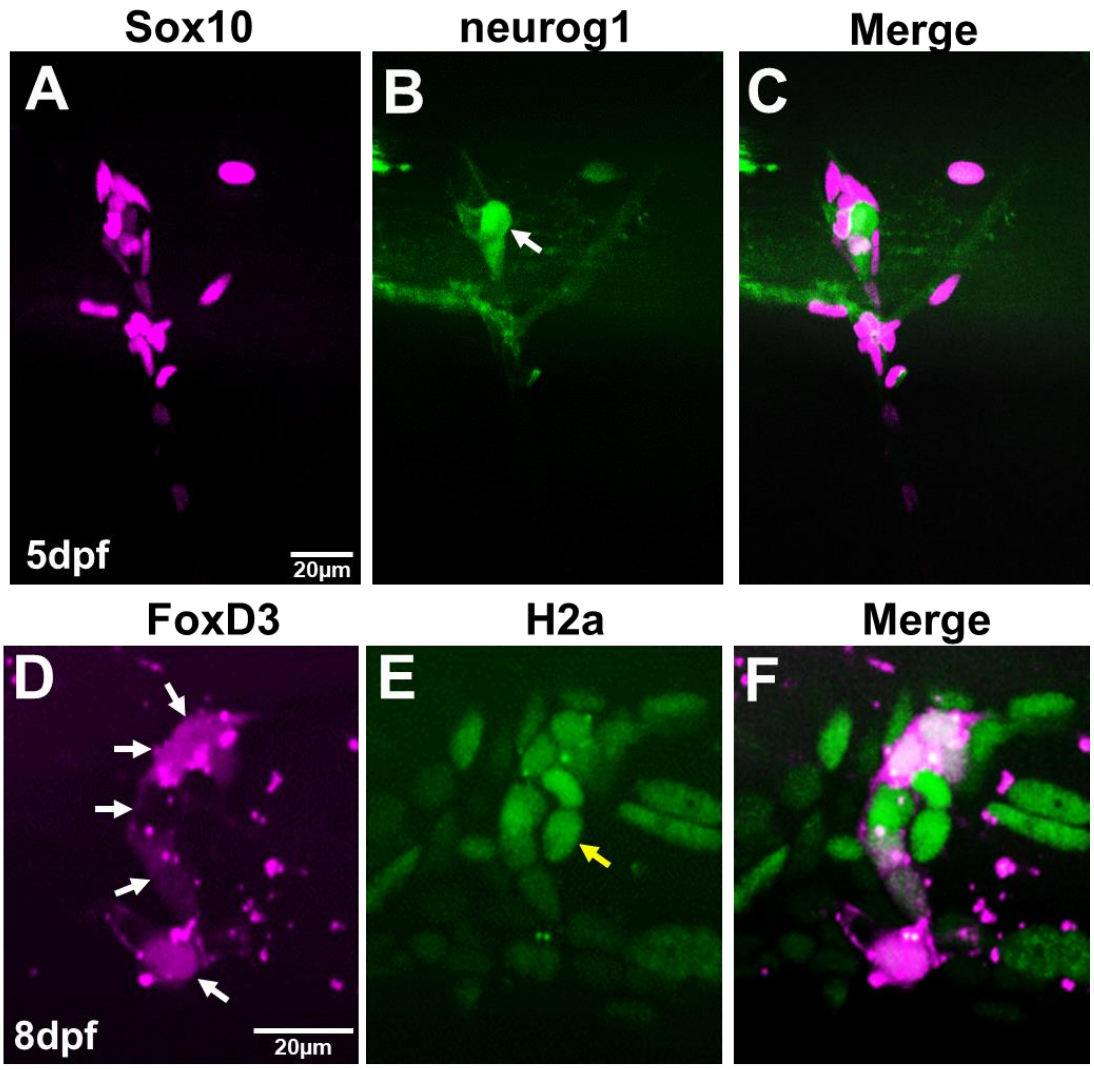

Figure 42: Follower TNC within the DRG express neuronal and glial markers.

(A, B, C) Confocal images of DRG in Sox10:mG x neurogenin1:GFP embryo at 5 days post fertilisation (dpf; white arrow highlights the primary neuron).

(D, E, F) Confocal images of DRG in FoxD3:mCherry x H2aFVA:H2A-GFP embryo at 8dpf. Peripheral cells express the glial marker FoxD3; note the absence of FoxD3 expression at the position of the primary neuron (indicated by a yellow arrow; white arrows indicate glial cells).

Anterior left, dorsal top.

Figure 43

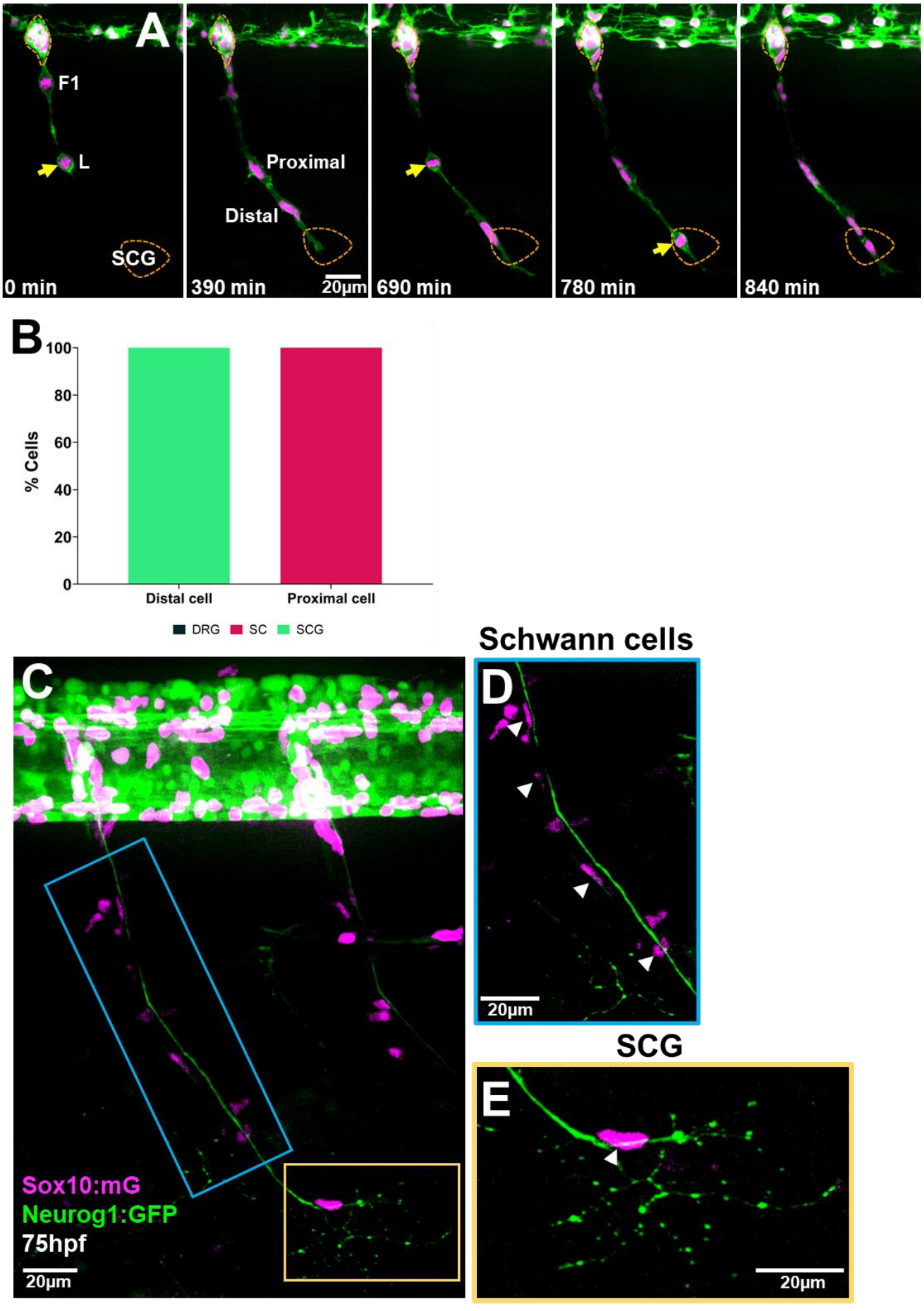
A
F1
L
SCG
0 min
Proximal
Distal
390 min
20μm
690 min
780 min
840 min
B
% Cells
100
80
60
40
20
0
Distal cell
Proximal cell
DRG
SC
SCG
C
Sox10:mG
Neurog1:GFP
75hpf
20μm
Schwann cells
D
20μm
SCG
E
20μm

Figure 43: Leaders' Distal daughters position suggest a clonal origin of the SCG.

(A) Selected frames of live imaging between 2-3dpf in a Sox10:mG embryo at the level of somite 20, showing followers within the DRG, leader dividing into Distal and Proximal cells and the Distal cell migrating to the SCG position, where it divides (yellow arrows indicate divisions; orange dotted line highlight the positions of the DRG and the SCG; L: leader, F1: first follower).

(B) Quantification of leader's daughters contribution to TNC derivatives (n=7).

(C) Confocal image of Sox10:mG x neurogenin1:GFP at 3dpf showing axon extending out of the DRG towards the SCG. Blue square enlarged in **(D)** and yellow enlarged in **(E)**.

(D) TNC localising around the axon (white arrowheads indicate TNC at the position of Schwann cells).

(E) Single TNC (leaders' Distal daughter) localising to the position of the SCG (white arrowhead indicates the position of the leaders' Distal daughter).

Chapter 3: Discussion

Leaders TNC divide asymmetrically

TNC migrate as single file chains with one leader cell guiding the migration of each chain. Leaders divide asymmetrically along their migratory path. They maintain their elongated shape, with ventral protrusions, and do not round up before division, positioning the division plane at the rear of the cell, giving rise to a small daughter that becomes a follower and a much bigger sibling at the front of the group that takes the leader's role. Interestingly, endothelial tip cells have been shown to divide asymmetrically in a similar manner. The larger daughter cell that adopts tip cell behaviour and a smaller cell that becomes a stalk cell. The asymmetric positioning of the mitotic spindle as well as the asymmetric inheritance of key mRNAs, such as VEGFR, have been reported to drive the asymmetric division of tip cells (Costa et al., 2016).

During other processes in embryonic development, such as bristle patterning in *Drosophila*, the asymmetric positioning of the mitotic spindle ensures an asymmetric inheritance of Notch components, which is fundamental for cell identity acquisition and subsequent differentiation (Schweisguth, 2015; Lu and Johnston, 2013). We have shown that in TNC Notch signalling is required for leaders and followers identity assignment. Hence, it is possible to propose that following the asymmetric division of leaders, Notch components may be asymmetrically inherited between its daughter cells. The fact that the new leader cell is immediately much larger than its sibling, suggests that this cell may inherit more Notch determinants, which in turn can reinforce its leader identity. Indeed, Notch components such as Numb have been shown to be inherited asymmetrically following the division of avian TNC, this in turn regulates fate determination (Wakamatsu et al., 2000). Notch has also been shown to control the expression of its signalling components and of fate determinants, such as α-adaptin and Numb, which via interaction with CXCR4 orchestrate the polarity and mitotic

spindle orientation during asymmetric cell division of mouse T cells (Charnley et al., 2020). Moreover, in endothelial cells, it has been reported that mRNA polarisation acts as a molecular compass that orients cell polarity and spatially directs tissue movement. mRNAs, such as the GTPase RAB13, are targeted to cell protrusions and orient blood vessel morphogenesis (Costa et al., 2020). Leaders TNC division is morphologically and behaviourally similar to endothelial tip cells, thus we speculate that asymmetric division of leaders sets differences between daughter cells and results in asymmetric inheritance of determinants, such as Notch components, which further enforces different cell identities in the daughter cells. Furthermore, leaders maintain ventral protrusions during and after division, which suggest that GTPases mRNA could be polarized to the cell protrusions akin to their distribution in endothelial cells. Thus similar mechanisms could be at play in leaders' asymmetric divisions.

Leaders and followers TNC give rise to different derivatives

We asked whether the migratory differences between leaders and followers and the asymmetric division of leaders translate into different fates. TNC give rise to Dorsal Root Ganglia, Schwann cells, Sympathetic Chain Ganglia and pigment cells (Raible and Eisen, 1994, 1996). Our data show that follower cells pause migration and coalesce lateral to the neural tube, solely give rise to the Dorsal Root Ganglia (DRG), while the ventral-most followers give rise to Schwann Cells (SC). Followers ability to pause in the correct DRG position and differentiate into neurons is regulated by Neuregulin-ErbB3 signalling (Honjo et al., 2008). Followers at this location give rise to both neurons and glia of the DRG, which raises a question regarding the mechanism that regulate followers' differentiation into these fates. It has been shown that Notch components, such as Notch1 and DeltaA, are expressed in glial cells within the zebrafish DRG, and Notch inhibition results in supernumerary neurons at the expense of glial cells (McGraw et al., 2012). Similarly, Notch signalling regulates avian

TNC glia and neuron differentiation within the DRG (Wakamatsu et al., 2000). Activation of Notch signalling in some of the DRG periphery cells favours glial differentiation (Mead and Yutzey, 2012), while Hedgehog signalling promotes neuronal differentiation, by regulating the expression of Neurogenin1 in centrally located cells (Ungos et al., 2003). Thus, the Notch seems a plausible signalling pathway that regulates followers TNC differentiation in the DRG.

Our data show that following leaders' asymmetric division, the two daughter cells adopt different fates. The smaller Proximal daughter becomes a SC, while the bigger Distal daughter resides in the position of the Sympathetic chain ganglia (SCG), indicating a clonal origin for the SCG. This is consistent with previous reports showing that in chick and zebrafish, early migration TNC give rise to the ventral-most derivatives (i.e. SCG; (McKinney et al., 2013; Raible and Eisen, 1994). The fact that leaders' daughters give rise to different derivatives suggest that these cells initiate distinct differentiation programs. Our observations show that the leaders' distal daughter remains at the SCG position for days after arriving at this location, where it proliferates. However, owing to the fact that SCG overt differentiation does not start until after 7 days post fertilisation, we were unable to directly test the Distal daughter differentiation into SCG. Although the asymmetric cell division is likely to play an important role in fate determination of leaders' daughters, it is also plausible that the leaders' daughters end positions and/or their proximity to local differentiation cues such as *BMP* could be responsible for fate determination, or indeed a combination of both could be at play. Taken together, our data show that TNC leaders divide asymmetrically and that leaders and followers give rise to different derivatives.

Taken together, our work has revealed that leaders and followers TNC are born from different progenitors, that leaders and followers exhibit different division patterns, initiate migration at different phases of the cell cycle and show an inversely proportional relationship between the durations of G_1 and S-phases. We also showed that cell cycle progression is required for TNC migration and that proper levels of Notch signalling is important for normal

TNC migration and identity assignment suggesting a link between cell cycle and Notch signalling. Our data showed that leaders divide asymmetrically, while followers divide symmetrically and that leaders and followers give rise to different derivatives.

Materials and methods

Zebrafish

Zebrafish were maintained in accordance with the UK Home Office regulations UK Animals (Scientific Procedures) Act 1986, amended in 2013 under project license P70880F4C. Embryos were obtained from the following strains:

Wild type, AB strain

Sox10:mG, Tg(-4.9sox10: Hsa.HIST1H2BJ-mCherry-2A-GLYPI-EGFP)

Sox10:Fucci, Tg(-4.9sox10 :mAGFP-gmnn-2A-mCherry-cdt1)

FoxD3:mCherry, Gt(foxd3-mCherry)ct110

hs:dnSu(H), vu21Tg (hsp70l:XdnSu(H)-myc)

hs:Gal4, kca4Tg Tg(hsp70l:Gal4)1.5kca4 (1)

UAS:NICD, kca3Tg Tg(UAS:myc-Notch1a-intra)

Sox10:Kalt4, Tg(-4.9sox10: Hsa.HIST1H2BJ-mCherry-2A-Kalt4ER)

Sox10:Dendra2, kg329Tg Tg(Sox10:H2B-Dendra2)

UAS:dnSu(H), Tg(UAS:dnSu(H)-myc)

Tg(h2afva:h2a-GFP)kca13

Offspring of the required genotypes were staged according to (Kimmel et al., 1995) and selected based on anatomical, developmental good health and the expression of fluorescent reporters when appropriate. Embryos were split randomly between experimental groups and maintained at 28.5°C in E3 medium.

mRNA micro-injections

pCS2+ PCNA-GFP vector was kindly provided by C. Norden (IGC, Portugal). mRNA was synthesised as described in the publication (Leung et al., 2011). In brief, the pCS2+ vector was linearised using NotI and mRNA synthesised using the SP6 mMessage Machine Kit (Ambion, Cat#) as per the manufacturer instructions. Embryos were injected at one to four cell stage with 30pg of PCNA-GFP mRNA in a volume of 1nl, incubated at 28.5°C and imaged at the appropriate stages.

Live Imaging and tracking

Imaging and analysis were carried as in Alhashem et al., 2021. In short, embryos were mounted in 1% agarose/E3 medium plus 40 µM Tricaine. Segments 6-12 were imaged in lateral views every 5 minutes from 16hpf for 16–18hr in an upright PerkinElmer Ultraview Vox system using 40X water immersion objective. In general, 70 µm z-stacks with 2 µm z-steps were obtained, however, 1 µm z-steps were obtained for cell volume rendering and calculation. Image stacks were corrected for drift using the Correct 3D Drift Fiji plugin and 3D single cell tracking with the View5D Fiji plugin. Tracks overlays were drawn using the MTrackJ and Manual Tracking Fiji plugins. Volume rendering and calculation were done in Imaris (Bitplane). Cell area measurements were done in Fiji using the freehand selection tool to draw around cell membranes. Cell speed measurements were calculated from 3D tracks using the following formula: ((SQRT((X1-X2)^2+(Y1-Y2)^2+(Z1-Z2)^2))/T)*60. Where X, Y and Z are the physical coordinates and T is the time-step between time-lapse frames. Cell directionality measurements were calculated using a previously published Excel macro (Gorelik and Gautreau, 2014). PCNA-GFP mRNA was expressed in majority of cells in the embryo, to aid in better visualisation, movies were cleaned using FIJI to retain only cells expressing both RFP and GFP. Image cleaning was done using a custom Fiji macro, as follows:

```
macro "Find Red Objects [s]" {
title = getTitle();
run("Split Channels");
selectWindow("C1-" + title); //select window with C1 in its name
getDimensions(width, height, channelCount, slices, frames);
run("Subtract Background...", "rolling=200 sliding stack");
setAutoThreshold("Default dark");
run("Threshold...");
setThreshold(5, 255);
setOption("BlackBackground", false);
run("Convert to Mask", "method=Default background=Dark");
run("Close");
run("Fill Holes", "stack");
run("Despeckle", "stack");
run("Dilate", "stack");
run("Dilate", "stack");
//now go over every slide
for(frame=1; frame<=frames; frame++){
for(slice=1; slice<=slices; slice++){
   selectWindow("C1-" + title);
   setSlice(slice);
   Stack.setFrame(frame);
   run("Create Selection");
   selectWindow("C2-" + title);
   setSlice(slice);
   Stack.setFrame(frame);
   run("Restore Selection");
   setBackgroundColor(0, 0, 0);
   run("Clear Outside", "slice");
}
}
}
```

Embryos genotyping

UAS:NICD, UAS:dnSu(H) or hs:dnSu(H) were genotyped by PCR after imaging using the following primers:

Transgenic	Forward	Reverse	Annealing temp.	Fragment size
UAS:NICD	CATCGCGTCTCAGCCTCAC	CGGAATCGTTTATTGGTGTCG	58°C	500bp
UAS:dnSu(H)	GCGGTGTGTGTACTTCAGTC	TCTCCCCAAACTTCCCTGTC	55°C	409bp
hs:dnSu(H)	CGGGCATTTACTTTATGTTGC	TGCATTTCTTGCTCACTGTTTC	55°C	1000bp

Whole Mount in Situ Hybridization, sectioning and Immunostaining

The whole mount *in situ* hybridization protocol used was adapted from https://zfin.org/ZFIN/Methods/ThisseProtocol.html. Riboprobes for notch1a, deltaB, deltaD, her4, cb1045 were kindly provided by Julian Lewis; sox10 and foxd3 were by Robert Kelsh (University of Bath, UK); crestin, mbp, bdh, myoD, by Steve Wilson (UCL, UK). In short, embryos were fixed overnight (O/N) in 4% Paraformaldehyde (PFA), dehydrated in 100% methanol then rehydrated, digested with proteinase K (10 µg/ml) and pre-hybridised with hybridisation buffer. Riboprobes were added at 65°C O/N, probes were removed by series of washes, embryos incubated with blocking solution then anti-dig antibody O/N then washed and colour detection was done by incubating embryos with NBT and BCIP substrate.

Embryos stained for *notch1a, deltaB, deltaD* and *her4* were sectioned. After the colour development, embryos were fixed O/N in 4% PFA at 4°C, washed 5x10min with PBS, embedded in Optimal cutting temperature compound (OCT), frozen by dipping the blocks in dry ice cold 70% ETOH, and sectioned to 12-15µm using a cryostat. Sections were thawed at room temperature (RT), incubated with blocking solution for 30min (10% goat serum, 2% BSA, 0.5% Triton, 10mM sodium azide in PBS) and in anti-GFP antibody overnight at 4°C.

Sections were washed with PBST 5x15min (0.5% Triton- PBS) and incubated with secondary antibody for 2h at RT°C. Sections were mounted in ProLong™ Gold Antifade Mountant (Molecular Probes Cat#P10144) and imaged.

Wholemount antibody staining was performed in embryos fixed for 2h in 4% PFA at RT, washed 4x10min in PBST and incubated with blocking solution for 2h and primary antibodies O/N at 4°C. Embryos were washed 5x30min in PBST, incubated in secondary antibodies O/N at 4°C, washed with PBST 6x30min and mounted in 1% agarose for imaging. Imaging of sectioned or wholemount antibody-stained embryos was performed in PerkinElmer Ultraview Vox system.

Antibody	**Supplier**	**Identifier**
Anti-GFP	Millipore	06-896
F59	DSHB	AB_528373
Anti-Myc	Cell Signaling	610182
Znp-1	DSHB	AB_2315626
Anti-Acetylated tubulin	Merk	T7451
Anti-dig	Sigma-Aldrich	41116161
Anti-PCNA PC10	Cell Signaling	2586
Anti-Cyclin D1	Cell Signaling	2978
Anti-BrdU	Abcam	ab6326
Secondary antibodies	Invitrogen	Alexa Fluor range

BrdU staining

BrdU incorporation assay was carried out as previously described (Verduzco and Amatruda, 2011). In short, embryos were incubated in 10mM BrdU (Abcam Cat#ab142567) for 3 hours, fixed in 4% PFA, digested with proteinase K, incubated in 2N HCl then 0.1M Sodium Tetraborate, incubated in blocking solution and followed by primary anti-BrdU then secondary antibodies.

Expression activation in inducible transgenic lines

Gene expression was induced by addition of 2.5 mM of Tamoxifen (Sigma-Aldrich Cat#H7904) to the E3 media at 12hpf in Sox10:Kalt4 embryos; or by heat shock in hs:Gal4 and hs:dnSu(H) embryos. Heat shock was performed at 12hpf by drastically changing the temperature of E3 media and incubating embryos for 1h at 39°C , thereafter embryos were grown at 28.5°C.

Drug treatments

Embryos were treated by adding cell cycle inhibitors to the E3 media. 20 mM Hydroxyurea (Sigma-Aldrich Cat#H8627), 300 µM Aphidicolin (Sigma-Aldrich Cat#A0781) 100 µM Genistein (Calbiochem Cat#345834), Teniposide (Sigma-Aldrich Cat#SML0609) or 1% DMSO (Sigma-Aldrich Cat#D8418) as a control, from 12hpf and incubated for 3-12h at 28.5°C. Notch signalling was inhibited at 12hpf by adding 100 µM DAPT (Merk Cat#D5942), 50 µM of Compound E (Bio-Teche Cat#12352200) or 1% DMSO as a control.

Generation of UAS:dnSu(H) transgenic line

Using the InFusion cloning system (Takara) the following constructs were inserted into the Ac/Ds vector (Chong-Morrison et al., 2018): 5xUAS sequence (Tol2Kit, http://tol2kit.genetics.utah.edu/index.php/Main_Page) was flanked at the 3’ and 5’ ends with

the rabbit β-globin intron sequences, GFP was cloned at the 3’ end, followed by SV40polyA sequence to generate the Ac/Ds dUAS:GFP vector. The cmlc2:egfp transgenesis marker (Tol2Kit) was cloned after GFP in the contralateral strand to prevent interaction between the UAS and the cmnl sequences. The *Xenopus* dnSu(H)-myc sequence (Latimer et al., 2005) was cloned into the Ac/Ds dUAS:GFP vector at the 5’ end of the 5xUAS sequence, followed by the SV40polyA sequence. Transgenesis was obtained by injecting Sox10:Kalt4 embryos with 1nl of 50pg of DNA plus 30pg of Ac transposase mRNA at 1 cell stage. Embryos carrying the transgene were selected by screening for heart fluorescence at 24hpf. Upon Gal4 expression dnSu(H)-myc protein was readily detected by antibody expression, but GFP fluorescence from the UAS sequence was not observed.

Generation of cell cycle transgenic lines

pCDNA3_E2F1 vector was kindly provided by M. Gomez, which contains the full length human E2F1 sequence. Using the InFusion cloning system (Takara) the full length E2F1 sequence (Helin et al., 1992) was inserted into the Ac/Ds dUAS:GFP vector (described) at the 3’ end to generate UAS:flE2F1 vector. To generate the UAS:dnE2F1, a stop codon was added to the E2F1 sequence at amino acid position 363 to produce a truncated dominant negative version, which was subsequently cloned into the Ac/Ds dUAS:GFP vector at the 3’ end. The 15aa-MyoD and nls sequences (Burstyn-Cohen and Kalcheim, 2002) were inserted in-frame at the 3’ end of the GFP in the the Ac/Ds dUAS:GFP vector. Sox10:Kalt4 embryos were injected with 1nl containing 50pg of DNA and 30pg of Ac transposase mRNA at 1 cell stage. Embryos carrying the transgene were selected by screening for heart fluorescence at 24hpf.

Photoconversion

Photoconversion was carried out as described in Alhashem et al., 2021. In brief, Sox10:dendra2 embryos were mounted in 3% methyl cellulose (Sigma-Aldrich Cat#M-0387), individual cells were marked with circular region of interest and photoconversion was done in

a Zeiss LSM 880 Microscope using 405nm UV Diode Laser at 40% laser intensity, pixel dwell 131.07 µsec for 2 iterations.

Embryo dissection, dissociation and FACS

Embryo dissection and dissociation were performed as described in Alhashem et al., 2021. Using forceps, the trunks were dissected, trypsin-EDTA was added and vigorously triturated, reaction was neutralised with foetal bovine serum and cells were washed then reconstituted using FACSmax Cell Dissociation Solution (Amsbio). Cells were split into different tubes and stained with 1 µg/ml 7-AAD (Biolegend Cat#420403) for 20 minutes and 5 µg/mL Hoechst 33342 (Invitrogen Cat# H3570) for 45 minutes. DNA content analysis by Fluorescence-activated cell sorting (FACS) was performed using a BD LSRFortessa™ Flow Cytometer by quantifying the amount of stained DNA.

Statistical analysis

All graphs and statistical analysis were carried out in GraphPad Prism 9. Every sample tested for tests for normality using the d'Agostino & Pearson, followed by the Shapiro-Wilk test. Samples with a normal distribution were either compared using unpaired two-tailed *t*-test or one way ANOVA. Those without a normal distribution were compared through a Mann-Whitney U test, Kruskal-Wallis test or Brown-Forsythe and Welch ANOVA tests. For all analyses, *P* values of under 0.05 were deemed statistically significant, with ****$P<0.0001$, ***$P<0.001$, **$P<0.01$, and *$P<0.05$.

Supplementary information

Supplementary movies are uploaded to OneDrive and can be accessed via this link:

Thesis Supplementary Movies

Movie S1: Leaders' progenitors divide asymmetrically into daughters with different sizes. Related to Figure 8.

Rotating 3D rendering of leaders' progenitor daughter cells immediately after division. Leader cell in yellow, follower in cyan, other non-rendered TNC in magenta. White arrow indicate leader cell.

Movie S2: Leaders and followers present different division patterns. Related to Figure 9.

Left panel: representative time-lapse of Sox10:mG showing a leader cell migrating then dividing (M>D); leader track in blue and leader's daughters in red and yellow.

Right panel: representative time-lapse of Sox10:mG showing a follower cell dividing then migrating (D>M); follower track in blue and follower's daughters in red and yellow.

White arrows indicate division position, time in minutes. Imaged from 16hpf to 28hpf.

Movie S3: PCNA-GFP reveals the cell cycle dynamics. Related to Figure 11.

Left panel: unprocessed time-lapse of Sox10:H2B-mCherry-Kalt4ER embryos injected with the cell cycle reporter PCNA-GFP mRNA. Note PCNA-GFP expression in non-TNC cells.

Right panel: processed version of the left panel time-lapse showing PCNA-GFP expression in TNC only.

TNC nuclei in magenta and PCNA-GFP in green; white arrowheads indicate cycling leader cell; time in minutes. Imaged from 20hpf to 27hpf.

Movie S4: Leaders and followers initiate migration at different phases of the cell cycle. Related to Figure 11.

Upper panel: processed time-lapse of TNC expressing PCNA-GFP showing a leader cell initiating migrating in S-phase.

Lower panel: processed time-lapse of TNC expressing PCNA-GFP showing a follower cell initiating migrating in G1.

PCNA-GFP in green; White arrowheads indicate the leader, follower and their daughter cells after division; yellow arrowhead indicate the point of division; time in minutes. Imaged from 16hpf to 26hpf.

Movie S5: Sox10:FUCCI confirms the PCNA cell cycle data. Related to Figure 12.

Representative time-lapse of Sox10:FUCCI showing leaders initiate migration in S-phase, while followers emigrate in G1.

G1 in magenta and S/G2 in green; magenta arrowheads indicate the leader and its daughters; cyan arrowheads indicate the follower cell; time in minutes; imaged from 16hpf to 18hpf.

Movie S6: S-phase arrest halts TNC migration. Related to Figure 15.

Left panel: time-lapse of Sox10:mG showing control (DMSO treated) TNC migrating normally. Imaged from 16hpf to 23hpf.

Right panel: time-lapse of Sox10:mG showing S-phase arrested (Aphidicolin treated) TNC unable to migrate out of the premigratory area. Imaged from 16hpf to 30hpf.

Leaders track in yellow, followers tracks in cyan and white; time in minutes.

Movie S7: Notch inhibition results in TNC migratory and identity defects. Related to Figure 23.

Upper and lower left panels: time-lapse of Sox10:mG in control (DMSO treated) condition showing normal TNC migration and leader-follower hierarchy. Imaged from 16hpf to 27hpf.

Upper and lower right panels: time-lapse of Sox10:mG in Notch inhibited (Compound E treated) condition showing TNC migration defects where most cells do not migrate past the notochord boundary and followers overtaking leaders. Imaged from 16hpf to 30hpf.

Upper panels fluorescently show cell nuclei in grey and membranes in green. Lower panels show nuclei in grey, leaders tracks in magenta and followers tracks in cyan; White arrowheads indicate leaders and white arrows indicate followers overtaken leaders. Time in minutes.

Movie S8: Notch LOF and GOF result in TNC migratory and identity aberrations. Related to Figures 27 and 29.

Upper and lower left panels: time-lapse of control Sox10:kalt4 showing normal TNC migration and leader-follower hierarchy. Imaged from 18hpf to 29hpf.

Upper and lower middle panels: time-lapse of Notch LOF Sox10:kalt4XUAS:dnSu(H) showing TNC migration and identity defects. Imaged from 20hpf to 29hpf.

Upper and lower right panels: time-lapse of Notch GOF Sox10:kalt4XUAS:NICD showing TNC migration and identity defects. Imaged from 18hpf to 29hpf.

Upper panels fluorescently show cell nuclei in. Lower panels show nuclei in grey, leaders tracks in magenta and followers tracks in cyan; White arrowheads indicate leaders and white arrows indicate followers overtaken leaders. Time in minutes.

Movie S9: Leaders divide asymmetrically, while followers divide symmetrically. Related to Figure 37.

Upper panel: time-lapse of Sox10:mG showing a leader cell maintaining its elongated shape and dividing asymmetrically into two daughters with different sizes. Imaged from 22hpf to 25hpf.

Lower panel: time-lapse of Sox10:mG showing a follower cell rounding up and dividing symmetrically into two daughters with similar sizes. Imaged from 20hpf to 23hpf.

White arrowheads indicate the leader, follower and their daughters after division; yellow arrowheads indicate the point of division; time in minutes.

Movie S10: Leaders divide asymmetrically into a big Distal cell and small Proximal cell. Related to Figure 39.

3D rendered time-lapse of a leader dividing asymmetrically. Note the elongated morphology of the leader while undergoing mitosis and the stark size difference between the Distal and Proximal cells.

Leader in yellow, Distal cell in magenta and Proximal cell in cyan.

Movie S11: Followers give rise to the DRG. Related to Figure 41.

Left panel: time-lapse of Sox10:mG imaged from 22hpf to 36hpf showing followers coalescing lateral to the neural tube to from the DRG, while the leader migrates more ventrally lateral to the dorsal aorta. Nuclei in magenta and membranes in green. L: leader, F1: first follower, F2: second follower, F3: third follower. Yellow arrowheads indicate the point of division. Time in minutes.

Right panel: cell tracks of the left panel time-lapse showing cell nuclei in grey. Leader and its daughters tracked in purple, follower 1 and its daughters in cyan, follower 2 and its daughters in green and follower 3 and its daughters in orange.

Movie S12: Leaders' Distal daughter reside and divide at the position of the SCG. Related to Figure 43.

Time-lapse of Sox10:mG imaged between 2dpf and 3dpf showing the leader's daughters migrating ventrally and dividing, with the Distal daughter residing and dividing at the position of the SCG suggesting a clonal origin of the SCG.

Yellow arrowheads indicate the point of division. F1: first follower, D 1.1 and D1.2: Distal cell first and second daughters respectively. Time in minutes.

Acknowledgements

I would like to thank and extend my gratitude to my supervisor Claudia Linker for being a great mentor and for her immense patience throughout my PhD. I also would like to thank my second supervisor Jon Clarke for the helpful discussions. Many thanks to all previous members of the Linker lab for being great and helpful colleagues. Thanks to Victoria Prince and Manuel Rocha for hosting me at UChicago and being great collaborators. Thanks to Caren Norden and Tatjana Sauka-Spengler for providing the PCNA-GFP construct and FoxD3 line. Huge thanks to my family for all their love and support. Many thanks to Cynthia Rodriguez for all her care and support throughout my PhD.

References

Abercrombie, M. & Heaysman, J. E. M. (1954) Observations on the social behaviour of cells in tissue culture: II. “Monolayering” of fibroblasts. *Experimental Cell Research*. [Online] 6 (2), 293–306.

Affolter, M. & Caussinus, E. (2008) Tracheal branching morphogenesis in Drosophila: new insights into cell behaviour and organ architecture. *Development*. [Online] 135 (12), 2055–2064.

del Álamo, D. et al. (2011) Mechanism and Significance of cis-Inhibition in Notch Signalling. *Current Biology*. [Online] 21 (1), R40–R47.

Alhashem, Z. et al. (2021) ‘Zebrafish Neural Crest: Lessons and Tools to Study In Vivo Cell Migration’, in Kyra Campbell & Eric Theveneau (eds.) *The Epithelial-to Mesenchymal Transition: Methods and Protocols*. Methods in Molecular Biology. [Online]. New York, NY: Springer US. pp. 79–106. [online]. Available from: https://doi.org/10.1007/978-1-0716-0779-4_9 (Accessed 24 March 2021).

Ambros, V (1999) Cell cycle and cell fate in C. elegans. *Development*. 1261947–1958.

Ambros, V. (1999) Cell cycle-dependent sequencing of cell fate decisions in Caenorhabditis elegans vulva precursor cells. *Development*. 126 (9), 1947–1956.

Baggiolini, A. et al. (2015) Premigratory and Migratory Neural Crest Cells Are Multipotent In Vivo. *Cell Stem Cell*. [Online] 16 (3), 314–322.

Bahrampour, S. & Thor, S. (2020) ‘The Five Faces of Notch Signalling During Drosophila melanogaster Embryonic CNS Development’, in Jörg Reichrath & Sandra Reichrath (eds.) *Notch Signaling in Embryology and Cancer: Notch Signaling in Embryology*. Advances in Experimental Medicine and Biology. [Online]. Cham: Springer International Publishing. pp. 39–58. [online]. Available from: https://doi.org/10.1007/978-3-030-34436-8_3 (Accessed 31 March 2021).

Bajpai, S. et al. (2021) Role of cell polarity dynamics and motility in pattern formation due to contact-dependent signalling. *Journal of The Royal Society Interface*. [Online] 18 (175), 20200825.

Barnum, K. J. & O’Connell, M. J. (2014) ‘Cell Cycle Regulation by Checkpoints’, in Eishi Noguchi & Mariana C. Gadaleta (eds.) *Cell Cycle Control*. Methods in Molecular Biology. [Online]. New York, NY: Springer New York. pp. 29–40. [online]. Available from: http://link.springer.com/10.1007/978-1-4939-0888-2_2 (Accessed 31 March 2021).

Barriga, E. H. et al. (2015) Animal models for studying neural crest development: is the mouse different? *Development*. [Online] 142 (9), 1555–1560.

Behan, P. O. & Chaudhuri, A. (2010) The sad plight of multiple sclerosis research (low on fact, high on fiction): critical data to support it being a neurocristopathy. *Inflammopharmacology*. [Online] 18 (6), 265–290.

Blanchoin, L. et al. (2014) Actin Dynamics, Architecture, and Mechanics in Cell Motility. *Physiological Reviews*. [Online] 94 (1), 235–263.

Blanco, R. & Gerhardt, H. (2013) VEGF and Notch in Tip and Stalk Cell Selection. *Cold Spring Harbor Perspectives in Medicine*. [Online] 3 (1), a006569.

Bocci, F. et al. (2020) Understanding the Principles of Pattern Formation Driven by Notch Signaling by Integrating Experiments and Theoretical Models. *Frontiers in Physiology*. [Online] 11. [online]. Available from: https://www.frontiersin.org/articles/10.3389/fphys.2020.00929/full (Accessed 28 January 2021).

Boström, J. et al. (2017) Comparative cell cycle transcriptomics reveals synchronization of developmental transcription factor networks in cancer cells. *PLOS ONE*. [Online] 12 (12), e0188772.

Bothma, J. P. et al. (2018) LlamaTags: A Versatile Tool to Image Transcription Factor Dynamics in Live Embryos. *Cell*. [Online] 173 (7), 1810-1822.e16.

Bowman, S. K. et al. (2008) The Tumor Suppressors Brat and Numb Regulate Transit-Amplifying Neuroblast Lineages in Drosophila. *Developmental Cell*. [Online] 14 (4), 535–546.

Bray, S. J. (2016) Notch signalling in context. *Nature Reviews Molecular Cell Biology*. [Online] 17 (11), 722–735.

Bretscher, M. S. (1983) Distribution of receptors for transferrin and low density lipoprotein on the surface of giant HeLa cells. *Proceedings of the National Academy of Sciences*. [Online] 80 (2), 454–458.

Bronner, M. E. & LeDouarin, N. M. (2012) Development and evolution of the neural crest: An overview. *Developmental Biology*. [Online] 366 (1), 2–9.

Bronner, M. E. & Simões-Costa, M. (2016) The neural crest migrating into the 21st century. *Current topics in developmental biology*. [Online] 116115–134.

Bronner-Fraser, M. & Fraser, S. (1989) Developmental potential of avian trunk neural crest cells in situ. *Neuron*. [Online] 3 (6), 755–766.

Bronner-Fraser, M. & Fraser, S. E. (1991) Cell lineage analysis of the avian neural crest. *Development*. 113 (Supplement 2), 17–22.

Bronner-Fraser, M. & Fraser, S. E. (1988) Cell lineage analysis reveals multipotency of some avian neural crest cells. *Nature*. [Online] 335 (6186), 161–164.

Burstyn-Cohen, T. et al. (2004) Canonical Wnt activity regulates trunk neural crest delamination linking BMP/noggin signaling with G1/S transition. *Development*. [Online] 131 (21), 5327–5339.

Burstyn-Cohen, T. & Kalcheim, C. (2002) Association between the Cell Cycle and Neural Crest Delamination through Specific Regulation of G1/S Transition. *Developmental Cell*. [Online] 3 (3), 383–395.

Campa, V. M. et al. (2008) Notch activates cell cycle reentry and progression in quiescent cardiomyocytes. *The Journal of Cell Biology*. [Online] 183 (1), 129–141.

Carlson, M. E. et al. (2008) Imbalance between pSmad3 and Notch induces CDK inhibitors in old muscle stem cells. *Nature*. [Online] 454 (7203), 528–532.

Carmona-Fontaine, C. et al. (2011) Complement Fragment C3a Controls Mutual Cell Attraction during Collective Cell Migration. *Developmental Cell*. [Online] 21 (6), 1026–1037.

Carney, T. J. et al. (2006) A direct role for Sox10 in specification of neural crest-derived sensory neurons. *Development*. [Online] 133 (23), 4619–4630.

Carrieri, F. A. et al. (2019) CDK1and CDK2regulate NICD1turnover and theperiodicity of the segmentation clock. *EMBO reports*. [Online] 20 (7), . [online]. Available from: https://onlinelibrary.wiley.com/doi/abs/10.15252/embr.201846436 (Accessed 2 October 2020).

Charnley, M. et al. (2020) A new role for Notch in the control of polarity and asymmetric cell division of developing T cells. *Journal of Cell Science*. [Online] 133 (5), . [online]. Available from: https://jcs.biologists.org/content/133/5/jcs235358 (Accessed 23 February 2021).

Chen, K. et al. (2020) The membrane-associated form of cyclin D1 enhances cellular invasion. *Oncogenesis*. [Online] 9 (9), 1–13.

Cheung, M. et al. (2005) The Transcriptional Control of Trunk Neural Crest Induction, Survival, and Delamination. *Developmental Cell*. [Online] 8 (2), 179–192.

Chia, W. et al. (2008) Drosophila neuroblast asymmetric divisions: cell cycle regulators, asymmetric protein localization, and tumorigenesis. *Journal of Cell Biology*. [Online] 180 (2), 267–272.

Chong-Morrison, V. et al. (2018) Re-purposing Ac/Ds transgenic system for CRISPR/dCas9 modulation of enhancers and non-coding RNAs in zebrafish. *bioRxiv*. [Online] 450684.

Chung, K.-F. et al. (2009) Isolation of Neural Crest Derived Chromaffin Progenitors from Adult Adrenal Medulla. *STEM CELLS*. [Online] 27 (10), 2602–2613.

Cohen, B. et al. (2010) Cyclin D1 is a direct target of JAG1-mediated Notch signaling in breast cancer. *Breast Cancer Research and Treatment*. [Online] 123 (1), 113–124.

Collazo, A. et al. (1993) *Vital dye labelling of Xenopus laevis trunk neural crest reveals multipotency and novel pathways of migration*. 14.

Cordero, D. R. et al. (2011) Cranial neural crest cells on the move: Their roles in craniofacial development. *American Journal of Medical Genetics Part A*. [Online] 155 (2), 270–279.

Cornell, R. A. & Eisen, J. S. (2002) Delta/Notch signaling promotes formation of zebrafish neural crest by repressing Neurogenin 1 function. *Development*. 129 (11), 2639–2648.

Cornell, R. A. & Eisen, J. S. (2005) Notch in the pathway: The roles of Notch signaling in neural crest development. *Seminars in Cell & Developmental Biology*. [Online] 16 (6), 663–672.

Costa, G. et al. (2016) Asymmetric division coordinates collective cell migration in angiogenesis. *Nature Cell Biology*. [Online] 18 (12), 1292–1301.

Costa, G. et al. (2020) RAB13 mRNA compartmentalisation spatially orients tissue morphogenesis. *The EMBO Journal*. [Online] 39 (21), e106003.

Cowan, C. R. & Hyman, A. A. (2004) Asymmetric cell division in C. elegans: cortical polarity and spindle positioning. *Annual Review of Cell and Developmental Biology*. [Online] 20427–453.

Cui, X. & Doe, C. Q. (1995) The role of the cell cycle and cytokinesis in regulating neuroblast sublineage gene expression in the Drosophila CNS. *Development*. 121 (10), 3233–3243.

Daudet, N. & Żak, M. (2020) 'Notch Signalling: The Multitask Manager of Inner Ear Development and Regeneration', in Jörg Reichrath & Sandra Reichrath (eds.) *Notch Signaling in Embryology and Cancer*. Advances in Experimental Medicine and Biology. [Online]. Cham: Springer International Publishing. pp. 129–157. [online]. Available from: http://link.springer.com/10.1007/978-3-030-34436-8_8 (Accessed 31 March 2021).

Devgan, V. et al. (2005) p21WAF1/Cip1 is a negative transcriptional regulator of Wnt4 expression downstream of Notch1 activation. *Genes & Development*. [Online] 19 (12), 1485–1495.

Douarin, N. M. L. et al. (2004) Neural crest cell plasticity and its limits. *Development*. [Online] 131 (19), 4637–4650.

Dunlop, C. E. et al. (2014) Ovarian germline stem cells. *Stem Cell Research & Therapy*. [Online] 5 (4), . [online]. Available from: https://www.ncbi.nlm.nih.gov/pmc/articles/PMC4282152/ (Accessed 20 March 2018).

Ehrhart-Bornstein, M. et al. (2010) Chromaffin Progenitor Cells from the Adrenal Medulla. *Cellular and Molecular Neurobiology*. [Online] 30 (8), 1417–1423.

Engin, F. et al. (2008) Dimorphic effects of Notch signaling in bone homeostasis. *Nature Medicine*. [Online] 14 (3), 299–305.

Erickson, C. A. & Goins, T. L. (1995) Avian neural crest cells can migrate in the dorsolateral path only if they are specified as melanocytes. *Development*. 121 (3), 915–924.

Facchetti, G. et al. (2017) Controlling cell size through sizer mechanisms. *Current Opinion in Systems Biology*. [Online] 586–92.

Fang, J. S. et al. (2017) Shear-induced Notch-Cx37-p27 axis arrests endothelial cell cycle to enable arterial specification. *Nature Communications*. [Online] 8 (1), 2149.

Fichelson, P. et al. (2005) Cell cycle and cell-fate determination in Drosophila neural cell lineages. *Trends in Genetics*. [Online] 21 (7), 413–420.

Fickentscher, R. & Weiss, M. (2017) Physical determinants of asymmetric cell divisions in the early development of Caenorhabditis elegans. *Scientific Reports*. [Online] 7 (1), 9369.

Formosa-Jordan, P. & Ibañes, M. (2014) Competition in Notch Signaling with Cis Enriches Cell Fate Decisions. *PLOS ONE*. [Online] 9 (4), e95744.

Friedl, P. & Gilmour, D. (2009) Collective cell migration in morphogenesis, regeneration and cancer. *Nature Reviews Molecular Cell Biology*. [Online] 10 (7), 445–457.

Gammill, L. S. & Roffers-Agarwal, J. (2010) Division of labor during trunk neural crest development. *Developmental Biology*. [Online] 344 (2), 555–565.

Ganguly, A. et al. (2012) The Role of Microtubules and Their Dynamics in Cell Migration *. *Journal of Biological Chemistry*. [Online] 287 (52), 43359–43369.

Georgia, S. et al. (2006) p57 and Hes1 coordinate cell cycle exit with self-renewal of pancreatic progenitors. *Developmental Biology*. [Online] 298 (1), 22–31.

Ghabrial, A. S. & Krasnow, M. A. (2006) Social interactions among epithelial cells during tracheal branching morphogenesis. *Nature*. [Online] 441 (7094), 746–749.

Giniger, E. (1998) A Role for Abl in Notch Signaling. *Neuron*. [Online] 20 (4), 667–681.

Gómez-López, S. et al. (2014) Asymmetric cell division of stem and progenitor cells during homeostasis and cancer. *Cellular and molecular life sciences: CMLS*. [Online] 71 (4), 575–597.

Gönczy, P. (2008) Mechanisms of asymmetric cell division: flies and worms pave the way. *Nature Reviews Molecular Cell Biology*. [Online] 9 (5), 355–366.

Gorelik, R. & Gautreau, A. (2014) Quantitative and unbiased analysis of directional persistence in cell migration. *Nature Protocols*. [Online] 9 (8), 1931–1943.

Guo, D. et al. (2009) Notch-1 regulates Akt signaling pathway and the expression of cell cycle regulatory proteins cyclin D1, CDK2 and p21 in T-ALL cell lines. *Leukemia Research*. [Online] 33 (5), 678–685.

Haas, P. & Gilmour, D. (2006) Chemokine Signaling Mediates Self-Organizing Tissue Migration in the Zebrafish Lateral Line. *Developmental Cell*. [Online] 10 (5), 673–680.

Harris, M. L. & Erickson, C. A. (2007) Lineage specification in neural crest cell pathfinding. *Developmental Dynamics*. [Online] 236 (1), 1–19.

Hartenstein, V. & Posakony, J. W. (1989) Development of adult sensilla on the wing and notum of Drosophila melanogaster. *Development*. 107 (2), 389–405.

Helin, K. et al. (1992) A cDNA encoding a pRB-binding protein with properties of the transcription factor E2F. *Cell*. [Online] 70 (2), 337–350.

Henion, P. D. & Weston, J. A. (1997) Timing and pattern of cell fate restrictions in the neural crest lineage. *Development*. 124 (21), 4351–4359.

Henrique, D. & Schweisguth, F. (2019) Mechanisms of Notch signaling: a simple logic deployed in time and space. *Development*. [Online] 146 (3), . [online]. Available from: https://dev.biologists.org/content/146/3/dev172148 (Accessed 2 February 2021).

Herbig, U. et al. (2006) Cellular Senescence in Aging Primates. *Science*. [Online] 311 (5765), 1257–1257.

High, F. A. et al. (2007) An essential role for Notch in neural crest during cardiovascular development and smooth muscle differentiation. *The Journal of Clinical Investigation*. [Online] 117 (2), 353–363.

Hirata, H. et al. (2020) Coordination between Cell Motility and Cell Cycle Progression in Keratinocyte Sheets via Cell-Cell Adhesion and Rac1. *iScience*. [Online] 23 (11), 101729.

Honjo, Y. et al. (2008) Neuregulin-mediated ErbB3 signaling is required for formation of zebrafish dorsal root ganglion neurons. *Development*. [Online] 135 (15), 2615–2625.

Huang, X. & Saint-Jeannet, J.-P. (2004) Induction of the neural crest and the opportunities of life on the edge. *Developmental Biology*. [Online] 275 (1), 1–11.

Hunter, G. L. et al. (2016) Coordinated control of Notch/Delta signalling and cell cycle progression drives lateral inhibition-mediated tissue patterning. *Development*. [Online] 143 (13), 2305–2310.

Huttenlocher, A. & Horwitz, A. R. (2011) Integrins in Cell Migration. *Cold Spring Harbor Perspectives in Biology*. [Online] 3 (9), a005074.

Jesuthasan, S. (1996) Contact inhibition/collapse and pathfinding of neural crest cells in the zebrafish trunk. *Development*. 122 (1), 381–389.

Joshi, I. et al. (2009) Notch signaling mediates G1/S cell-cycle progression in T cells via cyclin D3 and its dependent kinases. *Blood*. [Online] 113 (8), 1689–1698.

Kagawa, Y. et al. (2013) Cell Cycle-Dependent Rho GTPase Activity Dynamically Regulates Cancer Cell Motility and Invasion In Vivo. *PLOS ONE*. [Online] 8 (12), e83629.

Kalcheim, C. & Le Douarin, N. M. (1986) Requirement of a neural tube signal for the differentiation of neural crest cells into dorsal root ganglia. *Developmental Biology*. [Online] 116 (2), 451–466.

Killander, D. & Zetterberg, A. (1965) A quantitative cytochemical investigation of the relationship between cell mass and initiation of DNA synthesis in mouse fibroblasts in vitro. *Experimental Cell Research*. [Online] 40 (1), 12–20.

Kimmel, C. B. et al. (1995) Stages of embryonic development of the zebrafish. *Developmental Dynamics*. [Online] 203 (3), 253–310.

Klymkowsky, M. W. et al. (2010) Mechanisms driving neural crest induction and migration in the zebrafish and Xenopus laevis. *Cell Adhesion & Migration*. [Online] 4 (4), 595–608.

Kohrman, A. Q. & Matus, D. Q. (2017) Divide or Conquer: Cell Cycle Regulation of Invasive Behavior. *Trends in Cell Biology*. [Online] 27 (1), 12–25.

Konen, J. et al. (2017) Image-guided genomics of phenotypically heterogeneous populations reveals vascular signalling during symbiotic collective cancer invasion. *Nature Communications*. [Online] 8 (1), 15078.

Krispin, S. et al. (2010) Evidence for a dynamic spatiotemporal fate map and early fate restrictions of premigratory avian neural crest. *Development*. [Online] 137 (4), 585–595.

Kruger, G. M. et al. (2002) Neural Crest Stem Cells Persist in the Adult Gut but Undergo Changes in Self-Renewal, Neuronal Subtype Potential, and Factor Responsiveness. *Neuron*. [Online] 35 (4), 657–669.

Latimer, A. J. et al. (2005) her9 promotes floor plate development in zebrafish. *Developmental Dynamics*. [Online] 232 (4), 1098–1104.

Leonard, C. E. & Taneyhill, L. A. (2020) The road best traveled: Neural crest migration upon the extracellular matrix. *Seminars in Cell & Developmental Biology*. [Online] 100177–185.

Leslie, J. D. et al. (2007) Endothelial signalling by the Notch ligand Delta-like 4 restricts angiogenesis. *Development*. [Online] 134 (5), 839–844.

Leung, L. et al. (2011) Apical migration of nuclei during G2 is a prerequisite for all nuclear motion in zebrafish neuroepithelia. *Development*. [Online] 138 (22), 5003–5013.

Lewis, J. (1996) Neurogenic genes and vertebrate neurogenesis. *Current Opinion in Neurobiology*. [Online] 6 (1), 3–10.

Li, R. (2013) The Art of Choreographing Asymmetric Cell Division. *Developmental Cell*. [Online] 25 (5), 439–450.

Li, Y. et al. (2019) In Vivo Quantitative Imaging Provides Insights into Trunk Neural Crest Migration. *Cell Reports*. [Online] 26 (6), 1489-1500.e3.

Lièvre, C. S. L. & Douarin, N. M. L. (1975) Mesenchymal derivatives of the neural crest: analysis of chimaeric quail and chick embryos. *Development*. 34 (1), 125–154.

Lim, S. & Kaldis, P. (2013) Cdks, cyclins and CKIs: roles beyond cell cycle regulation. *Development*. [Online] 140 (15), 3079–3093.

Liu, Z. et al. (2015) Second-generation Notch1 activity-trap mouse line (N1IP::CreHI) provides a more comprehensive map of cells experiencing Notch1 activity. *Development*. [Online] 142 (6), 1193–1202.

Lodish, H. et al. (2000) Overview of the Cell Cycle and Its Control. *Molecular Cell Biology. 4th edition*. [online]. Available from: https://www.ncbi.nlm.nih.gov/books/NBK21466/ (Accessed 31 March 2021).

Lu, M. S. & Johnston, C. A. (2013) Molecular pathways regulating mitotic spindle orientation in animal cells. *Development*. [Online] 140 (9), 1843–1856.

Lukoseviciute, M. et al. (2018) From Pioneer to Repressor: Bimodal foxd3 Activity Dynamically Remodels Neural Crest Regulatory Landscape In Vivo. *Developmental Cell*. [Online] 47 (5), 608-628.e6.

Mammucari, C. et al. (2005) Integration of Notch 1 and Calcineurin/NFAT Signaling Pathways in Keratinocyte Growth and Differentiation Control. *Developmental Cell*. [Online] 8 (5), 665–676.

McGraw, H. F. et al. (2012) Postembryonic neuronal addition in Zebrafish dorsal root ganglia is regulated by Notch signaling. *Neural Development*. [Online] 723.

McGraw, H. F. et al. (2008) Zebrafish Dorsal Root Ganglia Neural Precursor Cells Adopt a Glial Fate in the Absence of Neurogenin1. *Journal of Neuroscience*. [Online] 28 (47), 12558–12569.

McKinney, M. C. et al. (2013) Evidence for dynamic rearrangements but lack of fate or position restrictions in premigratory avian trunk neural crest. *Development (Cambridge, England)*. [Online] 140 (4), 820–830.

McLennan, R. et al. (2015a) Neural crest migration is driven by a few trailblazer cells with a unique molecular signature narrowly confined to the invasive front. *Development*. [Online] 142 (11), 2014–2025.

McLennan, R. et al. (2010) Vascular endothelial growth factor (VEGF) regulates cranial neural crest migration in vivo. *Developmental Biology*. [Online] 339 (1), 114–125.

McLennan, R. et al. (2015b) VEGF signals induce trailblazer cell identity that drives neural crest migration. *Developmental Biology*. [Online] 407 (1), 12–25.

Mead, T. J. & Yutzey, K. E. (2012) Notch pathway regulation of neural crest cell development in vivo. *Developmental Dynamics*. [Online] 241 (2), 376–389.

Medici, D. et al. (2008) Snail and Slug Promote Epithelial-Mesenchymal Transition through β-Catenin–T-Cell Factor-4-dependent Expression of Transforming Growth Factor-β3. *Molecular Biology of the Cell*. [Online] 19 (11), 4875–4887.

Meier, R. et al. (2007) The Chemokine Receptor CXCR4 Strongly Promotes Neuroblastoma Primary Tumour and Metastatic Growth, but not Invasion. *PLOS ONE*. [Online] 2 (10), e1016.

Meulemans, D. & Bronner-Fraser, M. (2004) Gene-Regulatory Interactions in Neural Crest Evolution and Development. *Developmental Cell*. [Online] 7 (3), 291–299.

Molina, A. et al. (2020) G1 Phase Lengthening During Neural Tissue Development Involves CDC25B Induced G1 Heterogeneity. *bioRxiv*. [Online] 2020.11.06.370833.

Molinie, N. et al. (2019) Cortical branched actin determines cell cycle progression. *Cell Research*. [Online] 29 (6), 432–445.

Moro, E. et al. (2013) Generation and application of signaling pathway reporter lines in zebrafish. *Molecular Genetics and Genomics*. [Online] 288 (5), 231–242.

Mrozik, K. M. et al. (2018) N-cadherin in cancer metastasis, its emerging role in haematological malignancies and potential as a therapeutic target in cancer. *BMC Cancer*. [Online] 18 (1), 939.

Murphey, R. D. et al. (2006) A chemical genetic screen for cell cycle inhibitors in zebrafish embryos. *Chemical Biology & Drug Design*. [Online] 68 (4), 213–219.

Nader, G. P. F. et al. (2016) FAK, talin and PIPKIγ regulate endocytosed integrin activation to polarize focal adhesion assembly. *Nature Cell Biology*. [Online] 18 (5), 491–503.

Nagai, T. et al. (2020) Tactics of cancer invasion: solitary and collective invasion. *The Journal of Biochemistry*. [Online] 167 (4), 347–355.

Nandagopal, N. et al. (2018) Dynamic Ligand Discrimination in the Notch Signaling Pathway. *Cell*. [Online] 172 (4), 869-880.e19.

Nguyen, B.-C. et al. (2006) Cross-regulation between Notch and p63 in keratinocyte commitment to differentiation. *Genes & Development*. [Online] 20 (8), 1028–1042.

Nicenboim, J. et al. (2015) Lymphatic vessels arise from specialized angioblasts within a venous niche. *Nature*. [Online] 522 (7554), 56–61.

Noctor, S. C. et al. (2008) Distinct Behaviors of Neural Stem and Progenitor Cells Underlie Cortical Neurogenesis. *The Journal of comparative neurology*. [Online] 508 (1), 28–44.

Nooij, J. C. de et al. (1996) A Cyclin-Dependent Kinase Inhibitor, Dacapo, Is Necessary for Timely Exit from the Cell Cycle during Drosophila Embryogenesis. *Cell*. [Online] 87 (7), 1237–1247.

Noseda, M. et al. (2004) Notch Activation Induces Endothelial Cell Cycle Arrest and Participates in Contact Inhibition: Role of p21Cip1 Repression. *Molecular and Cellular Biology*. [Online] 24 (20), 8813–8822.

Nusser-Stein, S. et al. (2012) Cell-cycle regulation of NOTCH signaling during C. elegans vulval development. *Molecular Systems Biology*. [Online] 8. [online]. Available from: http://msb.embopress.org/cgi/doi/10.1038/msb.2012.51 (Accessed 14 November 2018).

O'Boyle, G. et al. (2013) Inhibition of CXCR4–CXCL12 chemotaxis in melanoma by AMD11070. *British Journal of Cancer*. [Online] 108 (8), 1634–1640.

Ohnuma, S. et al. (1999) p27Xic1, a Cdk Inhibitor, Promotes the Determination of Glial Cells in Xenopus Retina. *Cell*. [Online] 99 (5), 499–510.

Page, D. J. et al. (2019) Positive Feedback Defines the Timing, Magnitude, and Robustness of Angiogenesis. *Cell Reports*. [Online] 27 (11), 3139-3151.e5.

Paglini, M. G. & Rovasio, R. A. (1994) Cell cycle of neural crest cells in the early migratory stage in vivo. *Cell Proliferation*. [Online] 27 (9), 571–578.

Palomero, T. et al. (2006) NOTCH1 directly regulates c-MYC and activates a feed-forward-loop transcriptional network promoting leukemic cell growth. *Proceedings of the National Academy of Sciences*. [Online] 103 (48), 18261–18266.

Park, H.-C. et al. (2005) Oligodendrocyte Specification in Zebrafish Requires Notch-Regulated Cyclin-Dependent Kinase Inhibitor Function. *The Journal of Neuroscience*. [Online] 25 (29), 6836–6844.

Patel, J. et al. (2016) Self-Renewal and High Proliferative Colony Forming Capacity of Late-Outgrowth Endothelial Progenitors Is Regulated by Cyclin-Dependent Kinase Inhibitors Driven by Notch Signaling. *STEM CELLS*. [Online] 34 (4), 902–912.

Pauls, S. et al. (2001) A zebrafish histone variant H2A.F/Z and a transgenic H2A.F/Z:GFP fusion protein for in vivo studies of embryonic development. *Development Genes and Evolution*. [Online] 211 (12), 603–610.

Perez-Alcala, S. et al. (2004) LSox5 regulates RhoB expression in the neural tube and promotes generation of the neural crest. *Development*. [Online] 131 (18), 4455–4465.

Perry, J. A. & Kornbluth, S. (2007) Cdc25 and Wee1: analogous opposites? *Cell Division*. [Online] 2 (1), 12.

Pfeiffer, J. et al. (2018) Rapid progression through the cell cycle ensures efficient migration of primordial germ cells – The role of Hsp90. *Developmental Biology*. [Online] 436 (2), 84–93.

Phng, L.-K. & Gerhardt, H. (2009) Angiogenesis: A Team Effort Coordinated by Notch. *Developmental Cell*. [Online] 16 (2), 196–208.

Pomeranz, H. D. et al. (1991) Colonization of the post-umbilical bowel by cells derived from the sacral neural crest: direct tracing of cell migration using an intercalating probe and a replication-deficient retrovirus. *Development*. 111 (3), 647–655.

Raible, D. W. et al. (1992) Segregation and early dispersal of neural crest cells in the embryonic zebrafish. *Developmental Dynamics*. [Online] 195 (1), 29–42.

Raible, D. W. & Eisen, J. S. (1996) Regulative interactions in zebrafish neural crest. *Development*. 122 (2), 501–507.

Raible, D. W. & Eisen, J. S. (1994) Restriction of neural crest cell fate in the trunk of the embryonic zebrafish. *Development*. 120 (3), 495–503.

Rajan, S. G. et al. (2018) Tracking neural crest cell cycle progression in vivo. *Genesis (New York, N.Y. : 2000)*. [Online] 56 (6–7), e23214.

Rangarajan, A. et al. (2001) Notch signaling is a direct determinant of keratinocyte growth arrest and entry into differentiation. *The EMBO journal*. [Online] 20 (13), 3427–3436.

Reichrath, J. & Reichrath, S. (eds.) (2012) *Notch Signaling in Embryology and Cancer*. Advances in Experimental Medicine and Biology. [Online]. New York: Springer-Verlag. [online]. Available from: https://www.springer.com/gp/book/9781461408994 (Accessed 31 March 2021).

Riahi, R. et al. (2015) Notch1-Dll4 signaling and mechanical force regulate leader cell formation during collective cell migration. *Nature communications*. [Online] 66556.

Riccio, O. et al. (2008) Loss of intestinal crypt progenitor cells owing to inactivation of both Notch1 and Notch2 is accompanied by derepression of CDK inhibitors p27Kip1 and p57Kip2. *EMBO Reports*. [Online] 9 (4), 377–383.

Richardson, J. et al. (2016) Leader Cells Define Directionality of Trunk, but Not Cranial, Neural Crest Cell Migration. *Cell Reports*. [Online] 15 (9), 2076–2088.

Richter, S. et al. (2017) Small molecule screen in embryonic zebrafish using modular variations to target segmentation. *Nature Communications*. [Online] 8 (1), 1901.

Ridenour, D. A. et al. (2014) The neural crest cell cycle is related to phases of migration in the head. *Development*. [Online] 141 (5), 1095–1103.

Rinon, A. et al. (2011) p53 coordinates cranial neural crest cell growth and epithelial-mesenchymal transition/delamination processes. *Development*. [Online] 138 (9), 1827–1838.

Rios, A. C. et al. (2011) Neural crest regulates myogenesis through the transient activation of NOTCH. *Nature*. [Online] 473 (7348), 532–535.

Rizzo, P. et al. (2008) Cross-talk between Notch and the Estrogen Receptor in Breast Cancer Suggests Novel Therapeutic Approaches. *Cancer Research*. [Online] 68 (13), 5226–5235.

Rocha, M. et al. (2020) Neural crest development: insights from the zebrafish. *Developmental Dynamics*. [Online] 249 (1), 88–111.

Ronchini, C. & Capobianco, A. J. (2001) Induction of Cyclin D1 Transcription and CDK2 Activity by Notchic: Implication for Cell Cycle Disruption in Transformation by Notchic. *Molecular and Cellular Biology*. [Online] 21 (17), 5925–5934.

Roubinet, C. & Cabernard, C. (2014) Control of asymmetric cell division. *Current Opinion in Cell Biology*. [Online] 31 (Supplement C), 84–91.

Rowan, S. et al. (2008) Notch signaling regulates growth and differentiation in the mammalian lens. *Developmental Biology*. [Online] 321 (1), 111–122.

Sauka-Spengler, T. & Bronner-Fraser, M. (2008) A gene regulatory network orchestrates neural crest formation. *Nature Reviews Molecular Cell Biology*. [Online] 9 (7), 557–568.

Scarpa, E. et al. (2015) Cadherin Switch during EMT in Neural Crest Cells Leads to Contact Inhibition of Locomotion via Repolarization of Forces. *Developmental Cell*. [Online] 34 (4), 421–434.

Scarpa, E. & Mayor, R. (2016) Collective cell migration in development. *J Cell Biol*. [Online] 212 (2), 143–155.

Schaefer, M. et al. (2000) A protein complex containing Inscuteable and the Gα-binding protein Pins orients asymmetric cell divisions in Drosophila. *Current Biology*. [Online] 10 (7), 353–362.

Schweisguth, F. (2015) Asymmetric cell division in the Drosophila bristle lineage: from the polarization of sensory organ precursor cells to Notch-mediated binary fate decision. *Wiley Interdisciplinary Reviews. Developmental Biology*. [Online] 4 (3), 299–309.

Serbedzija, G. N. et al. (1994) Developmental potential of trunk neural crest cells in the mouse. *Development*. 120 (7), 1709–1718.

Shah, N. (1994) Glial growth factor restricts mammalian neural crest stem cells to a glial fate. *Cell*. [Online] 77 (3), 349–360.

Shahriyari, L. & Komarova, N. L. (2013) Symmetric vs. Asymmetric Stem Cell Divisions: An Adaptation against Cancer? *PLOS ONE*. [Online] 8 (10), e76195.

Shapiro, G. I. & Harper, J. W. (1999) Anticancer drug targets: cell cycle and checkpoint control. *The Journal of Clinical Investigation*. [Online] 104 (12), 1645–1653.

Shellard, A. & Mayor, R. (2016) Chemotaxis during neural crest migration. *Seminars in Cell & Developmental Biology*. [Online] 55 (Supplement C), 111–118.

Sieber-Blum, M. et al. (2004) Pluripotent neural crest stem cells in the adult hair follicle. *Developmental Dynamics: An Official Publication of the American Association of Anatomists*. [Online] 231 (2), 258–269.

Sieber-Blum, M. & Cohen, A. M. (1980) Clonal analysis of quail neural crest cells: they are pluripotent and differentiate in vitro in the absence of noncrest cells. *Developmental Biology*. [Online] 80 (1), 96–106.

Sjöqvist, M. & Andersson, E. R. (2019) Do as I say, Not(ch) as I do: Lateral control of cell fate. *Developmental Biology*. [Online] 447 (1), 58–70.

Stemple, D. L. & Anderson, D. J. (1992) Isolation of a stem cell for neurons and glia from the mammalian neural crest. *Cell*. [Online] 71 (6), 973–985.

Szabó, A. et al. (2016) In vivo confinement promotes collective migration of neural crest cells. *J Cell Biol*. [Online] 213 (5), 543–555.

Szabó, A. & Mayor, R. (2018) Mechanisms of Neural Crest Migration. *Annual Review of Genetics*. [Online] 52 (1), 43–63.

Tanaka, M. et al. (2009) Inhibition of Notch pathway prevents osteosarcoma growth by cell cycle regulation. *British Journal of Cancer*. [Online] 100 (12), 1957–1965.

Taubenberger, A. V. et al. (2020) The Mechanics of Mitotic Cell Rounding. *Frontiers in Cell and Developmental Biology*. [Online] 8. [online]. Available from: https://www.frontiersin.org/articles/10.3389/fcell.2020.00687/full (Accessed 26 January 2021).

Theveneau, E. et al. (2010) Collective Chemotaxis Requires Contact-Dependent Cell Polarity. *Developmental Cell*. [Online] 19 (1), 39–53.

Théveneau, E. et al. (2007) Ets-1 Confers Cranial Features on Neural Crest Delamination. *PLOS ONE*. [Online] 2 (11), e1142.

Theveneau, E. & Mayor, R. (2012) Neural crest delamination and migration: From epithelium-to-mesenchyme transition to collective cell migration. *Developmental Biology*. [Online] 366 (1), 34–54.

Timmerman, L. A. et al. (2004) Notch promotes epithelial-mesenchymal transition during cardiac development and oncogenic transformation. *Genes & Development*. [Online] 18 (1), 99–115.

Ubezio, B. et al. (2016) Synchronization of endothelial Dll4-Notch dynamics switch blood vessels from branching to expansion Tanya T Whitfield (ed.). *eLife*. [Online] 5e12167.

Ungos, J. M. et al. (2003) Hedgehog signaling is directly required for the development of zebrafish dorsal root ganglia neurons. *Development*. [Online] 130 (22), 5351–5362.

Vega-López, G. A. et al. (2015) Functional analysis of Hairy genes in Xenopus neural crest initial specification and cell migration. *Developmental Dynamics*. [Online] 244 (8), 988–1013.

Vega-Lopez, G. A. et al. (2018) Neurocristopathies: New insights 150 years after the neural crest discovery. *Developmental Biology*. [Online] 444S110–S143.

Venkatraman, L. et al. (2016) Time to Decide? Dynamical Analysis Predicts Partial Tip/Stalk Patterning States Arise during Angiogenesis. *PLOS ONE*. [Online] 11 (11), e0166489.

Verduzco, D. & Amatruda, J. F. (2011) Analysis of Cell Proliferation, Senescence and Cell Death in Zebrafish Embryos. *Methods in cell biology*. [Online] 101. [online]. Available from: https://www.ncbi.nlm.nih.gov/pmc/articles/PMC3870180/ (Accessed 26 January 2021).

Vermeulen, K. et al. (2003) The cell cycle: a review of regulation, deregulation and therapeutic targets in cancer. *Cell Proliferation*. [Online] 36 (3), 131–149.

Wakamatsu, Y. et al. (2000) Fate determination of neural crest cells by NOTCH-mediated lateral inhibition and asymmetrical cell division during gangliogenesis. *Development*. 127 (13), 2811–2821.

Walmod, P. S. et al. (2004) Cell-cycle-dependent regulation of cell motility and determination of the role of Rac1. *Experimental Cell Research*. [Online] 295 (2), 407–420.

White, P. M. et al. (2001) Neural Crest Stem Cells Undergo Cell-Intrinsic Developmental Changes in Sensitivity to Instructive Differentiation Signals. *Neuron*. [Online] 29 (1), 57–71.

Wirtz-Peitz, F. et al. (2008) Linking Cell Cycle to Asymmetric Division: Aurora-A Phosphorylates the Par Complex to Regulate Numb Localization. *Cell*. [Online] 135 (1), 161–173.

Wiszniak, S. & Schwarz, Q. (2019) Notch signalling defines dorsal root ganglia neuroglial fate choice during early neural crest cell migration. *BMC Neuroscience*. [Online] 20 (1), 21.

Yeo, S.-Y. et al. (2007) Fluorescent protein expression driven by her4 regulatory elements reveals the spatiotemporal pattern of Notch signaling in the nervous system of zebrafish embryos. *Developmental Biology*. [Online] 301 (2), 555–567.

Zalc, A. et al. (2014) Antagonistic regulation of p57 ^{kip2} by Hes/Hey downstream of Notch signaling and muscle regulatory factors regulates skeletal muscle growth arrest. *Development*. [Online] 141 (14), 2780–2790.

Zatulovskiy, E. & Skotheim, J. M. (2020) On the Molecular Mechanisms Regulating Animal Cell Size Homeostasis. *Trends in Genetics*. [Online] 36 (5), 360–372.

Zhang, J.-M., Wei, Q., et al. (1999) Coupling of the cell cycle and myogenesis through the cyclin D1-dependent interaction of MyoD with cdk4. *The EMBO Journal*. [Online] 18 (4), 926–933.

Zhang, J.-M., Zhao, X., et al. (1999) Direct inhibition of G1 cdk kinase activity by MyoD promotes myoblast cell cycle withdrawal and terminal differentiation. *The EMBO Journal*. [Online] 18 (24), 6983–6993.

Zhang, L. et al. (2008) Cell cycle progression is required for zebrafish somite morphogenesis but not segmentation clock function. *Development (Cambridge, England)*. [Online] 135 (12), 2065–2070.

Zhang, S. et al. (2018) Notch signaling via regulation of RB and p-AKT but not PIK3CG contributes to MIA PaCa-2 cell growth and migration to affect pancreatic carcinogenesis. *Oncology Letters*. [Online] 15 (2), 2105–2110.